

**PRINCETON UNIVERSITY'S  
PRISM CLEANROOM  
ANNUAL RESEARCH  
REPORT 2018**



## A MESSAGE FROM THE DIRECTORS

Dear Stakeholders of the PRISM Cleanroom at Princeton University,

This report briefly outlines the types of research taking place at Princeton that utilize in the resources of the PRISM Cleanroom, Soft Materials Processing Lab, and/or Packaging Lab. The information was provided by researchers themselves, who then vetted the formatted pages.

The daily pricing model of our facility is unique in that it allows for uninhibited exploration and the creation of robust preliminary data. This mechanism encourages the great diversity in research areas contained in these pages, encourages learning by students of all levels and disciplines, and enables an effective way to support new research ideas and highly competitive proposals.

We thank the faculty, researchers, and lab members who helpfully provided this information demonstrating the great impact these facilities are having on the overall research mission of Princeton.

For the collection of the data and the creation of this report we acknowledge the substantial efforts of Dan McNesby, Cheyenne Brown and Elizabeth Squassoni-Jachimczuk.

Thank you for your continued support and enjoy learning about some of the exciting research happening at Princeton!

Ian Harvey, PRISM Cleanroom Director



Craig B. Arnold, PRISM Director



## TABLE OF CONTENTS

COVER PAGE.....	1
MESSAGE FROM THE DIRECTORS.....	2
TABLE OF CONTENTS.....	3
PRISM CLEANROOM TOOL LIST.....	6
LIST OF MICROFABRICATION COURSES (ACADEMIC AND SHORT COURSES).....	7
NEW PROCESSES INTRODUCED BY STAFF.....	9
PRISM CLEANROOM RESEARCH REPORTS	
<b>AST (Astrophysical Sciences)</b>	
<b>EFTHIMION, PHILIP C.</b>	
<i>High-Resolution X-Ray Spectroscopy Studies of Ion and Electron Temperature Profiles in Buried Layer Targets.....</i>	12
<b>CEE (Chemical and Biological Engineering)</b>	
<b>BOURG, IAN C.</b>	
<i>Quartz Wetting By Water and CO<sub>2</sub> and the Potential Impact of Organic Residues.....</i>	13
<b>ELE (Electrical Engineering)</b>	
<b>GMACHL, CLAIRE F.</b>	
<i>Lateral Tailoring of Gain and Current Profile in High Power Edge Emitting Lasers.....</i>	14
<i>Hybrid III-V &amp; II-VI Infrared Photodetectors.....</i>	15
<i>16<math>\mu</math>m GaAs Quantum Cascade Laser.....</i>	16
<i>Optoelectronic Plasmonic Metamaterials with a Quantum Cascade Structure.....</i>	17
<b>HOUCK, ANDREW A.</b>	
<i>Hyperbolic and Flat Band Lattices in Circuit Quantum Electrodynamics.....</i>	18
<i>Developing Protected Superconducting Circuits for Quantum Computation.....</i>	19
<i>Nanowire Superinductance Fluxonium Qubit.....</i>	20
<i>Lattice Quantum Simulation with Circuit QED.....</i>	21
<i>Quantum Optimal Control.....</i>	22
<i>Granular Aluminum Kinetic Inductors.....</i>	23
<i>Superconducting Research for Quantum Computing.....</i>	24
<i>Many Body Quantum Optics and Light Matter Interactions in Superconducting Circuits.....</i>	25
<i>Many Body Quantum Simulation Using Superconducting Circuits.....</i>	26
<b>LYON, STEPHEN A.</b>	
<i>Superconducting Kinetic Inductance Devices for Electron Spin Resonance.....</i>	27
<i>Devices to Control Surface Electron Transport on Helium.....</i>	28
<i>Electrons on Helium.....</i>	29
<i>Silicon Quantum Dots.....</i>	30
<i>Investigating the Origin of Shallow Traps at the Si-SO<sub>2</sub> Interface in Quantum Dots.....</i>	31
<b>PRUCNAL, PAUL R.</b>	
<i>Phototonic Integrated Circuits for Neuromorphic and Microwave Processing.....</i>	32

## TABLE OF CONTENTS

### **RAND, BARRY P.**

<i>Toward Electrically Pumped Lasing in Hybrid Organic-Inorganic Perovskite Semiconductors</i> .....	33
<i>Thin Film Optoelectronic Device Applications</i> .....	34
<i>Benchmarking of Digital Logic Styles for High-Performance OTFT Circuits</i> .....	35

### **SENGUPTA, KAUSHIK**

<i>Future Programmable Millimeterwave Systems</i> .....	36
<i>A Multi-Port Dual Polarized Antenna Couples mm-Wave Receiver with Pattern Programmability and Capability of Passive Rejection of Interferers</i> .....	37
<i>mmWave Reconfigurable Power Amplifiers for 5G</i> .....	38
<i>THZ Imager Chip</i> .....	39

### **SHAYEGAN, MANSOUR**

<i>Probing Exotic Phases of Interacting Electrons in Low-Dimensional Systems</i> .....	40
<i>Exotic Phases of Electrons in Interacting 2D Systems</i> .....	41
<i>Probing Exotic Phases of Interacting Electrons in Low-Dimensional Systems</i> .....	42
<i>Probing Nematic Phases with a Composite Fermions Sea</i> .....	43

### **STURM, JAMES C.**

<i>Efficient Power Transfer Between Large-Area/Flexible Substrates Using ZnO Schottky Diodes Deposited By Plasma-Enhanced ALD</i> .....	44
<i>Oxide Materials and Interfaces for Photovoltaics</i> .....	45
<i>Si/SiGe 2DEGs Grown by UHV CVD for Quantum Computing Applications</i> .....	46
<i>Microfluidic</i> .....	47
<i>Microfluidic Devices as the In Vitro Tumor Model</i> .....	48
<i>High-Performance Thin Film Transistors for Large Area Circuits and Systems Applications</i> .....	49
<i>Flexible Microelectrode Array</i> .....	50
<i>GHZ Large-Area Electronics for Interfacing a Large Number of IOT Sensors</i> .....	51

### **THOMPSON, JEFFREY D.**

<i>Atomic Source of Single Photons in the Telecom Band</i> .....	52
<i>New Materials for Quantum Systems</i> .....	53

## **MAE (Mechanical and Aerospace Engineering)**

### **ARNOLD, CRAIG B.**

<i>LIFT (Laser Induced Forward Transfer)</i> .....	54
<i>Understanding Piezoelectrochemical Materials</i> .....	55

### **COHEN, DANIEL J.**

<i>Controlling Tissue Collective Migration</i> .....	56
--	----

### **HULTMARK, MARCUS N.**

<i>Nano-Scale Thermal Anemometry Probes</i> .....	57
<i>Design and Manufacturing of Nano-Scale Thermal Anemometry Probes in Compressible Flows</i> .....	58

## TABLE OF CONTENTS

<b>KASDIN, N. JEREMY</b>	
<i>Subscale Starshade Testing</i> .....	59
<b>STONE, HOWARD A.</b>	
<i>Construction and Design of a Microfluidic Channel Geometry for Studying the Formation of Separation Bubbles</i> .....	60
<i>Engineering the Chromosome Segregation Machinery to Catalyze Life</i> .....	61
<i>Flow-Induced Gelation of Microfiber Suspensions</i> .....	62
<i>CO<sub>2</sub> Driven Diffusiophoresis and Particle Separation</i> .....	63
<b>MOL (Molecular Biology)</b>	
<b>MURPHY, COLEEN T.</b>	
<i>C. Elegans in PDMS Chip</i> .....	64
<b>YAN, NIENG</b>	
<i>Transfer Two-Dimensional Materials onto TEM Grids</i> .....	65
<b>PHY (Physics)</b>	
<b>GALBIATI, CRISTIANO</b>	
<i>Amorphous Selenium Device Fabrication for Neutrinoless Double Beta Decay Search</i> .....	66
<b>LEIFER, ANDREW M.</b>	
<i>Male Neural Dynamics and Behavior Response to Hermaphrodite Sensory Cues</i> .....	67
<b>ONG, NAI PHUAN</b>	
<i>Many Body Quantum Simulation Using Superconducting Circuits</i> .....	68
<i>Fabrication of Devices for Transport Experiments of Topological Materials</i> .....	69
<i>Superconductivity in the Weyl Semimetal MoTe<sub>2</sub></i> .....	70
<i>Electronic Devices Using Topological Materials</i> .....	71
<b>STAGGS, SUZANNE T.</b>	
<i>Simons Observatory (Li)</i> .....	72
<i>Simons Observatory (Wang)</i> .....	73
<b>TULLY, CHRISTOPHER G.</b>	
<i>Graphene Single Electron Transistor for Neutrino Detector</i> .....	74
<b>WU, SANFENG</b>	
<i>Topological Quantum Phases in 2D Materials (Jia)</i> .....	75
<i>Topological Quantum Phases in 2D Materials (Onyszczyk)</i> .....	76
OTHER RESEARCH PERFORMED IN THE PRISM CLEANROOM.....	77
EXAMPLES OF CITATIONS RESULTING FROM RESEARCH UTILITIZING THE PRISM CLEANROOM.....	78

## PRISM CLEANROOM TOOL LIST

### DEPOSITION - PVD

- Angstrom sputter (3x4"; Nb, Al, Ti)
- Angstrom sputter (4x4" configurable: Al, Cr, Ti, AlNiCo, Mo, Ho, Al 1% Si, Co, Ge, Au, Pt, Ni) (Pending)
- Angstrom sputter (3x3" configurable: CoO, MnO, NiO, ZnO, ZnO w/ 2% Al<sub>2</sub>O<sub>3</sub>, Fe<sub>2</sub>O<sub>3</sub>, SiO<sub>2</sub>, TiO<sub>2</sub>, Al<sub>2</sub>O<sub>3</sub>)
- Angstrom dual chamber e-beam evaporator, six dedicated pockets (Ti, Pt, Au, Ni, Ge, Al)
- Denton e-beam Evaporator (four pockets; In, dielectrics, Ti, Sn, Ag, Al, Pt, Ge, Ni, Au, SiO<sub>2</sub>, Si, Cr, Cu)
- Angstrom Nexdep e-beam evaporator (six pockets, *NO* In, Cu, Sn, dielectrics)
- Angstrom Covap thermal evaporator (dedicated Ti, Au, Cr, Al)

### PLASMA ETCH

- Si precision etch for vertical, smooth sidewalls, no foot; (pending)
- GaAs on GaAlAs precision etch for vertical, smooth sidewalls, (pending)
- SAMCO 200iPB RIE (III-V and compound semiconductor); Cl<sub>2</sub>, BCl<sub>3</sub>, SiCl<sub>4</sub>, Ar, and O<sub>2</sub>
- PlasmaTherm APEX SLR metal etcher: Cl<sub>2</sub>, BCl<sub>3</sub>, Ar, O<sub>2</sub>, SF<sub>6</sub>, and CHF<sub>3</sub>
- PlasmaTherm APEX SLR diamond etcher: Cl<sub>2</sub>, O<sub>2</sub>, H<sub>2</sub>, N<sub>2</sub>, and Ar
- SAMCO 800iPB Deep RIE (Si) using Bosch; SF<sub>6</sub>, C<sub>4</sub>F<sub>8</sub>, O<sub>2</sub>, CF<sub>4</sub>, and Ar
- STS Multiplex ICP Etcher (Metals); Cl<sub>2</sub>, BCl<sub>3</sub>, Ar, O<sub>2</sub>, SF<sub>6</sub>, and CHF<sub>3</sub>
- TePla M4L isotropic ash; O<sub>2</sub>, Ar, and CF<sub>4</sub>
- PlasmaPro 80 RIE; SF<sub>6</sub>, CF<sub>4</sub>, CHF<sub>3</sub>, O<sub>2</sub>, Ar, and N<sub>2</sub> use: Si, SiO<sub>2</sub>, SiN<sub>x</sub>, SiC, Al, Al<sub>2</sub>O<sub>3</sub>
- PlasmaTherm 720 SLR RIE shallow etching of Si, SiO<sub>2</sub>, SiN<sub>x</sub>, some metals, and III/V's: Cl<sub>2</sub>, BCl<sub>3</sub>, H<sub>2</sub>, Ar, O<sub>2</sub>, SF<sub>6</sub>, CF<sub>4</sub>

### ALD, CVD & THERMAL PROCESSES

- Cambridge ALD thermal Al<sub>2</sub>O<sub>3</sub>
- Oxford PEALD low temperature Al<sub>2</sub>O<sub>3</sub>
- Oxford PlasmaPro PECVD SiO<sub>2</sub>, SiN<sub>x</sub>, α-Si

- RTP: one each: Si, III-V; forming gas
- RCA processing hood; Semi-Tool SRD's
- Tube Furnaces: w/d ox, solid state diff., TEOS, SiN<sub>x</sub>, polySi, anneal

### NANO & MICRO LITHOGRAPHY

- Raith E-Line e-beam writer, 5-30keV
- Heidelberg DWL66+ with grayscale and backside alignment, 900nm and 2μm
- Nanonex Nanoimprinter
- Suss MA6, MJB4; Cr etch; HMDS prime

### CHARACTERIZATION & METROLOGY

- Hitachi S-4700 FESEM
- KLA Tencor P-15 Profilometer, Gaertner Ellipsometer, NanoSpec Reflectometer

### PACKAGING

- ADT Dicing Saw (taping, UV curing tools)
- Wire Bonding: K&S Wedge, Questar Wedge, West-Bond Ball-Wedge
- Logitech Lapping/Polishing System,
- West-Bond Manual Epoxy Die Bonder
- Tresky Flip Chip (thermal evap. In, Cu)

### SOFT MATERIALS & MICROFLUIDICS

- Heidelberg microPG101 (direct laser patterning of SU-8, 2μm and 5μm)
- Suspended nanoparticle and protein printer (two of these)
- SCS Parylene coating
- NxQ 4006 Mask Aligner
- PDMS Processing Tools, Plasma surface activation and wet processing, UV / ozone cleaning
- Critical point dryer, VWR 1410 Vacuum Oven, KLA Tencor D-120 Profilometer
- 3D prototype (plastic) printing
- FormLabs Form2 3D prototyping (plastic)

### STAFF SERVICES

- Microfluidics concept / simulate / design / fabricate / test support
- Process and architectural design using cleanroom tools

## TOOL AND PROCESS SPECIFIC SHORT COURSES

- PRISM Cleanroom Orientation 1 - A PRISM Cleanroom laboratory safety lecture and a tour of PRISM Cleanroom Orientation 2 - A practical training inside the cleanroom at the acid fume hood focused on piranha etch and BOE etch.
- ADT Dicing Saw short course
- Questar Wedge Wire Bonder short course
- K&S Wedge Wire Bonder short course
- Logitech Lapping/Polishing Station short course
- Tresky Flip Chip Bonder short course
- RCA Hood short course – RCA cleaning procedure of the whole cassette of silicon wafers prior to high-temperature processing steps
- CVD Equipment 1034 Oxidation and Annealing Furnaces short course
- CVD Equipment 1033 Oxidation Furnace short course
- CVD Equipment 1033 LPCVD Furnaces short course
- Gaertner Ellipsometer short course
- Hitachi S-4700 SEM short course
- KLA Tencor P-15 Profilometer short course
- NanoSpec Reflectometer short course
- Nanonex Nanoimprinter short course
- Raith E-beam Writer short course
- KLA Tencor D-120 Profilometer short course
- PDMS Processing Tools short course
- Critical Point Dryer short course
- Cambridge ALD short course
- Oxford ALD short course
- Angstrom Covap Thermal Evaporator short course
- Angstrom Dielectrics Sputterer short course
- Angstrom Dual Chamber E-beam Evaporator short course
- Angstrom Metals Sputterer short course
- Angstrom Nexdep E-beam Evaporator short course
- Denton E-beam Evaporator short course
- Edwards Thermal Evaporator short course
- Ultraviolet/Ozone Cleaning System short course
- VWR 1410 Vacuum Oven short course
- CVD2 Stack Furnace short course
- Oxford ICP-CVD short course
- Oxford PlasmaPro80 RIE short course
- PlasmaTherm 720 SLR RIE short course
- SAMCO 200iPB RIE III-V short course
- SAMCO 800iPB Deep RIE (si) short course
- STS Multiplex ICP Etcher (Metals) short course
- TePla M4L Plasma Asher short course
- SSI Solaris 150 RTP Systems short course
- Automatic Develop Station short course
- Brewer Science Spin Processor short course
- Heidelberg DWL66+ short course
- NxQ 4006 Mask Aligner short course
- Photoresist Spinners short course
- Polos Chrome Etch Processor short course
- Suss MA6 Mask Aligner short course
- Suss MJB4 Mask Aligner short course
- YES Vacuum Oven short course
- PlasmaTherm APEX SLR (Metals) short course
- PlasmaTherm APEX SLR (Semiconductors) short course
- Heidelberg microPG101 short course
- Semi-Tool Spin Rinse Dryers short course

More information at: <https://prism-cleanroom.princeton.edu/tools.php>

## FUNDAMENTAL PROCESSING PRINCIPLES COURSES

- PVD (Physical Vapor Deposition)
- Photolithography

### **Academic Course:**

- MSE 305 Engineering in the Micro/Nano Maker Space (course offered in Spring 2019)



**Roman Akhmechet**

**The Princeton Institute for the Science and Technology of Materials (PRISM)**

During conventional contact lithography process with g-line positive tone resists, it is near impossible to achieve straight side walls. At the same time, pattern transfer of photoresist into the underlying material with RIE process can translate the resist sidewall into the final device layer. Therefore, there is a need to manipulate the sidewall profile of the soft resist mask. By using ammonia image reversal process, it is possible to tailor the sidewall profile of AZ4330 photoresist, and, under certain condition, to

achieve a perfectly straight 90 degree sidewall. The process consists of overexposing the photoresist, then taking the sample through ammonia image reversal bake in the YES oven. Finally, there is a flood exposure step before developing.

With a highly directional RIE process, this straight resist sidewall can be transferred into a straight sidewall in the underlying etched material.

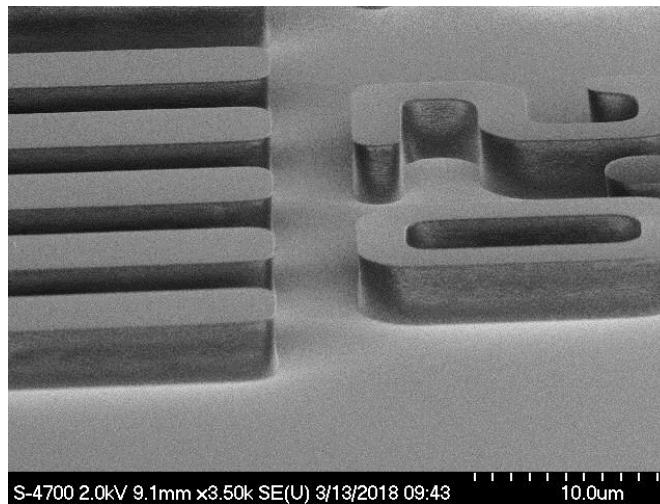


**Figure 1:** Near perfect straight sidewalls in 3.4 micron thick AZ4330, 13 second MJB4 exposure.

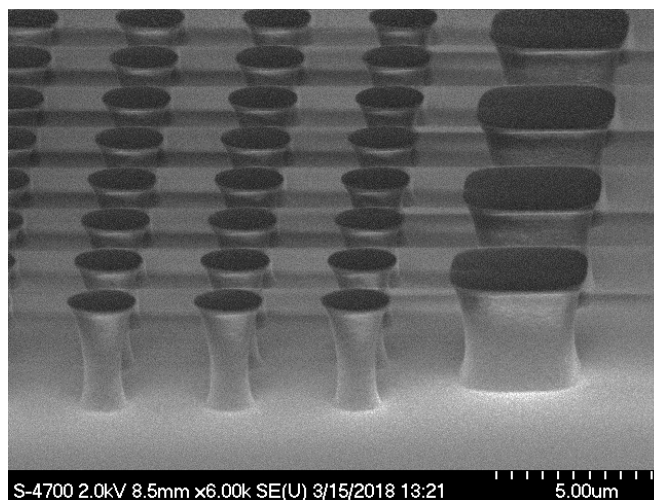


**Figure 2:** Slightly inverted slope, 5 second MJB4 exposure.

Zuzanna Lewicka

The Princeton Institute for the Science and Technology of Materials (PRISM)

To test the cleanliness of the PRISM Cleanroom furnaces and thermal oxide quality, the minority carrier recombination lifetime was measured using the WCT-120 lifetime tester (Figure 1) from Sinton Instruments (<https://www.sintoninstruments.com>).

The measured lifetime is an effective lifetime consisting of bulk and surface components [1]. The effective lifetime gives a strong indication of the furnace cleanliness because it directly relates to defects and impurities in silicon wafers. During thermal oxidation of the silicon wafer, contamination (e.g. sodium, iron, and other metallic impurities) on the furnace tube and other components within the furnace, at high temperature, migrate through the furnace tube and diffuses easily to the wafer. These impurities would create recombination centers on the surface and in the bulk silicon and decrease the effective minority-carrier lifetime. Only in a clean furnace, the low defect, high quality oxide layer can be formed. The effective lifetime measured for a high quality oxide layer on RCA cleaned silicon substrate should be significantly higher than lifetime measured for new wafers taken right out of the box. The new wafer can have some surface damage created in the factory by dicing and polishing that will decrease the effective lifetime. Lower interface defect density and the higher lifetime can be achieved by RCA wafer cleaning and growth of a high quality thermal SiO<sub>2</sub> film. Annealing in forming gas of an oxidized surface can decrease the density of interface traps even more [2].

The WCT-120 lifetime tester was used to measure effective minority carrier recombination lifetimes for silicon wafers using Quasi-Steady-State Photoconductance Decay (QSS-PCD) method [3]. The measurement was done on the new n- and p-type FZ-Si wafers taken right out of the box (n-Si no treatment and p-Si no treatment) as well as on the new wafers taken right out of the box and

dipped in diluted 10:1 hydrofluoric acid (n-Si dHF and p-Si dHF) and on the wafers that were RCA cleaned and run through the PRISM Cleanroom furnaces (n-Si/SiO<sub>2</sub> and p-Si/SiO<sub>2</sub>). Cleanliness of two atmospheric furnaces: CVD Equipment 1033 and CVD Equipment 1034 was tested. Silicon wafers FZ-Si p-type (10 Ω-cm) and FZ-Si n-type (2.3 Ω-cm) were oxidized at 1050 °C for two hours. In addition, the effect of post-oxidation forming gas annealing (N<sub>2</sub>H<sub>2</sub>, 30 min at 400 °C) for n-type wafer in CVD Equipment 1034 system (n-Si/SiO<sub>2</sub> in 1034 + N<sub>2</sub>/H<sub>2</sub>) was also analyzed. Figure 2 and Figure 3 present the data summary of the experiment and effective lifetimes vs. minority-carrier density for n-type and p-type silicon wafers analyzed in this study. In Table 1 the effective lifetimes measured at a minority-carrier density of 10<sup>15</sup>cm<sup>-3</sup> are compared for all analyzed samples.

Effective lifetimes of 61 μs and 55 μs were measured at a minority-carrier density of 10<sup>15</sup>cm<sup>-3</sup> for n-type Si wafers with coatings of thermal oxide grown at 1050 °C in CVD 1033 and CVD 1034 systems, respectively (Figure 2, Table 1). A forming gas anneal after dry oxide growth was able to further improve lifetime (89 μs). The measurements done on the n-type Si wafers taken right out of the box (n-Si no treatment) and the new wafers taken right out of the box and dipped in diluted hydrofluoric acid (n-Si dHF) characterized significantly lower lifetimes of 4 μs and 6 μs, respectively. Similar results were also obtained for p-type silicon wafers at a minority-carrier density of 10<sup>15</sup> cm<sup>-3</sup> (Figure 3, Table 2). The lifetimes measured for thermal-oxides grown on p-type Si wafers in 1033 and 1034 systems were 50 μs and 30 μs, respectively. Uncoated by thermal oxide p-type wafers had lower lifetimes: 9 μs and 15 μs.

In conclusion, a high quality oxide layer on a silicon substrate can be formed in CVD Equipment 1034 and 1034 PRISM Cleanroom furnaces.



**Figure 1:** Sinton's lifetime tester.

Si wafer treatment	Effective Lifetime measured at a minority-carrier density of $10^{15}\text{cm}^{-3}$	
	n-type	p-type
No treatment (new from the box)	4 $\mu\text{s}$	9 $\mu\text{s}$
Diluted HF dip	6 $\mu\text{s}$	15 $\mu\text{s}$
RCA clan and oxidation in CVD 1033 furnace	61 $\mu\text{s}$	50 $\mu\text{s}$
RCA clan and oxidation in CVD 1034 furnace	55 $\mu\text{s}$	30 $\mu\text{s}$
RCA clan, oxidation in CVD 1034 furnace and $\text{N}_2\text{H}_2$ annealing	89 $\mu\text{s}$	NA

**Table 1:** Minority carrier recombination lifetimes measured at a minority-carrier density of  $10^{15}\text{cm}^{-3}$  for all analyzed samples.

**Figure 2:** Effective Lifetime vs. Minority-Carrier Density for n-type silicon wafers.

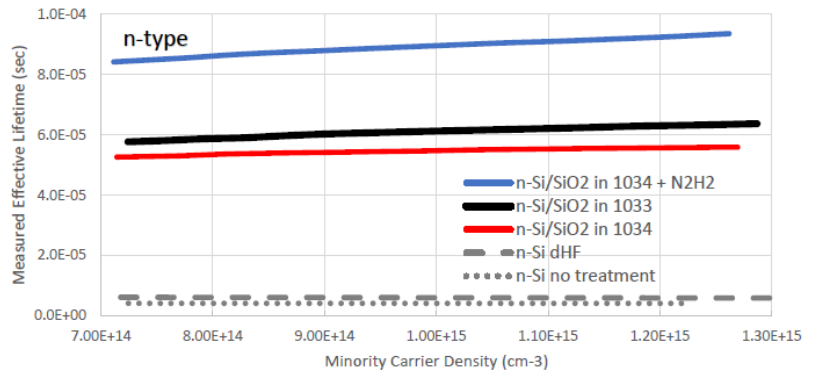
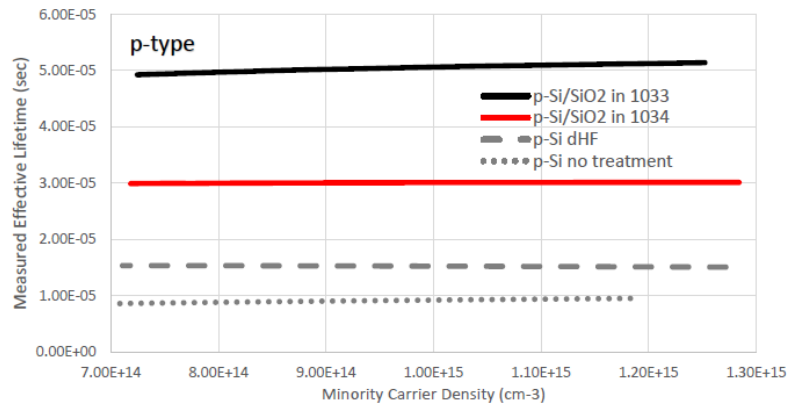


**Figure 3:** Effective Lifetime vs. Minority-Carrier Density for p-type silicon wafers.



**Acknowledgement:** Measurements performed using the Sinton's lifetime tester in Prof. James C. Sturm Laboratory. I am grateful to Alexander Berg from Prof. Sturm Lab for providing samples and helping in the minority carrier recombination lifetime measurement.

**CITATIONS**

[1] D. Schroder, "Carrier lifetimes in silicon", IEEE Transactions on Electron Devices, vol. 44, no. 1, pp. 160–170, Jan 1997.  
 [2] A. Sushobhan, "Crystalline-Silicon/Organic Heterojunctions for Solar Photovoltaics", PhD Thesis, Princeton University 2011.  
 [3] R. Sinton, A. Cuevas, and M. Stuckings, "Quasi-steady-state photoconductance, a new method for solar cell material and device characterization," in Photovoltaic Specialists Conference, 1996, Conference Record of the Twenty Fifth IEEE, 13-17 1996, pp. 457–460.

Researcher: **Brian Kraus**

Advisor: **Philip C. Eftthimion (AST)**

Sponsorship: **DOE & Lawrence Livermore National Laboratory**

Our group from the Princeton Plasma Physics Laboratory is using the PVD equipment in PRISM to prepare foils with buried layers for use as targets in short-pulse laser experiments. We are working towards a campaign at the Titan laser to map electron and ion temperature profiles of solids heated to extreme temperatures. The experiment would be the first measurement of ion temperature via x-ray lineshapes in a short-pulse plasma, a goal attainable with extreme resolving power of  $>9000$  (exceeding the resolution of previous Titan experiments by a factor of 40). By adapting decades of spectroscopy experience to the dense conditions generated by laser-solid interactions, we can simultaneously measure electron temperature, ion temperature, and plasma density from the spectra of different ion species. These comprehensive spectral measurements may be of wide interest as a vehicle for studying ion and electron dynamic separately; in our case, a comparison of the temperature profiles of each species will give information on the electron-ion equilibration time, which may be longer than the duration of emission in the presence of fast electrons. Thin tracer layers of mid-Z metals (Ti and Mn) will be buried under a tamper at depths

between 0 and 4 microns, and their He-like emission spectra will be recorded by two spectrometers with high resolving power. The proposed experiments are tailored to avoid opacity broadening, quantify Stark broadening, and limit axial gradients with the buried layer platform. With these influences subtracted, the Doppler width of a line remains a diagnostic of ion temperature. Line ratios from the same spectrum indicate the electron temperature. To ensure that buried layers remain contained, a multiple monochromatic imaging diagnostic will spectrally resolve pinhole images of the ablation plume, quantifying the spatial extent of highly-charged ions. The Titan laser is well-suited to these goals, as high intensity is needed to provide sufficient photon flux for high-resolution measurements. Results from these experiments on Titan will directly inform high-resolution spectroscopy diagnostics on NIF, such as the complementary time-resolved dHIRES spectrometer for helium-like Kr. Furthermore, a well-constrained ion temperature measured via spectroscopy could be applied to electron-ion coupling in a variety of platforms, which is of great interest for warm dense matter and high-energy-density (HED) experiments.

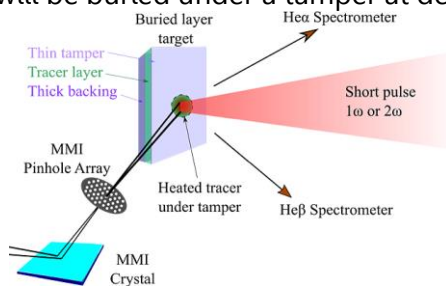


**Figure 1:** The experimental setup at JLF in Livermore, CA, where a PRISM-produced foil target is heated to extreme conditions with a short-pulse laser.

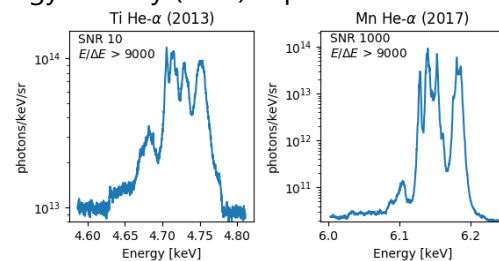


**Figure 2:** Two x-ray spectra from Ti and Mn layers deposited inside an Al foil. Each line corresponds to an atomic transition of  $Ti^{20+}$  and  $Mn^{23+}$ .

## CITATIONS

- The awarded time at Lawrence Livermore National Laboratory's Jupiter Laser Facility takes place over September-October 2018.

Researcher: **Emily Wei-Hsin Sun**  
 Advisor: **Ian C. Bourg (CEE)**  
 Sponsorship: **Princeton University**

Fundamental physical and chemical features governing multiphase flow in water-CO<sub>2</sub>-quartz nanopore systems directly impact the mobility and trapping of supercritical CO<sub>2</sub> injected into the subsurface as part of Carbon Capture and Sequestration (CCS). CCS is a potentially important approach to mitigating anthropogenic emissions, and depends largely on the capillary trapping capacities of subsurface formations. However, published experimental data on relevant properties, such as water-CO<sub>2</sub> contact angles (CA), vary widely. The fundamental basis of this variability remains poorly known, though surface contamination

and/or roughness is hypothesized to be a significant source. An important remaining knowledge gap in CCS is the influence of organic residues naturally present in sedimentary rocks on water-CO<sub>2</sub>-solid wetting and multiphase flow. We carry out a series of MD simulations to probe CAs in the presence of organic molecules. Using small organic molecules as proxies, we simulate a CO<sub>2</sub> bubble in a water-filled 6.6 nm quartz nanopore with varying fluid pressures. We find that high concentrations of organics may influence the water-CO<sub>2</sub> wetting behavior of quartz. We hope to supplement our MD findings with observations from microfluidic experiment.

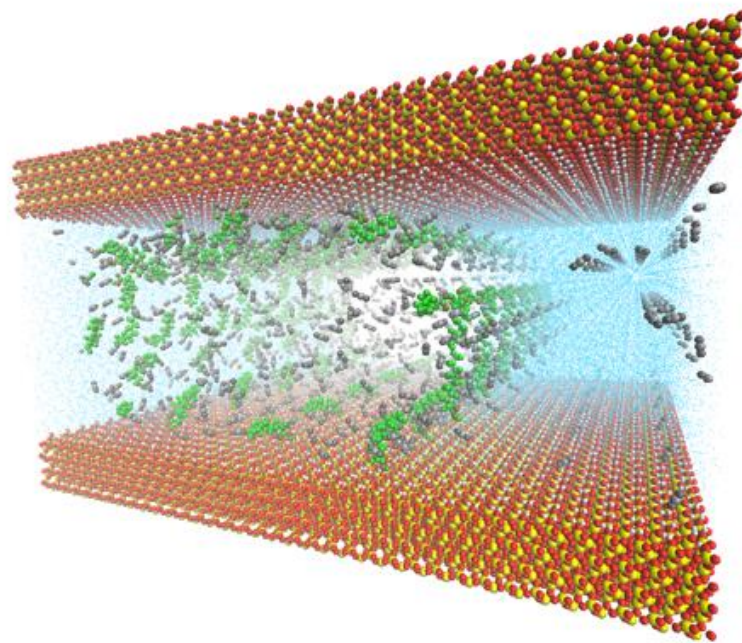


**Figure 1:** Molecular Dynamics simulation of a supercritical CO<sub>2</sub> bubble in water moving through a quartz nanopore.

## CITATIONS

- In preparation: Sun, E. W.-H., Bourg, I. C. (2018)

Researcher: **Sara Kacmoli**  
 Advisor: **Claire F. Gmachl (ELE)**  
 Sponsorship: **Industrial**

In conventional lithography, upon exposure and development, the photoresist is expected to be fully removed from the substrate. Steep sidewalls and rectangular cross-sections of the remaining resist pattern are desired in many applications. On the contrary, in grayscale lithography, complex photoresist profiles and topographies are created. They are achieved by varying the exposure dose according to a custom-made grayscale table. Creating profiles that match the needs of the user requires a process of optimization of many parameters of the direct laser lithography system, specifically Heidelberg DWL 66+. These parameters include intensity, focus, gray values in the design, filters, resist thickness etc. The gradient resist profiles are then transferred into other materials via various etching, deposition or other patterning processes. They are useful in creating innovative

micro structures to improve existing devices and systems.

For example, we study the incorporation of these grayscale features in semiconductor laser processing in order to tailor the gain and current profile of devices as desired. Another application is the development of multi-level retroreflector structures to be incorporated in long-path mid-infrared sensing systems for trace gases. In these systems, after light passes through a medium of interest, it is collected and analyzed. Retroreflector patterns transferred onto a flexible substrate will return the light back to the source for collection and analysis. In general, grayscale lithography finds widespread use in micro electro-mechanical systems (MEMS) research. The amount of flexibility and control that grayscale lithography provides is advantageous in any 3D structure construction.

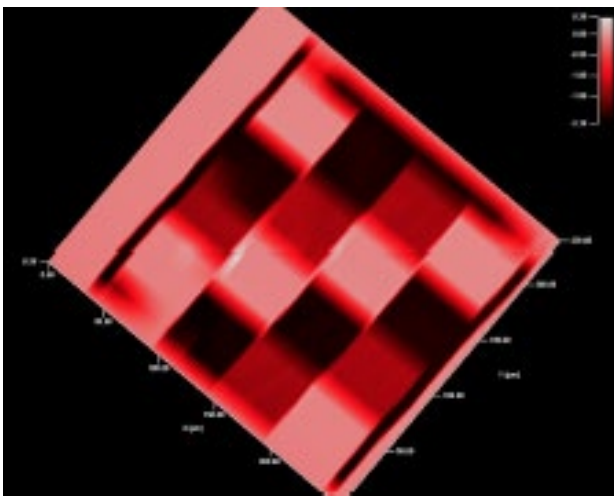


**Figure 1:** Surface scan of a retroreflector structure with multiple layers of photoresist. Because of ray optics, the light is always reflected back towards its source. Light, medium and dark red areas relate to resist plateaus with step heights of  $\sim 1\mu\text{m}$  between them.

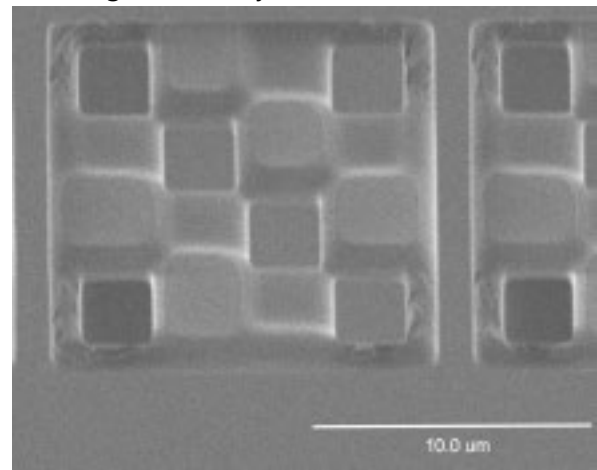


**Figure 2:** Scanning electron microscope (SEM) image of a scaled down retroreflector structure shown at a tilt. The step height between each step is  $\sim 0.8\mu\text{m}$ .

## CITATIONS

- New project-no publications yet

Researcher: **Yasin Kaya**

Advisor: **Claire F. Gmachl (ELE)**

Sponsorship: **Princeton University**

High-speed and sensitive broadband mid-infrared (MIR) detectors are critical for numerous defense and healthcare applications. Currently, mercury cadmium telluride (MCT) detectors are widely used for these applications but they suffer from growth related materials problems. We are investigating an alternative material system, InGaAs/InAlAs (III-V) and ZnCdSe/ZnCdMgSe (II-VI) as an alternative to MCT detectors in MIR region. These hybrid wafers are grown lattice match to InP by molecular beam epitaxy method. The hybrid wafer is process into mesa structures

by photo-lithography and wet etching techniques. Figure 1 shows a representative design of the hybrid detector. Performance of the hybrid detector is characterized by (Fourier Transform Infrared Spectroscopy) FTIR and calibrated black body sources. Figure 2 shows the spectral response of a representative hybrid detector centered at 5  $\mu\text{m}$  in the II-VI and 8  $\mu\text{m}$  in III-V material systems. Ongoing work continues to improve the performance and broad coverage of the hybrid detectors.

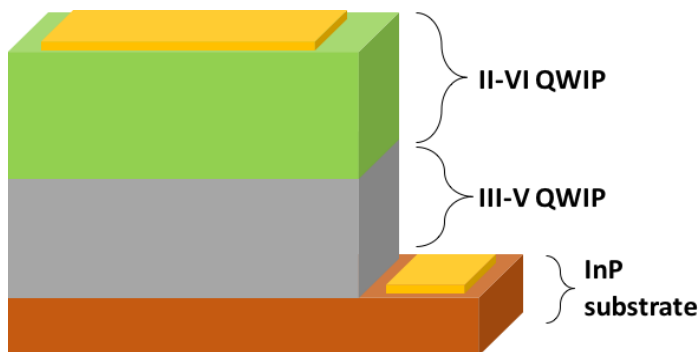


**Figure 1:** Hybrid detector design.

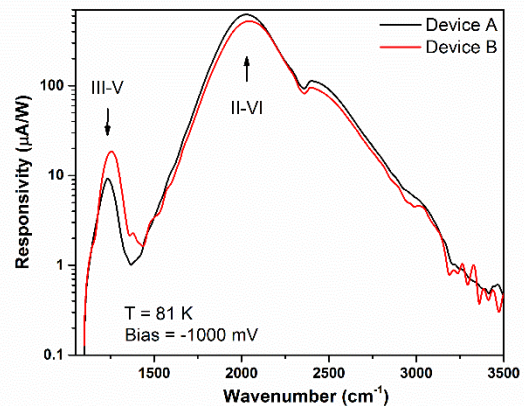


**Figure 2:** Responsivity vs wavenumber for two representative hybrid detectors.

## CITATIONS

- None

Researcher: **Ming Lyu**

Advisor: **Claire F. Gmachl (ELE)**

Sponsorship: **Princeton University**

Long wavelength infrared light sources have been of great interest for sensing and communication. For example, 16  $\mu\text{m}$  laser beams have been widely used for selective multiphoton dissociation of  $\text{UF}_6$  [1]. In addition, this wavelength range contains absorption peaks of benzene (14.8  $\mu\text{m}$ ) and some of its derivatives such as phenol (14.5  $\mu\text{m}$ ) or aniline (19.8  $\mu\text{m}$ )[2]. Detection of these chemicals is essential for environmental monitoring because its hazards to human. However, commercial 16 $\mu\text{m}$  laser devices are not yet available. Since its invention in 1994[3], quantum cascade lasers (QCLs) have been a major source for mid-infrared light, but traditional InP-based QCLs have low performance at 16 $\mu\text{m}$  due to two-phonon absorption of InP in this region.

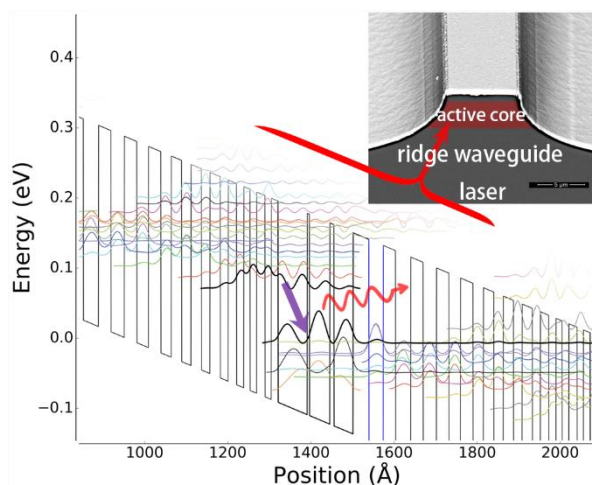


**Figure 1:** Band diagram of a 16  $\mu\text{m}$  GaAs/AlGaAs quantum cascade laser

GaAs/AlGaAs heterostructure is widely used for semiconductor devices and in the THz QCLs but is not yet widely used for higher frequency like 16  $\mu\text{m}$  (19THz)[4]. We are exploring this material to achieve much-needed 16 $\mu\text{m}$  laser device. Figure 1 shows the band diagram of our GaAs/AlGaAs QC structure, where electrons transit from upper to lower state and emit photons, and then are injected to the next upper state. Figure 2 shows the partial cross-section of an etched mesa, which used to calibrate electrical and optical properties of the QC structure. The QC material is grown by molecular beam epitaxy (MBE) in Prof. Loren Pfeiffer's group. We use the cleanroom primarily for photo-lithography, scanning electron microscope imaging, etching and metal deposition.

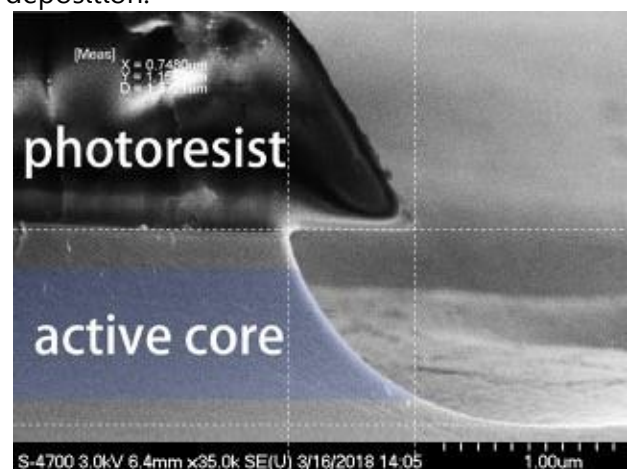


**Figure 2:** Scanning electron microscope cross-section image of an etched GaAs/AlGaAs mesa

## CITATIONS

- [1] Y. Okada et al. Journal of Molecular Structure, 410(Supplement C): 299 (1997)
- [2] SDBSWeb : <http://sdbweb.db.aist.go.jp> (National Institute of Advanced Industrial Science and Technology, 2007)
- [3] J. Faist et al. Science 264, 553 (1994)
- [4] Ulrich et al. Applied physics letters, 80(20), 3691-3693 (2002).
- M. Lyu et al, "Design and Optimization of 14-20 $\mu\text{m}$  Wavelength GaAs/AlGaAs Quantum Cascade Lasers", IR workshop (2017), Arizona



Researcher: **Yezhezi Zhang**  
 Advisor: **Claire F. Gmachl (ELE)**  
 Sponsorship: **NSF**

Multilayer plasmonic metamaterials exhibit anisotropic hyperbolic dispersion and enable non-magnetic negative refraction for potential applications such as superlensing and optical cloaking. However, since they mostly exhibit optical properties of metals, these materials can be lossy and are not suitable for those applications. To provide optical loss compensation, one may integrate an active gain-medium into the plasmonic metamaterials; however, many schemes such as dye-doped metamaterials degrade easily or are not electronically tunable. Moreover, there is no active metamaterial with loss compensation in

the mid-infrared (mid-IR) spectral region. In this work, we incorporated quantum cascade (QC) structures into plasmonic metamaterials and studied the optical responses of these metamaterials at zero bias by taking reflection and transmission measurements at varying incident angles. We have shown that the negative refractivity is preserved after the incorporation of QC structures, making it promising for active loss compensation. We are currently studying the effect of applied bias on the optical responses and working towards the realization of active mid-IR metamaterials.

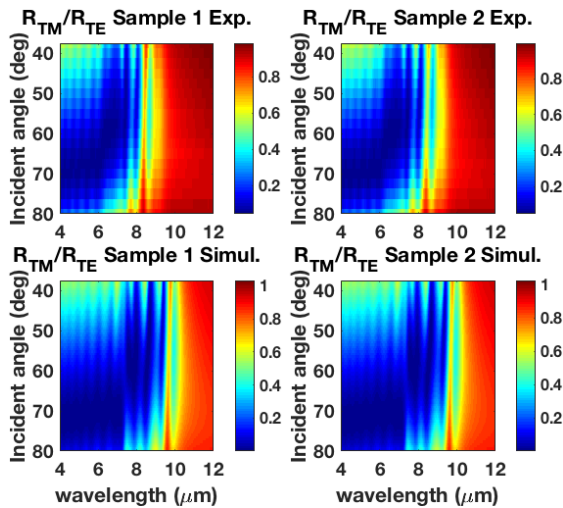


**Figure 1:** Experiment and (transfer matrix) simulation results of  $R_{TM}/R_{TE}$ . Left two: sample 1 with 40 repeats and no QC structure; right two: sample 2 with 40 repeats and QC structure A. It is observed that the incorporation of QC structures has no significant impact on the  $R_{TM}/R_{TE}$  ratios.

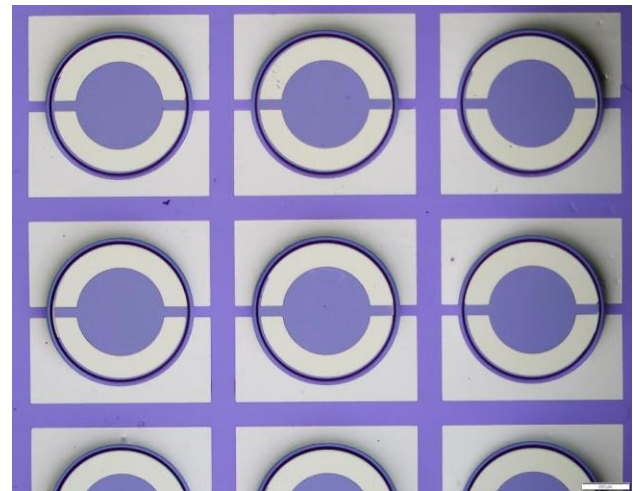


**Figure 2:** Split-ring contacts prepared for studying the effect of applied bias on the optical responses.

## CITATIONS

- Y. Zhang, W. Fan, A. Y. Song, D. L. Sivco, and C. F. Gmachl, "Optoelectronic Plasmonic Metamaterials with a Quantum Cascade Structure," in *Conference on Lasers and Electro-Optics*, OSA Technical Digest (online) (Optical Society of America, 2018), paper FM4J.5.
- Y. Zhang, W. Fan, A. Y. Song, D. L. Sivco, and C. F. Gmachl, "Optical Response of Plasmonic Metamaterials with Quantum Cascade Structure for Loss Compensation," in *SPIE Photonics West, 2018*.

Researcher: **Mattias Fitzpatrick**  
 Advisor: **Andrew A. Houck (ELE)**  
 Sponsorship: **NSF, DOE**

After close to two decades of research and development, superconducting circuits have emerged as a rich platform for both quantum computation and quantum simulation. Lattices of superconducting coplanar waveguide (CPW) resonators have been shown to produce artificial materials for microwave photons, where weak interactions can be introduced either via non-linear resonator materials or strong interactions via qubit-resonator coupling. Here, we introduce a technique using networks of CPW resonators to create a new class of materials

which constitute regular lattices in an effective hyperbolic space with constant negative curvature. We show numerical simulations of a class of hyperbolic analogs of the kagome lattice which show unusual densities of states with a spectrally-isolated degenerate flat band. We also present an experimental realization of one of these lattices, exhibiting the aforementioned band structure. This paper represents the first step towards on-chip quantum simulation of materials science and interacting particles in curved space.

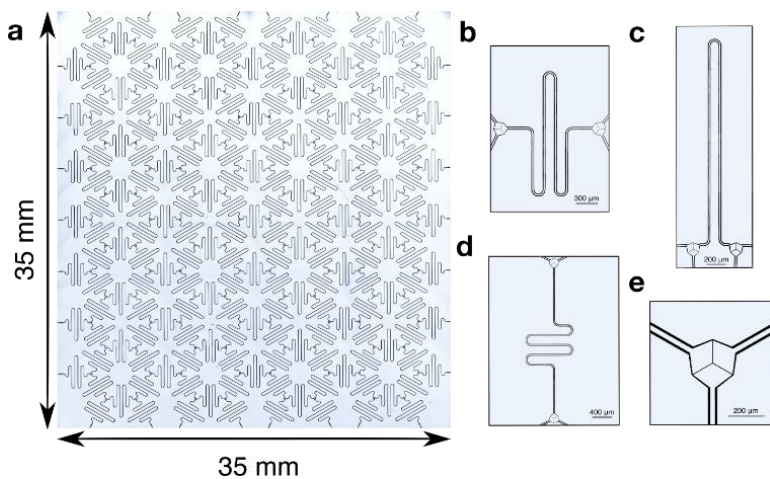
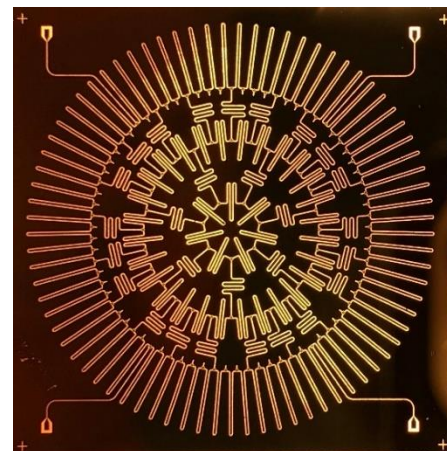


**Figure 1:** (a) Picture of a Euclidean lattice of CPW microwave resonators, modified from [15]. (b)-(d) Three mathematically identical resonators with different shapes but the same resonance frequencies and hopping rates. (e) Close-up of a capacitive coupler like the ones used in (a)-(d) to connect three resonators together. The effective hopping rate at this junction is set by the capacitance between the three arrow-shaped center pins.

**Figure 2:** Image of device fabricated in the cleanroom to study photons in hyperbolic space.



**CITATIONS**

- Alicia J. Kollar, Mattias Fitzpatrick, and Andrew A Houck, Hyperbolic Lattices in Circuit Quantum Electrodynamics, arXiv:1802.09549
- Mattias Fitzpatrick, Neereja M. Sundaresan, Andy C. Y. Li, Jens Koch, and Andrew A Houck, Observation of a Dissipative Phase Transitions in a One-Dimensional Circuit QED Lattice, Phys. Rev. X, 011016

Researcher: **Andras Gyenis**  
 Advisor: **Andrew A. Houck (ELE)**  
 Sponsorship: **ARO**

Disordered superconducting materials provide a new capability to implement novel circuit designs due to their high kinetic inductance. Here, we realize a fluxonium qubit in which a long NbTiN nanowire shunts a single Josephson junction. We explain the measured fluxonium energy spectrum with a nonperturbative theory accounting for the multimode structure of the device in a large frequency range. Making use of multiphoton Raman spectroscopy, we address

forbidden fluxonium transitions and observe multilevel Autler-Townes splitting. Finally, we measure lifetimes of several excited states ranging from  $T_1=620$  ns to  $T_1=20$   $\mu$ s by applying consecutive  $\pi$ -pulses between multiple fluxonium levels. Our measurements demonstrate that NbTiN is a suitable material for novel superconducting qubit designs.

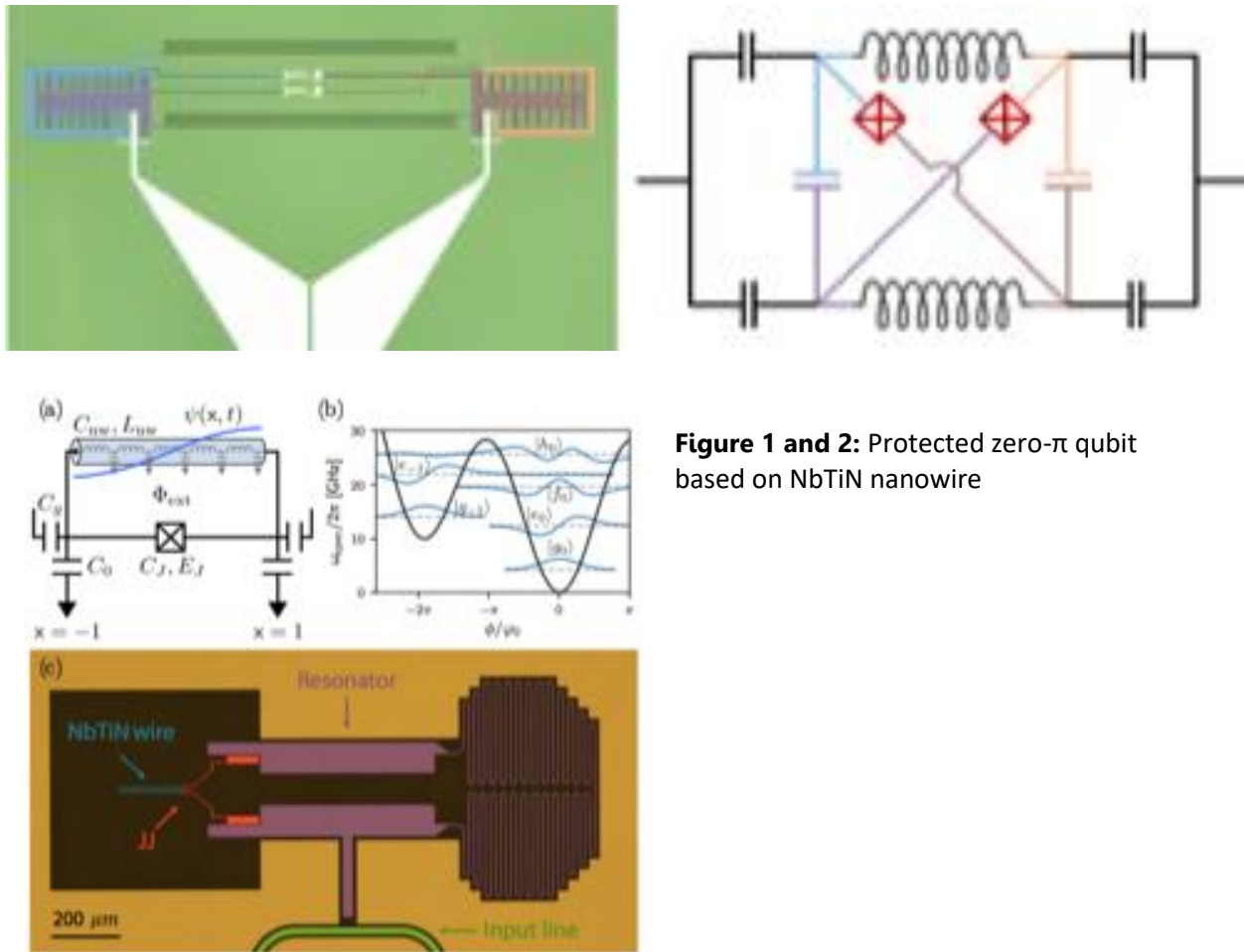


**Figure 1 and 2:** Protected zero- $\pi$  qubit based on NbTiN nanowire

**CITATIONS**

- arXiv:1805.00938

Researcher: **Thomas Hazard**  
 Advisor: **Andrew A. Houck (ELE)**  
 Sponsorship: **ARO**

Due to their high kinetic inductance, disordered superconducting materials provide a new capability to implement novel circuit designs. Here, we realize a fluxonium qubit consisting of an inductively shunted Josephson junction where the inductance is realized by a long NbTiN nanowire. We explain the measured fluxonium energy spectrum with a nonperturbative theory accounting for the multimode structure of the device in a large frequency range. Making use of multiphoton Raman spectroscopy, we address forbidden fluxonium transitions and observe multilevel Autler-Townes splitting. Finally, we

measure lifetimes of several excited states ranging from  $T_1 = 620$  ns to  $T_1 = 20$   $\mu$ , by applying consecutive  $\pi$  pulses between multiple fluxonium levels. Our measurements demonstrate that NbTiN is a promising material for superconducting qubit designs. The multimode theory developed here is an important step towards understanding large circuits beyond the lumped element approximation, such as the  $\pi$  qubit, where the distributed nature of the circuit elements is critical to device design.

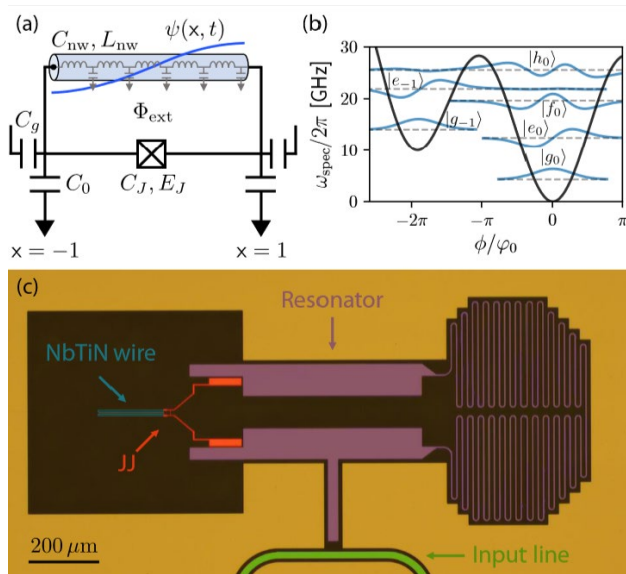


**Figure 1:** A simplified circuit diagram for the nanowire superinductance fluxonium qubit displaying the first antisymmetric standing wave nanowire mode in blue. A false colored optical image of the device with the NbTiN nanowire shown in blue, the single Josephson junction and gate capacitors in red, the readout resonator in purple and the input transmission line in green.

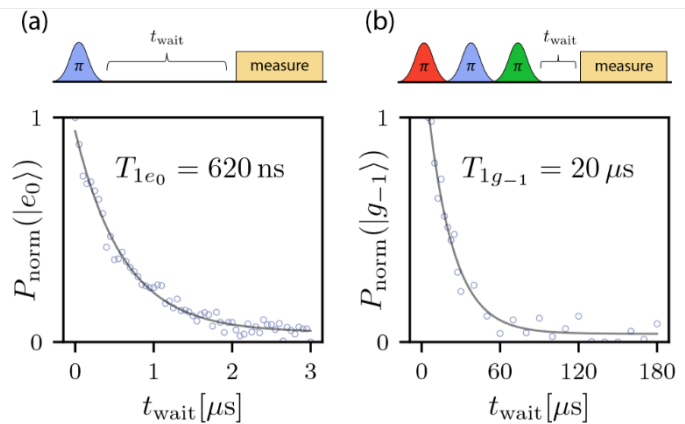


**Figure 2:**  $T_1$  measurements of the (a)  $e_0$  plasmon and (b)  $g_{-1}$  fluxon excited states. The populations are fit with a single exponential to extract the lifetime.

**CITATIONS**

- arXiv:1805.00938

Researcher: **Alicia Kollar, Jacob Bryon, Pranav Mundada**  
 Advisor: **Andrew A. Houck (ELE)**  
 Sponsorship: **NSF, MURI**

The field of circuit QED has emerged as a rich platform for both quantum computation and quantum simulation. The unique deformability of coplanar waveguide (CPW) microwave resonators enables realization of artificial photonic materials with novel lattice structures. We will present two classes of such examples. First, we will show that these techniques can be used to produce periodic lattices in a hyperbolic space of constant negative curvature. Second, we present examples of Euclidean lattices which exhibit gapped flat bands. Because CPW resonators are one-dimensional objects, the

lattices formed are naturally line graphs. We will show that line graphs lead naturally to flat bands and that criteria for when they are gapped can be derived from graph-theoretic techniques. The resulting gapped flat-band lattices are typically forbidden in standard atomic crystallography, but readily realizable in superconducting circuits. With the addition of high-kinetic-inductance materials or transmon qubits these systems will constitute a table-top simulator of interacting and quantum mechanical particles in strong curvature.

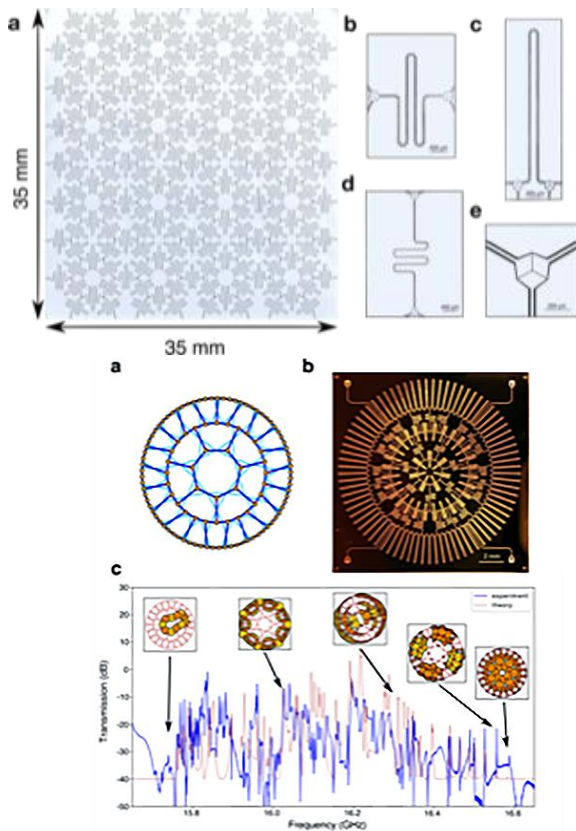


**Figure 1:** Circuit QED lattices. a, Picture of a Euclidean lattice of CPW microwave resonators. b-d, Three mathematically identical resonators with different shapes but the same resonance frequencies and hopping rates. e, Close-up of a capacitive coupler like the ones used in a-d to connect three resonators together. The effective hopping rate at this junction is set by the capacitance between the three arrow-shaped centre pins.

**Figure 2:** The heptagon-kagome device. a, Resonator layout (dark blue) and effective lattice (light blue) for a circuit that realizes two shells of the heptagon-kagome lattice. Orange circles indicate three-way capacitive couplers. b, Photograph of a physical device which realizes the layout and effective graphs in a. The device was fabricated in a 200 nm niobium film on a sapphire substrate and consists of 140 CPW resonators with fundamental resonance frequencies of 8 GHz, second harmonic frequencies of 16 GHz, and hopping rates of  $-147.4$  MHz at the second harmonic. Four additional CPW lines have been included at each corner of the device to couple microwaves into and out of the device for transmission measurements. Short stubs protruding inward from the outermost three-way couplers in the device are high frequency  $\lambda/4$  resonators which maintain a consistent loading of the sites in the outer ring, ensuring uniform on-site energies. c, Simulated and actual transmission ( $S_{21}$ ) for the device in b, demonstrating reasonable agreement between theory and experiment. Eigenstates at various frequencies are included as insets. The diameter of the circles indicates the magnitude of the wavefunction and the colour its sign. The flat-band state (far left) is included for reference although it does not show up prominently in transmission.

## CITATIONS

- <https://arxiv.org/pdf/1802.09549.pdf>
- <https://journals.aps.org/prx/pdf/10.1103/PhysRevX.7.011016>
- <https://arxiv.org/pdf/1801.10167.pdf>

Researcher: **Zhaoqi Leng**  
Advisor: **Andrew A. Houck (ELE)**  
Sponsorship: **IARPA**

As qubit coherence time sets a limit on the total time available for performing quantum gates, realizing high-fidelity, fast quantum gates is critical for enabling long-depth quantum circuits in the non-fault-tolerant regime and represents a path way towards fault tolerant quantum computation. Here, we will explore using black-

box optimization to tune up quantum gates for two transmon qubits coupled via a bus cavity. This optimization procedure does not require any knowledge of gradients derived from the system Hamiltonian, and thus it is ideal for automatic gate optimization on large quantum systems.

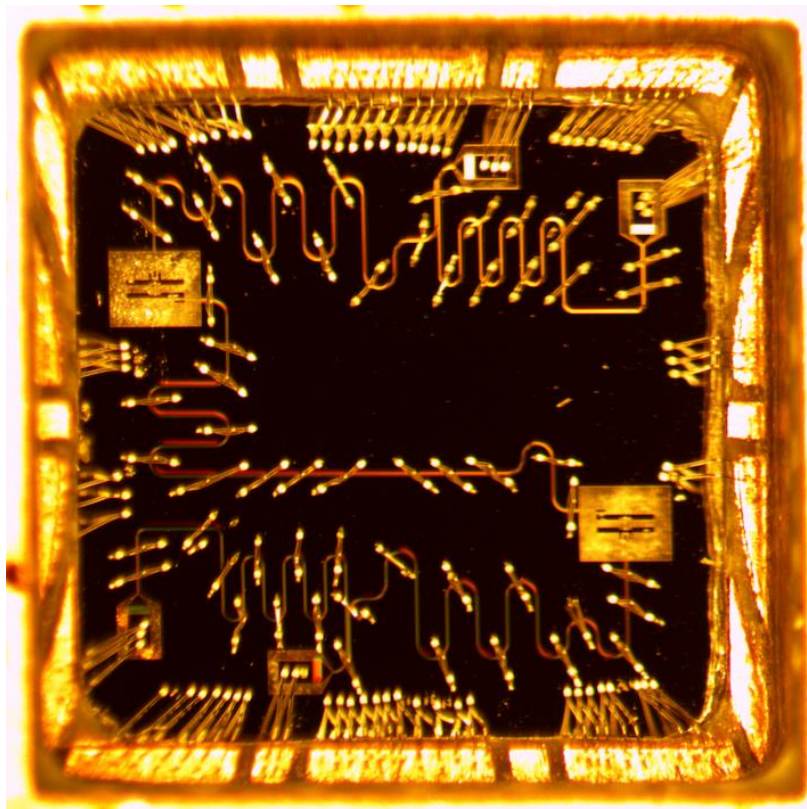


**Figure 1:** Device image. Two transmon qubits are coupled by a bus cavity

## CITATIONS

- <https://journals.aps.org/pr/abstract/10.1103/PhysRevA.93.060302>
- <https://journals.aps.org/pr/abstract/10.1103/PhysRevA.97.042348>

Researcher: **Alex Place**  
Advisor: **Andrew A. Houck (ELE)**  
Sponsorship: **ARO**

This project explores a novel material with an anomalously large kinetic inductance, granular aluminum. High kinetic inductance materials may be used to realize the next generation of qubits, including qubits with topological protection against decoherence. Further, granular aluminum behaves nonlinearly. Almost

every qubit requires a nonlinear element—most qubits use Josephson junctions to provide their nonlinearity, but the junctions introduce a significant amount of noise. This project will pursue several junctionless-qubit designs which will eliminate this common source of decoherence.

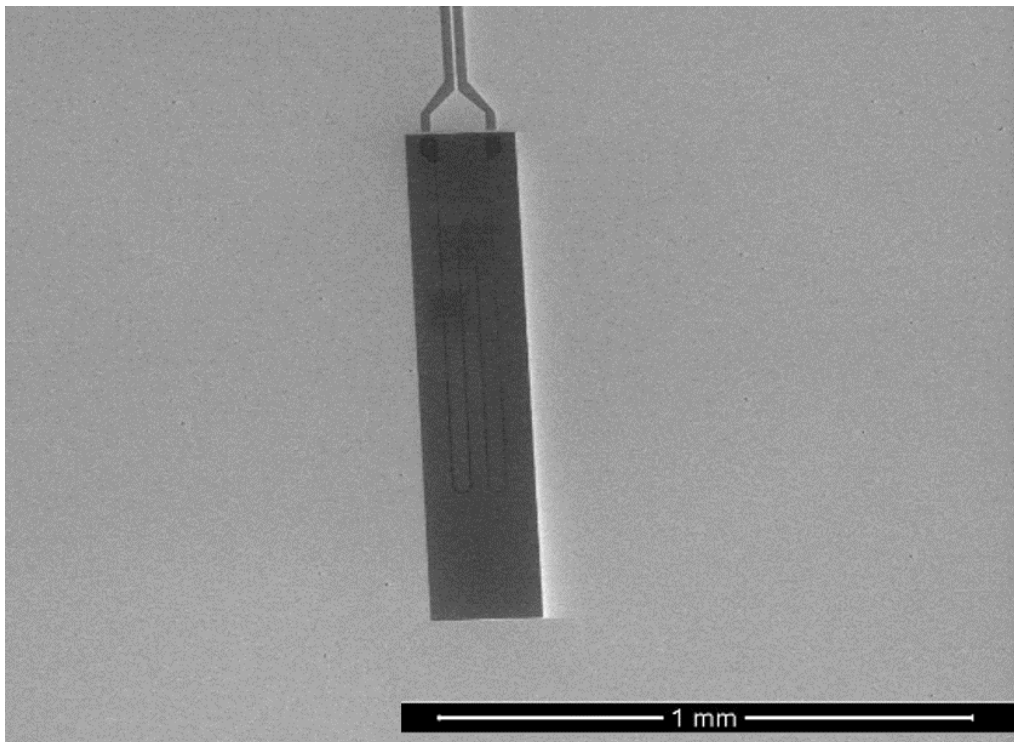


**Figure 1:** Scanning electron microscopy image of a helium fluxonium qubit with a granular Aluminum nanowire inductor.

## CITATIONS

- None

Researcher: **Anjali Premkumar**  
Advisor: **Andrew A. Houck (ELE)**  
Sponsorship: **ARO**

Quantum computing has the potential to aid faster computation and communication, solve time consuming brute force problems, facilitate quantum cryptography, and simulate physical quantum systems. Researchers across academia and industry are exploring superconducting qubits as a promising implementation of quantum computing. My PhD research in

Professor Andrew Houck's group will involve designing new qubits, fabricating them in the clean room, and testing them in a dilution refrigerator. Our devices consist of Aluminum Josephson junctions coupled to Niobium coplanar waveguides. The coplanar waveguides act as resonators which allow for nondestructive qubit state readout.

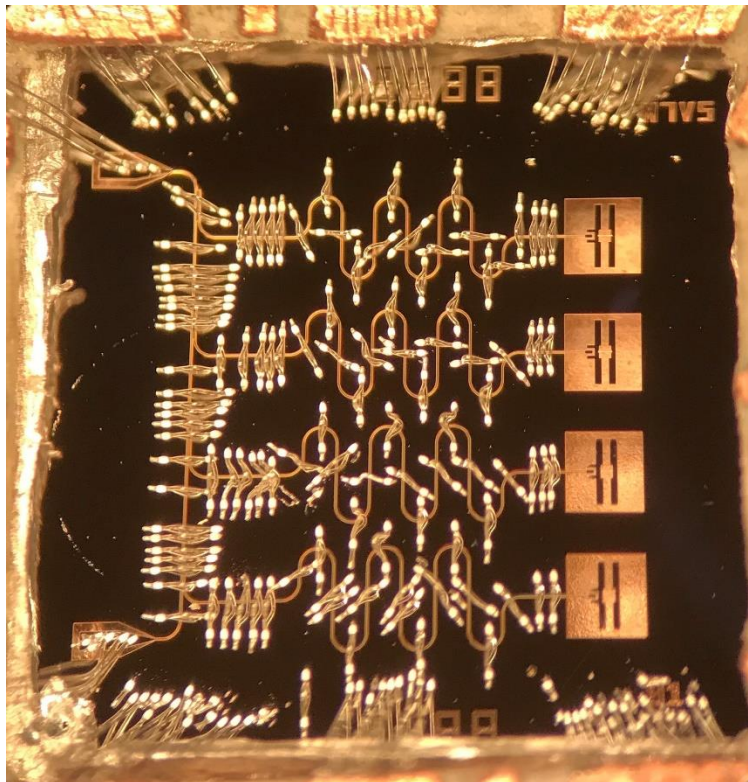


**Figure 1:** Transmon superconducting qubits in a circuit quantum electrodynamics architecture.

## CITATIONS

- N/A



Researcher: **Basil Smitham**  
 Advisor: **Andrew A. Houck (ELE)**  
 Sponsorship: **NSF**

Coupling qubits strongly to a photonic crystal gives rise to many exotic physical scenarios, beginning with single and multi-excitation qubit-photon dressed bound states comprising induced spatially localized photonic modes, centered around the qubits, and the qubits themselves. The localization of these states changes with qubit detuning from the band-edge, offering an avenue of in situ control of bound state interaction. In a previous experiment and paper in our lab by Neereja Sundaresan, we fabricated a device with two qubits coupled to a superconducting microwave photonic crystal and were able to realize tunable on-site and inter-bound state interactions. We observed a fourth-order two photon virtual process between

bound states indicating strong coupling between the photonic crystal and qubits. My research project focuses on extending this work by using specially calibrated drives to tune the spatial profile and scaling of the interactions between the bound states, with an eye towards creating chains of one-dimensional chains of bound states with tunable and potentially long-range interactions. The widely tunable, strong and robust interactions demonstrated by coupling superconducting qubits to photonic crystals are promising benchmarks towards creating larger, more complex systems of bound states and realizing quantum many-body models.

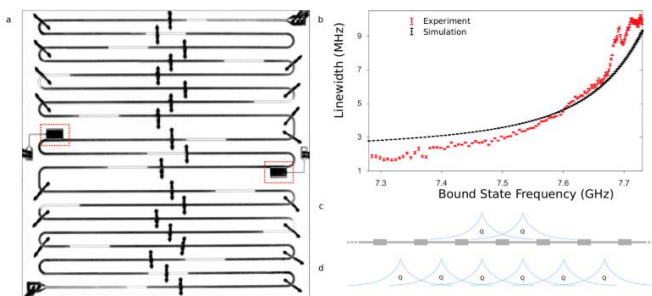


**Figure 1:** A platform for interacting dressed bound states. (a) A 16-site microwave photonic crystal is realized by alternating sections of high and low impedance coplanar waveguide. Two transmon qubits (multi-level, anharmonic energy ladder) are in neighboring unit cells in the middle of the device, centered in the high impedance sections for maximal coupling to the band edge at 7.8 GHz (all values presented in units of  $(2\pi)$  Hz. i.e.  $-\omega_{BE} = 7.8 (2\pi)$  GHz). For this experiment, the pass band (band gap) refers to states above (below) the band-edge frequency. Each qubit is individually tunable in frequency via a local flux bias line. (b) Bound state linewidth an indirect measure of localization varies with qubit frequency. The wide range over which photon localization can be tuned indicates the feasibility of realizing a chain of strongly interacting bound states. Experimentally measured and simulated linewidths are shown in red and black, respectively. (c) The interaction between bound states will be determined by overlap of their localized photonic envelopes with the qubits. (d) In a larger system, this localization-length-dependent interaction of the bound states would preserve the importance of the spatial organization of qubits in determining the many-body structure of the interactions.

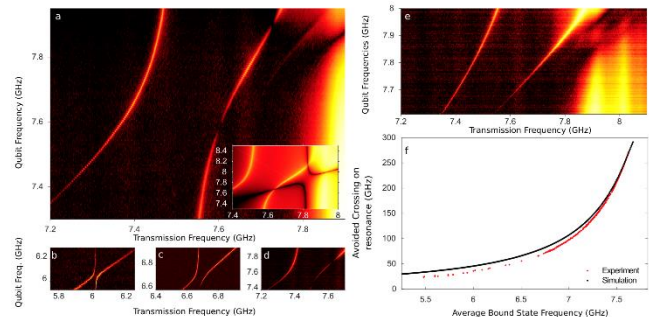


**Figure 2:** Interacting Bound States-Interaction between bound states is characterized by the avoided crossing seen in transmission while tuning one qubit (y-axis) through resonance with the other (fixed). (a) An avoided crossing of 240 MHz is observed when the fixed qubit is at 7.73 GHz. The two points where transmission amplitude of a bound state dims are understood as the bound state peak being resonant with the qubit frequency. a (inset) Hopping model simulation of the one-excitation manifold is consistent with experimental observation. The lamb shift in the hopping model originates from next-nearest neighbor interaction between coupled cavities. (b), (c), (d) Tunable bound state interaction strength is illustrated in example bound state avoided level crossings for a fixed qubit whose bare frequency is circa 6.125, 6.75, and 7.625 GHz. As qubits are detuned further from the band edge, bound states are more tightly localized, reducing overlap and thus reducing interaction. (e) Measuring bound state separation as qubits are simultaneously tuned, maintaining resonance, shows changing bound state interaction strength with frequency. (f) Bound state avoided crossing as a function of average bound state frequency. A steady reduction in interaction strength occurs with detuning from the band edge (moving deeper into the bandgap) due to increasing localization of the bound states. Hopping model simulation (black) captures this detuning-dependent behavior.

CITATIONS

- N. M. Sundaresan, R. Lundgren, G. Zhu, A. V. Gorshkov, and A. A. Houck, arXiv:1801.10167 (2018).

Researcher: **Andrei Vrajitoarea, Simon Bilodeau**  
 Advisor: **Andrew A. Houck (ELE)**  
 Sponsorship: **ARO/NSF**

Present quantum technologies based on superconducting circuits rely on the only non-dissipative and non-linear electronic element, the Josephson junction, for manipulating quantum information and engineering photon-photon interactions. Anharmonic Josephson circuits play a central role in implementing near term quantum computers yet suffer from limited coherence. Alternative architectures encode quantum information using microwave photons stored in superconducting resonators which have shown two orders of magnitude improvement in coherence. Since these quantum memories are harmonic, Josephson qubits are still needed for preparing and transferring quantum states. In this work we present a new paradigm in exploiting the Josephson non-linearity which would allow

logical operations to be performed directly on the oscillator Hilbert space while still retaining improved coherence. We implement a two cavity architecture with flux-tunable inductive coupling using a superconducting quantum interference device. The coupling can be parametrically modulated to selectively activate a three wave mixing process for generating anharmonicity by strong hybridization of the two photon state. We demonstrate direct Rabi driving and measure the Wigner function of arbitrary superpositions in the single photon manifold. Measured relaxation and coherence times are limited by the resonator intrinsic losses. This architectural shift in engineering nonlinear oscillators offers potential for designing quantum networks with improved coherence.

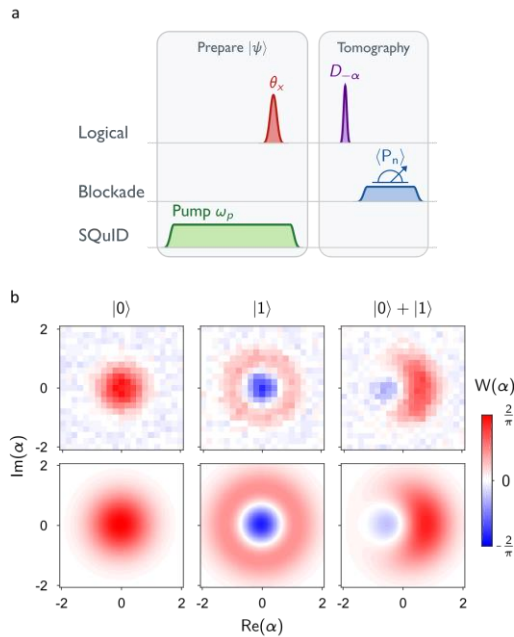


**Figure 1:** Characterizing the cavity state by measuring the Wigner function

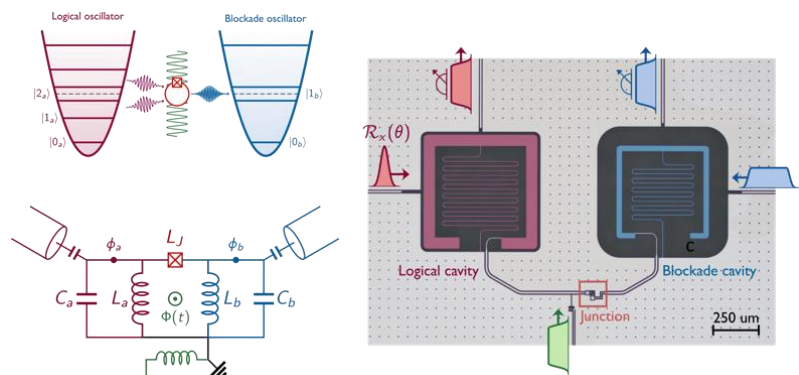


**Figure 2:** Device description and layout

**CITATIONS**

- Manuscript currently being written

Researcher: **Abraham Asfaw**  
 Advisor: **Stephen A. Lyon (ELE)**  
 Sponsorship: **NSF**

Superconducting devices have enabled tremendous improvements in the detection sensitivity of pulsed electron spin resonance. In our work, we take advantage of the kinetic inductance of disordered superconductors such as NbTiN to fabricate devices that extend the

applicability of superconducting resonators to various aspects of electron spin resonance, including multi-frequency experiments as well as long-coherence measurements in stabilized magnetic fields.

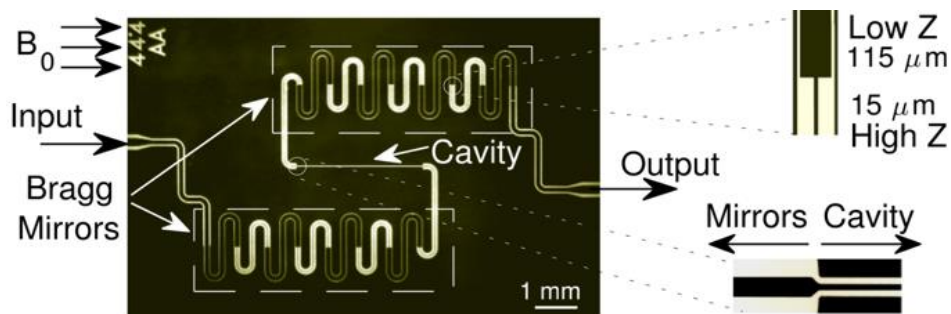


**Figure 1:** Rapidly frequency-tunable superconducting resonators for multi-frequency pulsed electron spin resonance. The devices are fabricated from 20 nm thick NbTiN grown on sapphire. The chips are patterned using photolithography (Heidelberg DWL66+) and etched by an SF6/Ar etch (STS Metals Etcher). The work is completed by dicing in an ADT Dicing Saw and wirebonding with the Questar autobonder.

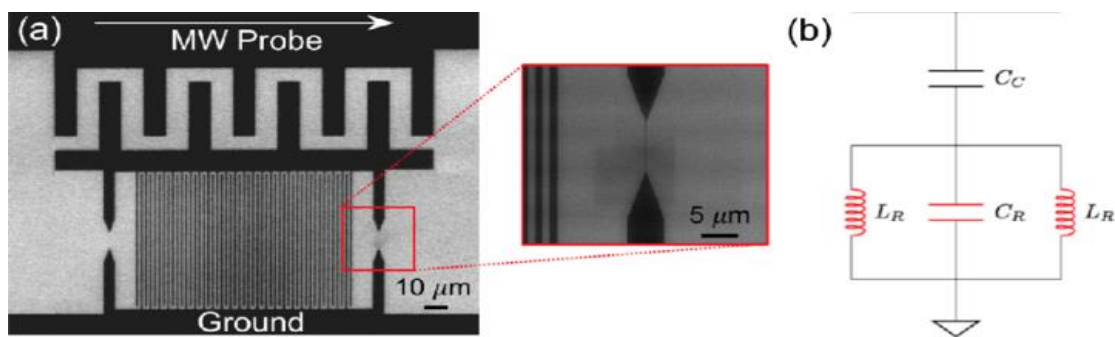


**Figure 2:** Superconducting Kinetic Inductance Field-Frequency Sensors (SKIFFS) for measuring small magnetic field fluctuations in moderate background magnetic fields fabricated from 7 nm thick NbTiN on sapphire using electron-beam lithography (Raith e-LiNE) followed by an SF6/Ar etch (STS Metals Etcher).

**CITATIONS**

- A. T. Asfaw, E. I. Kleinbaum, T. M. Hazard, A. Gyenis, A. A. Houck and S. A. Lyon, SKIFFS: Superconducting Kinetic Inductance Field- Frequency Sensors for Sensitive Magnetometry in Moderate Background Magnetic Fields, submitted. [arXiv:1807.09860]
- A. T. Asfaw, A. J. Sigillito, A. M. Tyryshkin, T. Schenkel and S. A. Lyon, Multi-frequency spin manipulation using rapidly tunable superconducting coplanar waveguide microresonators, Appl. Phys. Lett. 111, 032601 (2017).

Researcher: **Abraham Asfaw**  
 Advisor: **Stephen A. Lyon (ELE)**  
 Sponsorship: **NSF**

Electrons on helium constitute a promising platform for quantum computation. In our work, we are fabricating devices for control and manipulation of individual electrons on helium,

akin to the quantum dot devices used in solid-state systems. The devices require photolithography and electron-beam lithography in a multi-layer process.

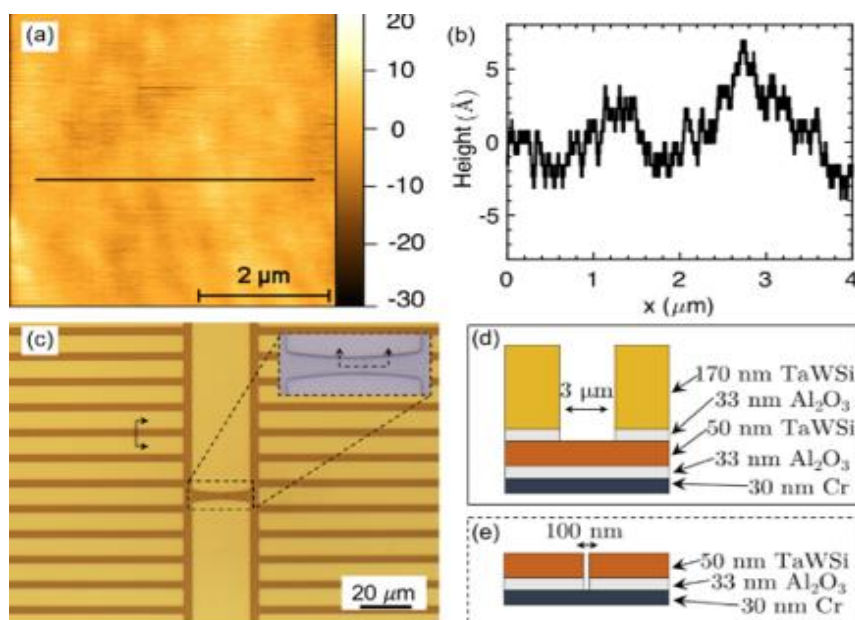


**Figure 1:** Devices for controlling electrons in 200 nm deep helium-filled microchannels. The work in MNFL combines several layers of deposition (Angstrom Metals Sputterer, Cambridge ALD), photolithography (Heidelberg DWL66+), and etching in either SF<sub>6</sub> or BCl<sub>3</sub> (STS Metals Etcher, Apex metals etcher).

## CITATIONS

- A. T. Asfaw, E. I. Kleinbaum and S. A. Lyon, Transport Measurements of Surface Electrons in 200 nm Deep Helium-Filled Microchannels Above Amorphous Metallic Electrodes, submitted. [arXiv:1807.00788]

Researcher: **Kyle Castoria**  
Advisor: **Stephen A. Lyon (ELE)**  
Sponsorship: **NSF**

This research focuses on studying electrons bound to the surface of superfluid helium. This system provides a very clean surface for the electrons with which we can study interesting 2DEG phenomena like the quantum melting of a Wigner crystal. Due to the isolation of the electrons from their environment, this system is

also a candidate physical implementation of a memory qubit for quantum computers. For our research, we must control the electrons via gates submerged below the liquid helium surface. The fabrication of these gates requires the use of the MFNL.

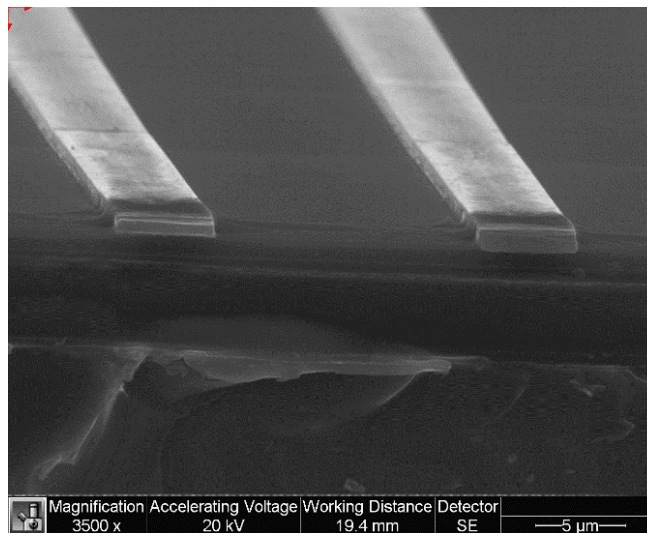


**Figure 1**

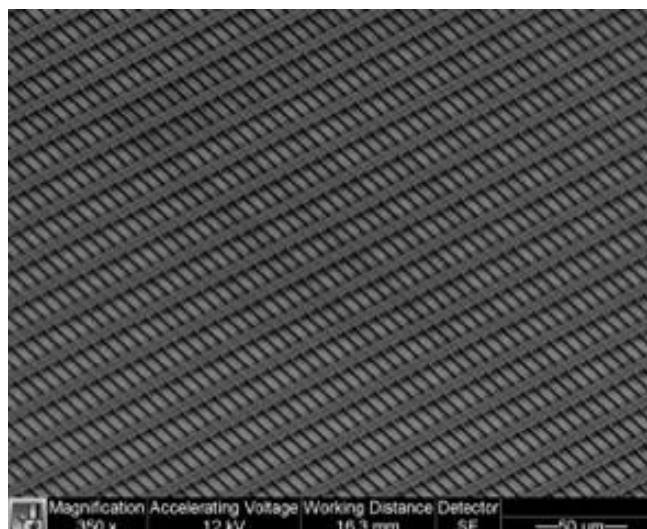


**Figure 2**

## CITATIONS

- S. A. Lyon, Phys. Rev. A: At., Mol., Opt. Phys., 2006, 74, 052338.

Researcher: **Jin-Sung Kim**  
 Advisor: **Stephen A. Lyon (ELE)**  
 Sponsorship: **NSF**

Spins confined in Metal-Oxide-Silicon (MOS) quantum dot devices are promising qubits in a quantum processor, demonstrating long coherence times, a large valley splitting, and coherent interactions with donor qubits. Furthermore, the mature fabrication infrastructure of the CMOS industry offers a tantalizing roadmap towards scaling to extremely large quantum systems on a single silicon chip. Despite the incredible advances in materials and fabrication developed by the CMOS industry and continued by the silicon quantum electronics community, many challenges remain in building a silicon quantum processor. One of the biggest challenges in this field is the presence of disorder at the Si/SiO<sub>2</sub> interface.

My work involves the development and characterization of a low-disorder MOS double quantum dot device fabricated in the PRISM cleanroom in conjunction with the Princeton QDNL cleanroom. To realize these low-disorder devices, I first developed a fabrication process in the PRISM cleanroom yielding the highest reported mobility thin-oxide MOSFET with

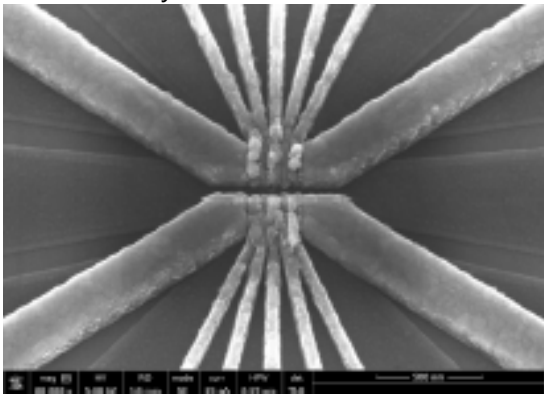


**Figure 1:** MOS Double quantum dot device. Nanolithography was performed in the QDNL. Silicon etching and aluminum oxide deposition was performed in the PRISM cleanroom.

critical densities (the lowest electron density required to form a conducting pathway) on par with the lowest critical densities measured in any MOS device. Leveraging these high-quality samples as an experimental platform, I have demonstrated with electron spin resonance measurements that standard annealing procedures are sufficient in passivating shallow electron traps, the most detrimental and least understood defect for quantum dot devices.

Finally, I demonstrate the performance of our quantum dot devices. I correlate for the first time mesoscopic defect measurements with ensemble defect densities, demonstrating a method of determining high-quality substrates for quantum dot devices. In addition, I show that our fabricated devices demonstrate a quiet charge noise environment and a valley splitting large enough to support high-fidelity spin operations. The culmination of this work defines a framework for understanding disorder in quantum devices and demonstrates a promising platform for scaling to larger quantum systems in MOS.



**Figure 2:** Large-area MOSFET for electron spin resonance measurements, fabricated in the PRISM cleanroom.

## CITATIONS

- Appl. Phys. Lett. 110, 123505 (2017)

Researcher: **Ryoto Sekine**  
 Advisor: **Stephen A. Lyon (ELE)**  
 Sponsorship: **Engineering Physics**

In the process of fabricating Si-SiO<sub>2</sub> quantum dots for quantum computing purposes, small traps in the potential well confining electrons have been observed. These hinder the ability to use these as reliable qubits, and ideally should be removed. We hypothesize that the shallow traps originate from the slight work function

variations between the grains in the polycrystalline metal gate. If this is the case, using amorphous metal gates which have much more uniform work functions should remove the shallow traps, and this is what we investigate under this grant.

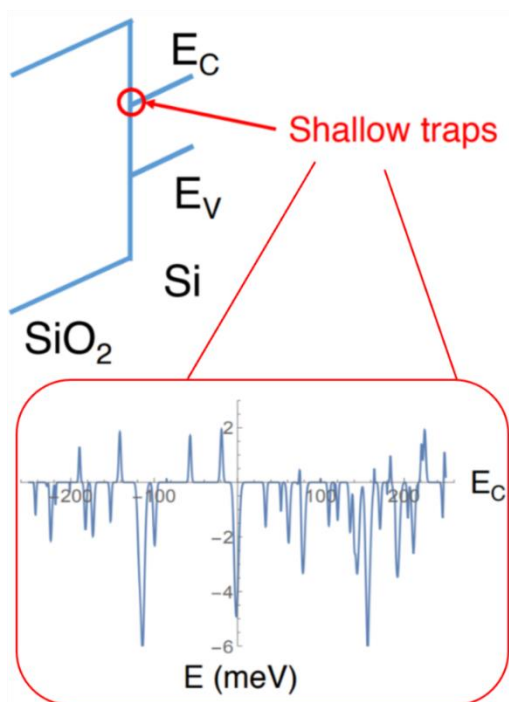


**Figure 1:** A depiction of the location and magnitude of the shallow traps that we are interested in.

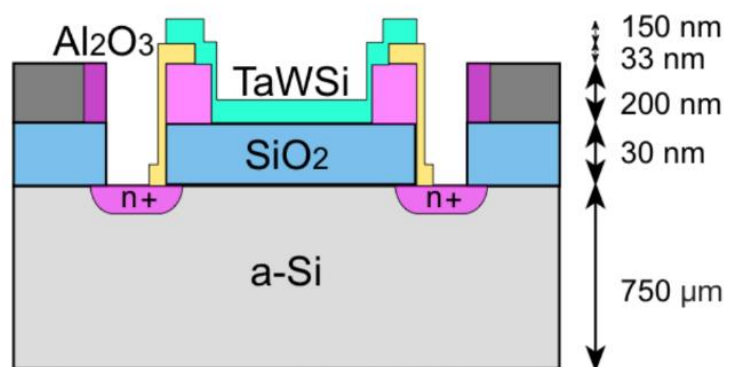


**Figure 2:** Schematic of a device fabricated with an amorphous metal (here TaWSi) gate.

## CITATIONS

- No publications thus far

Researcher: **Eric Blow**  
 Advisor: **Paul R. Prucnal (ELE)**  
 Sponsorship: **Industrial and NSF**

Integrated photonics is an emerging field which leverages the high bandwidths of optical signal processing to provide novel solutions to modern communication and computing obstacles. The Lightwave Communication Research Lab designs integrated photonic systems for neuromorphic processing and microwave applications. These

systems have unprecedented processing power compared to conventional technologies. The research group utilizes the PRISM facilities to fabricate test devices and packaging of large-scale photonic integrated circuits as shown below.

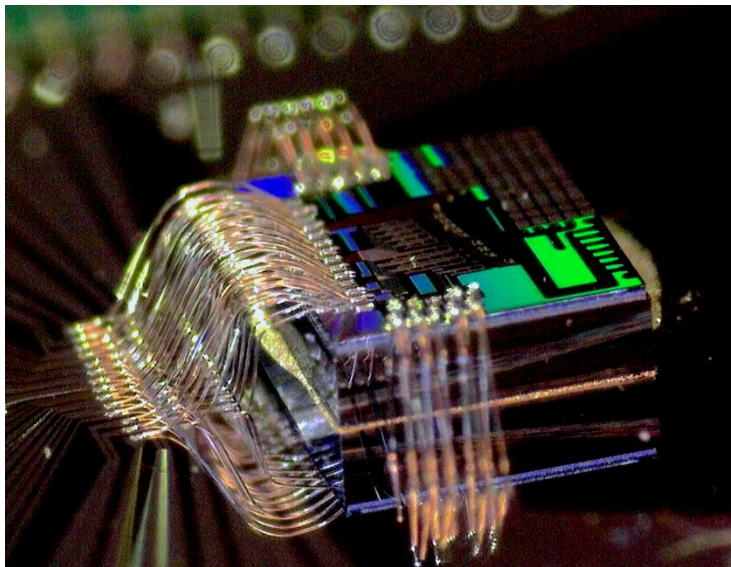


**Figure 1:** Photonic Integrated Neural Network Wirebonded to Si Interposer

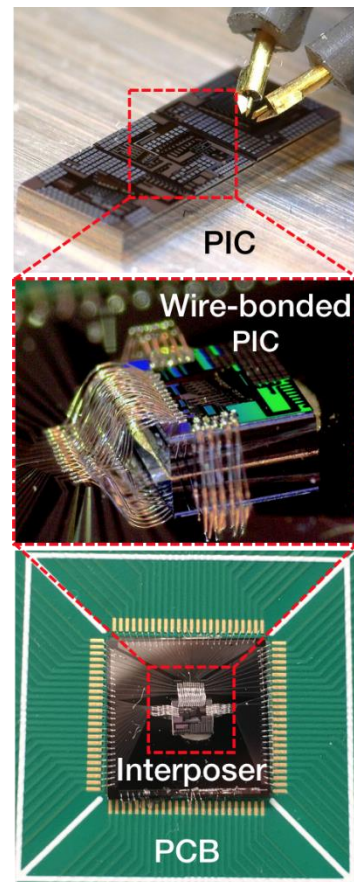


**Figure 2:** Lightwave Lab Packaging Approach to Large Scale Photonic Integrated Circuits

**CITATIONS**

- <http://ee.princeton.edu/research/prucnal/content/recent-publications>



Researcher: **William Gunnarsson**  
Advisor: **Barry P. Rand (ELE)**  
Sponsorship: **AFOSR**

Hybrid organic inorganic perovskites have emerged as promising gain media for tunable, solution-processed semiconductor lasers. However, continuous-wave operation has not been achieved so far. Here, we demonstrate that optically pumped continuous-wave lasing can be sustained above threshold excitation intensities of  $\sim 17$  kW/sq cm for over an hour in methylammonium lead iodide (MAPbI<sub>3</sub>) distributed feedback lasers that are maintained below the MAPbI<sub>3</sub> tetragonal-to-orthorhombic phase transition temperature of T 160 K. In contrast with the lasing death phenomenon that occurs for pure tetragonal-phase MAPbI<sub>3</sub> at T >

160 K, we find that continuous-wave gain becomes possible at T 100 K from tetragonal-phase inclusions that are photogenerated by the pump within the normally existing, larger-bandgap orthorhombic host matrix. In this mixed-phase system, the tetragonal inclusions function as carrier recombination sinks that reduce the transparency threshold, in loose analogy to inorganic semiconductor quantum wells, and may serve as a model for engineering improved perovskite gain media. (Taken from Y. Jia, et al. Nature Photonics, Volume 11, pages 784-788 (2017)).

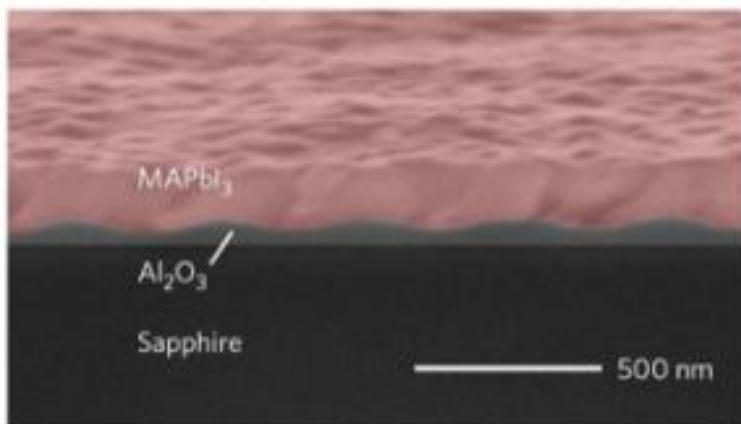


**Figure 1:** Cross-sectional scanning electron microscope (SEM) image of a MAPbI<sub>3</sub> film deposited on an alumina distributed feedback grating.

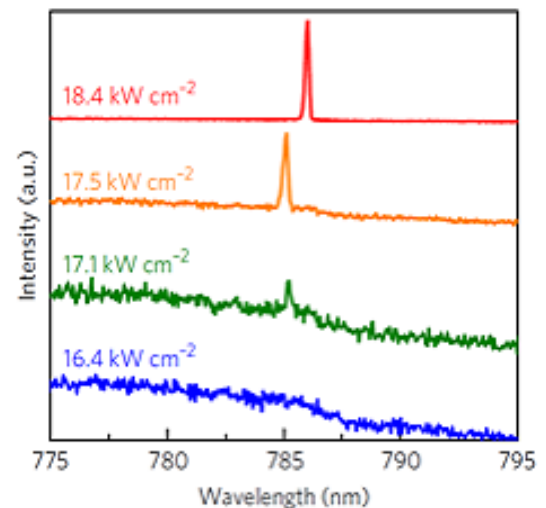


**Figure 2:** Emission spectra under optical pumping at the intensities listed above each spectrum.

## CITATIONS

- Y. Jia, et al. Nature Photonics, Volume 11, pages 784-788 (2017).

Researcher: **Kwangdong Roh**  
 Advisor: **Barry P. Rand (ELE)**  
 Sponsorship: **AFOSR**

Extensive research has established organic-inorganic hybrid perovskites as a promising material for optoelectronic device applications. Especially for lasers, many optically driven amplified spontaneous emission and lasing reports have been demonstrated across the near infrared to the green in various configurations (distributed feedback (DFB), distributed Bragg reflectors, photonic crystals, etc.) and pumping regimes (from pulsed to continuous-wave excitation) at low threshold, allowed by the tunable bandgap energy by controlling halide stoichiometry or material dimensionality. However, most reports lack red-emitting lasing action at room temperature due to undesirable halide phase separation that produce iodide-rich and bromide-rich domains in mixed-halide perovskites under intense illumination, resulting in a red gap problem where bandgap becomes pinned to the lower iodide-rich phase. We develop a red-emitting 2nd-order DFB laser operating at room temperature from solution-processed organic-inorganic hybrid perovskite

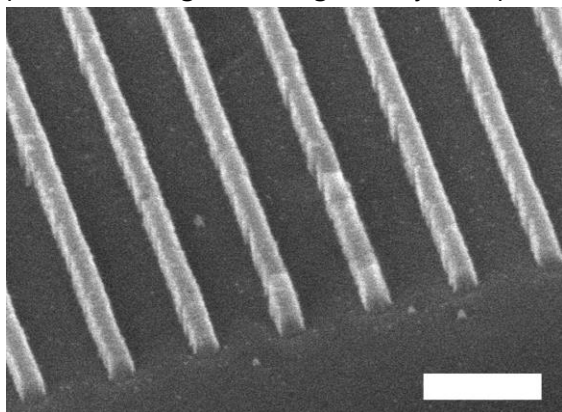


**Figure 1:** SEM image of a quartz grating with a pitch of 372 nm and a groove of 75 nm in angled view (scale bar is 500 nm)

thin films. Ultra-flat mixed-halide perovskite layers were prepared on a quartz grating which have been fabricated by electron beam lithography and plasma reactive-ion-etching processes to achieve single-mode surface-emitting laser emission for at least a few tens of minutes ( $\sim 10^6$  pulses) with a threshold of  $85 \mu\text{J}/\text{cm}^2$  and full-width-half-maximum of less than 1.5 nm under picosecond-pulsed optical excitation. We effectively suppress phase separation by properly choosing self-assembled long-chain organic ammonium halide additives to enable stable lasing action over a wide range of wavelengths near the red. Our results provide a significant step towards full-color visible laser device applications from cost-effective halide perovskite material system.

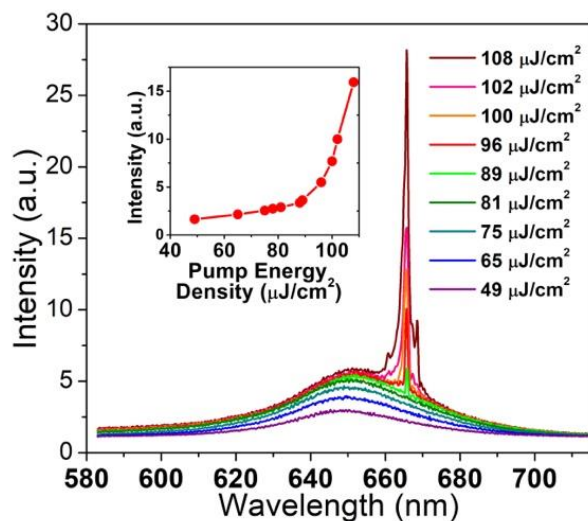


**Figure 2:** Emergence of single-mode DFB laser with increasing excitation intensity. (Inset) Emission intensity as a function of pump energy density showing a lasing threshold of  $85 \mu\text{J}/\text{cm}^2$ .

## CITATIONS

- Chen, Songtao, et al. "A photonic crystal laser from solution based organo-lead iodide perovskite thin films." *Acs Nano* 10.4 (2016): 3959-3967.
- Zhao, Lianfeng, et al. "In situ preparation of metal halide perovskite nanocrystal thin films for improved light-emitting devices." *ACS nano* 11.4 (2017): 3957-3964.

Researcher: **Zhuozhi Yao**  
 Advisor: **Barry P. Rand (ELE) David Wentzlaff (ELE)**  
 Sponsorship: **N/A**

Organic Thin-film Transistors (OTFTs) experienced substantial progress in recent decades. Choosing an appropriate circuit style is the key to improving an OTFT circuit's functionality and reliability. Conventionally, p-type only logic is widely implemented for OTFT circuits since the mobility of a p-type semiconductor is orders of magnitude larger than that of an n-type semiconductor.

Complementary logic suffers from its imbalance of mobility and complicated fabrication process. However, the recent development of n-type organic semiconductors changes the scenario since high-performance complementary-type OTFT circuits have been reported from different groups. Benchmarking various logic styles will therefore be helpful for circuit optimization.

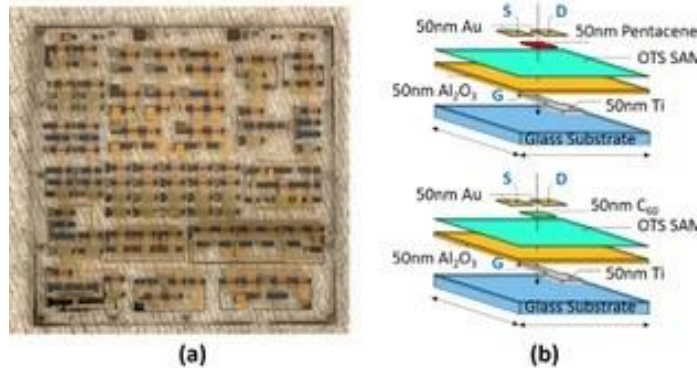


**Figure 1:** (a) Photograph of a 3×3 cm OTFT circuits sample (b) Schematic view of pentacene and C<sub>60</sub> OTFTs

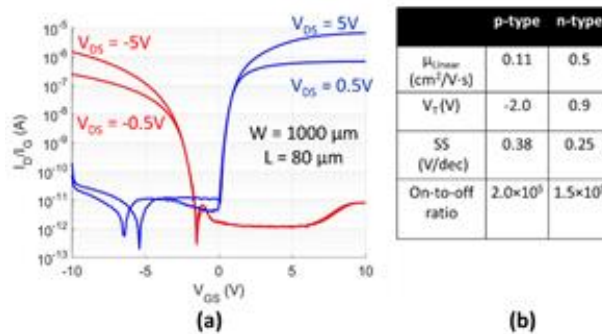


**Figure 2:** (a)  $I_D$ - $V_{GS}$  transfer characteristics and (b) DC parameters of pentacene and C<sub>60</sub> OTFTs

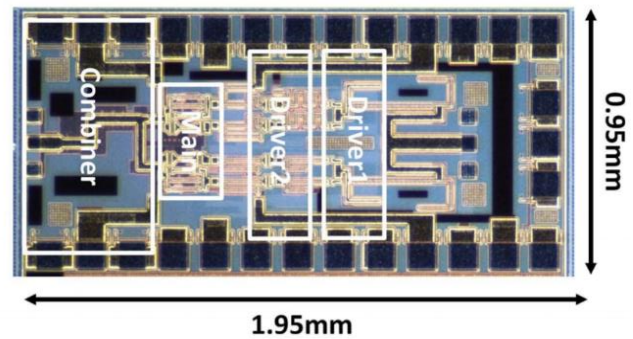
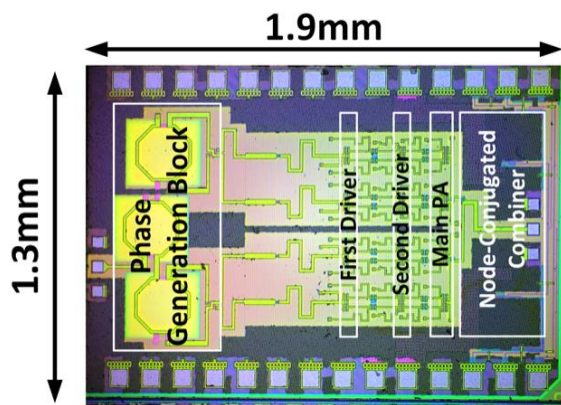
**CITATIONS**

- None

Researcher: **Chandrakanth Reddy Chappidi**  
 Advisor: **Kaushik Sengupta (ELE)**  
 Sponsorship: **NSF, ONR, MURI (AFOSR)**

The electromagnetic spectrum between 30-300 GHz, called as the millimeter-Wave will serve as the future spectrum for wireless connectivity and sensing. This opens up a future spectrum orders of magnitude larger than we have ever had access to and requires fundamentally new architectures and signal processing to be able to use this efficiently. This work proposes the concept of programmable universal mmWave front-ends. Dynamic frequency reconfiguration while ensuring high spectral can become key towards optimal utilization of spectral resources for future cognitive radios. This is extremely

challenging to achieve simultaneously with high energy efficiency and spectral efficiency. In this work, we present a mm-Wave transmitter architecture based on a generalized multi-port load-pulling approach to enable simultaneously broadband and back-off efficiency. As a proof of concept, scalable, broadband transmitter architectures are proposed in CMOS and SiGe processes. The prototype PA chips work across record bandwidths and record efficiencies across 30-55GHz with Psat of 23.7dBm at peak PAE of 27.7% in 0.13 m SiGe process, and with peak Psat of 19.3dBm and across 37-73GHz in 65nm bulk CMOS process."



**Figures 1 and 2:** Chip micrographs for mmWave programmable transmitters.

## CITATIONS

- C.Chappidi and K.Sengupta, "Broadband mm-Wave PAs with Simultaneous Back-off Efficiency enhancement across 30-55 GHz: A Multi-port Network Synthesis Approach," IEEE J. Solid-State Circuits (JSSC), Sept. 2018.
- Chandrakanth Chappidi and Kaushik Sengupta, "A Digitally Reconfigurable PA Architecture with Simultaneous Frequency and Back-off Programmability," IEEE RFIC, Jun. 2017.
- Chandrakanth Chappidi and Kaushik Sengupta, "A W-Band SiGe Power Amplifier with Psat of 23 dBm and PAE of 16.8% at 95GHz" IMS, Jun. 2017.
- Chandrakanth R.Chappidi and Kaushik Sengupta, "Globally Optimal Matching Networks with Lossy Passives and Efficiency Bounds," IEEE Transactions on Circuits and Systems-I, Sept. 2017.
- C.Chappidi and K.Sengupta, "A 37-73 GHz CMOS PA with Multi-port Dynamic Load Modulation and Broad-band Back-off Efficiency Enhancement for 5G Applications," submitted.

Researcher: **Xuyang Lu**  
 Advisor: **Kaushik Sengupta (ELE)**  
 Sponsorship: **AFOSR**

Future mmWave wireless devices for cellular communication, sensing and other applications will operate in an increasingly heterogeneous environment. Therefore, element-level pattern synthesis that can dynamically reconfigure to optimal patterns in the presence of near-field interferers. The concept is illustrated in Fig. 1. In this work, we present a dual-polarized 6-port antenna structure co-designed and integrated with a 6-port 70 GHz mmWave receiver architecture that can be configured to 192 element patterns (including polarization) using matching network with a 1-bit switchable MOM capacitor banks. The schematics of the LNA, mixer and IF amplifier are shown in Fig. 2. Fig. 3 shows the simulated reconfigurable patterns

showing beam shaping, element maxima and notch control. The receiver pattern of an edge port (Port 1) can be programmed to generate a two-beam pattern or single beam patterns pointing to  $+40^\circ$  or  $-30^\circ$  in the H plane. Fig. 4 shows the measurement setup and the chip micrograph. The chip is realized on a 65-nm CMOS process and measures 2 mm x 2 mm. The chip under test is bonded to a Rogers PCB where the LO power and IF is fed through PCB transmission lines into the chip through wire bonds. The wirelessly measured EIS at 70 GHz for 500MHz channel bandwidth and 25dB SNR is -52 dBm. A 100Msyms/sec QAM 16 link is demonstrated with EVM = 5.45%.

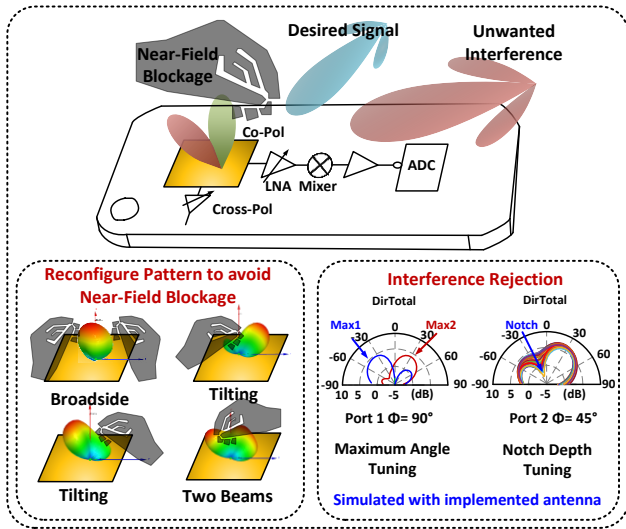


**Figure 1:** Element-level pattern shaping at mmWave frequencies can allow mitigation of complex electromagnetic environment including presence of strong near-field perturbations and passive rejection of directional interferers.

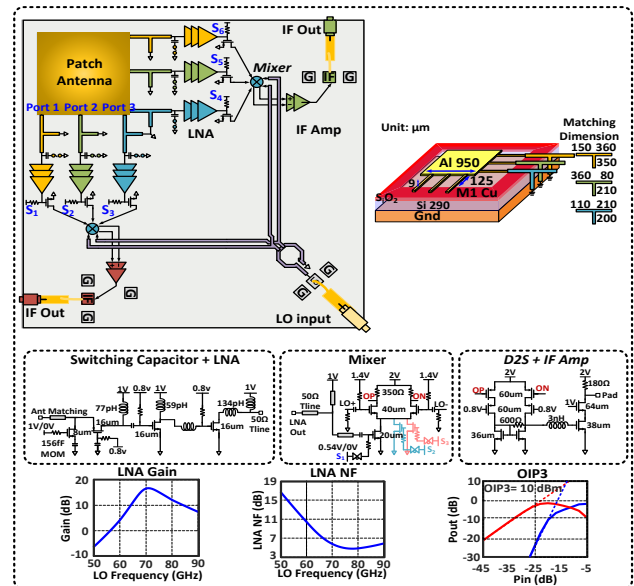


**Figure 2:** 6-port patch antenna with the reconfigurable matching network allowing pattern shaping and the simulated circuit performances.

**CITATIONS**

[1] Y. J. Sung, "Reconfigurable Patch Antenna for Polarization Diversity," IEEE Trans. on Antennas and Propag., vol. 56, no. 9, pp. 3053-3054, Sept. 2008.

Researcher: **Tushar Sharma**  
 Advisor: **Kaushik Sengupta (ELE)**  
 Sponsorship: **DARPA**

The mmwave reconfigurable power amplifiers are an important topic of research for the 5G communication system. We intend to work on new technologies which can support the demands of reconfigurable, broadband high efficiency transmitter architectures which can

support development of efficient and reliable communication systems. Under this project, we aim to tape out different chips using gallium nitride (GaN), Indium Phosphide (InP) technologies.

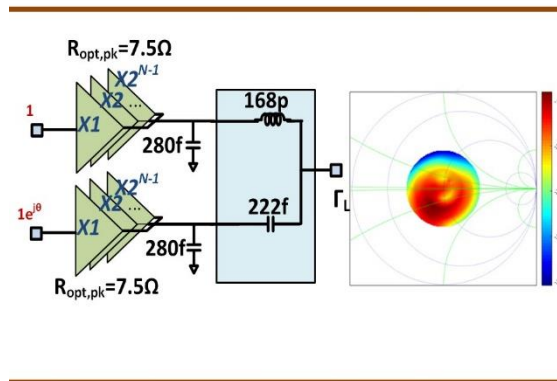


**Figure 1:** Reconfigurable Power Amplifier Architecture.

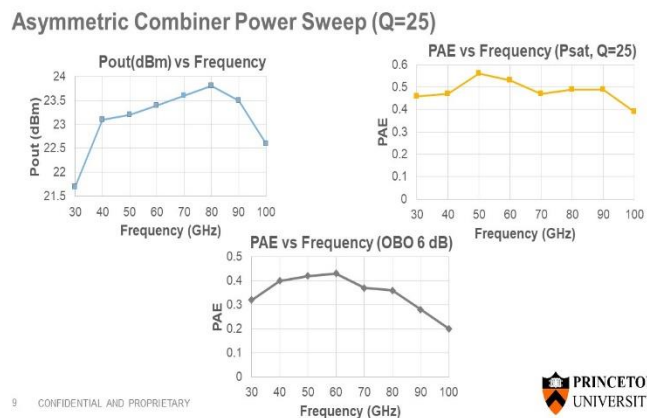


**Figure 2:** Simulated Indium Phosphide (InP) Reconfigurable Power Amplifiers from 30-100 GHz.

## CITATIONS

- C.R.Chappidi and K.Sengupta, "Frequency Reconfigurable mm-Wave Power Amplifier with Active Impedance Synthesis in an Asymmetrical Non-Isolated Combiner: Analysis and Design," IEEE J. Solid State Cir-cuits, vol. 52, no. 8, pp. 1990-2008, Aug. 2017
- C.R.Chappidi, X.Wu and K.Sengupta, "A digital mm-wave PA architecture with simultaneous frequency and back-off reconfigurability," IEEE RFICSymp. Dig. Papers, 2017, pp. 328-331.

Researcher: **TJ Smith, Dan Stanley, Anna Broome**  
 Advisor: **Kaushik Sengupta (ELE)**  
 Sponsorship: **ONR, EE Senior Thesis Fund, EE Slingshot Fund**

The THz spectrum, extending from 0.3–3.0 THz, wedged between RF and IR, has demonstrated game-changing potential in a wide array of applications including high-resolution radars and imaging, chemical spectroscopy, contraband detection, and ultra-fast wireless communication. However, the spectrum is popularly known as the THz gap due to the lack of technology in the spectrum, either for signal generation or detection, particularly ones that are low-cost and operable at room temperature. In this work, we create a single-chip, 100-pixel THz camera operating in the 2.5–3.5 THz frequency range to allow active video rate imaging (30 fps) with a QCL source. We use silicon IC technology, specifically a 65 nm industry-standard CMOS process, for low-cost,

room temperature operation. The chip consists of a 10x10 array of THz pixels, each of which contain the entire chain of detection including a rectangular patch antenna, rectifying detectors, a low noise amplifier, and read-out and multiplexing circuitry. The chip's digital circuitry and output amplifier are capable of over-clocking to 300,000 fps, allowing for post-sampling averaging to increase SNR by a factor of roughly 10x (20 dB). The chip achieves a simulated NEP in the range of nW/√Hz and a responsivity of 68 kV/W, allowing fast response and high integration, and enabling a wide range of novel applications in the THz range. The chip measures only 1 mm<sup>2</sup> in size.

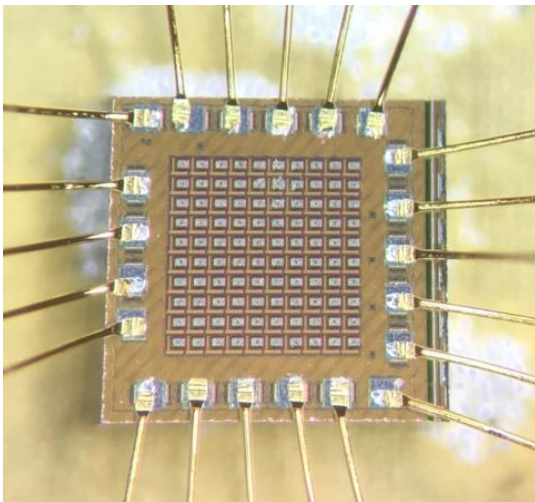


**Figure 1:** Micrograph of the wire-bonded image sensor

Technology	Array Size	Freq. (THz)	Max Res. (V/W)	Min NEP (pW/√Hz)	Image Mode	Ref.
65 nm CMOS	10 x 10	2.8	67.9k	32.9	Video (30 fps)	This work
180 nm CMOS	Single pixel	0.86	3.3k	106	Integrated ADC	[11]
65 nm CMOS	32 x 32	0.856	115k	1200	Video (25 fps)	[14]
130 nm CMOS	8 x 8	0.823	3.46k	12.6	Lock-in	[4]
SBD 130 nm CMOS	4 x 4	0.28	336	29	Lock-in	[15]

**Table 1:** Comparison of this work to similar works

**CITATIONS**

- None

Researcher: **Md. Shafayat Hossain**  
 Advisor: **Mansour Shayegan (ELE)**  
 Sponsorship: **NSF, DMR, DOE, MRSEC**

We propose an experimental investigation of electron interaction physics in high-quality, quantum-confined semiconductor structures. Our research include studies of the electronic transport properties at low temperatures and high magnetic fields where electron correlation phenomena dominate. The emphasis of the work will be on several systems, including high-quality two-dimensional electron systems (2DESs) confined to selectively-doped AlAs quantum wells (QWs), and electron and hole systems confined to wide or double QWs of GaAs. The 2DESs in AlAs have parameters that are very different from those of the standard 2DESs in GaAs: they have a much larger and anisotropic effective mass, a much larger effective g-factor, and they occupy multiple conduction band valleys. The electron or hole systems in wide or double GaAs QWs, on the other hand, possess an additional subband or layer degree of freedom. Both AlAs and bilayer systems provide crucial and important test-beds for new

many-body physics. Several exotic phases of these systems will be studied, including the fractional quantum Hall effect (FQHE), composite fermions, Wigner crystal, and stripe phases. As shown in Fig. 1, we pattern a surface superlattice of negative electron beam resist using electron beam lithography. Thanks to the difference between the thermal contraction coefficient of the resist and GaAs, a strain is generated during the cooldown of the sample. This strain is propagated to the 2DES via piezoelectric effect and gives rise to a minute density modulation. We applied this technique to study exotic phases in GaAs that has prospects in topological quantum computation.<sup>1</sup> We also implemented valley superlattice<sup>2</sup> in AlAs QWs which has applications in valleytronics. We show a representative AlAs sample glued on top of a piezo actuator in Fig. 2 which we use for our experiments on AlAs QWs such as in the realization of a valley superlattice<sup>2</sup>.

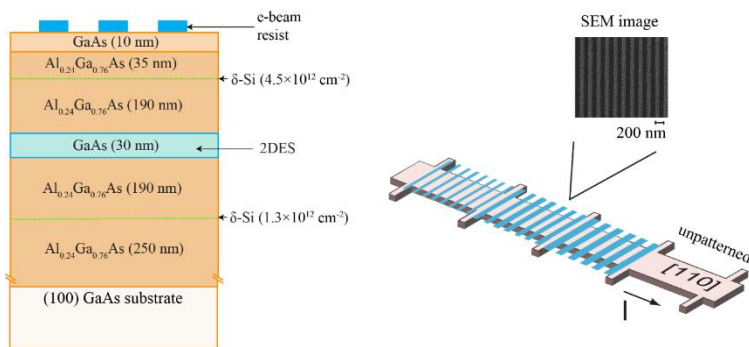


**Figure 1:** Structure of our GaAs QW (left). A Hall bar mesa is patterned using standard photolithography techniques. The superlattice (blue stripes) are patterned on the surface of the sample using electron beam lithography.

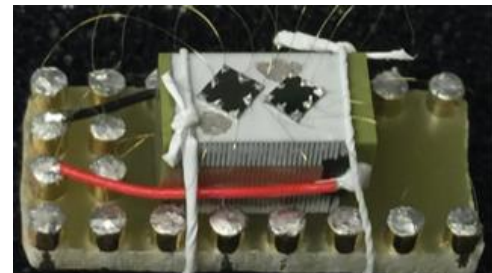


**Figure 2:** AlAs QW samples glued on top of a piezo actuator for applying in-plane strain which we use to tune the valley occupancy.

## CITATIONS

<sup>1</sup> Md Shafayat Hossain, Meng K. Ma, M. A. Mueed, L. N. Pfeiffer, K. W. West, K. W. Baldwin, and M. Shayegan, Direct Observation of Composite Fermions and Their Fully-Spin-Polarized Fermi Sea near  $\nu=5/2$ , Phys. Rev. Lett. 120, 256601 (2018).

<sup>2</sup> M. A. Mueed, Md Shafayat Hossain, I. Jo, L. N. Pfeiffer, K. W. West, K. W. Baldwin, and M. Shayegan, Realization of a Valley Superlattice, Phys. Rev. Lett. 121, 036802 (2018).



Researcher: **James Loy**

Advisor: **Mansour Shayegan (ELE)**

Sponsorship: **Moore**

In selectively-doped semiconductor structures, the electrons are spatially separated from the dopant atoms to reduce scattering by the ionized impurities. Thanks to the reduced disorder and scattering, such clean structures provide nearly ideal systems for studies of electron-electron interaction phenomena, especially at low temperatures and high magnetic fields where the thermal and kinetic energies of the electrons are quenched. The dominant electron interaction leads to various fascinating and exotic ground states that are often unexpected. Studies of such states are at the forefront of condensed matter research. They could lead to a better fundamental understanding of interaction phenomena, and they might help advance new concepts such as topological quantum computing. We experimentally investigate electron interaction physics in high-quality, quantum-confined semiconductor structures. The program will include studies of the electronic transport properties at low temperatures and high

magnetic fields where electron correlation phenomena dominate. The emphasis of the work will be on several systems, including high-quality two-dimensional electron systems (2DESs) confined to selectively-doped AlAs quantum wells (QWs), and electron and hole systems confined to wide or to double QWs of GaAs. The 2DESs in AlAs have parameters that are very different from those of the standard 2DESs in GaAs: they have a much larger and anisotropic effective mass, a much larger effective g-factor, and they occupy multiple conduction band valleys. The electron or hole systems in wide or double GaAs QWs, on the other hand, possess an additional subband or layer degree of freedom. Both AlAs and bilayer systems provide crucial and important test-beds for new many-body physics. Several exotic phases of these systems will be studied during the course of this project, including the fractional quantum Hall effect (FQHE), composite fermions, Wigner crystal, and stripe phases.

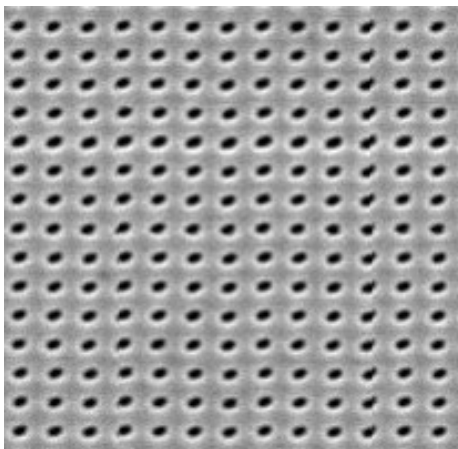


**Figure 1:** 2D Array of dots that produce a 2D periodic potential that interacts with our 2DES's.

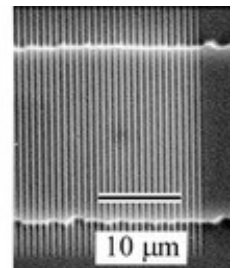
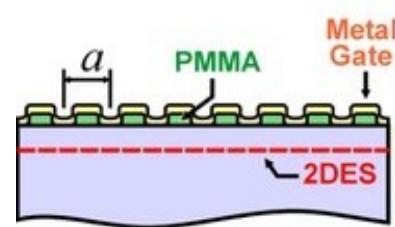


**Figure 2:** Sideview of sample showing a technique for 2DES density modulation via a topgate with variable voltage, with periodic PMMA spacers. SEM image shows the resulting periodic striping from the top of the device.

## CITATIONS

- Md. Shafayat Hossain, M. A. Mueed, Meng K. Ma, Y. J. Chung, L. N. Pfeiffer, K. W. West, K. W. Baldwin, and M. Shayegan, Anomalous coupling between magnetic and nematic orders in quantum Hall systems, *Phys. Rev. B* 98, 081109(R) (2018).
- M. A. Mueed, Md. Shafayat Hossain, I. Jo, L. N. Pfeiffer, K. W. West, K. W. Baldwin, and M. Shayegan, Realization of a Valley Superlattice, *Phys. Rev. Lett.* 121, 036802 (2018).

Researcher: **Meng Ma**  
 Advisor: **Mansour Shayegan (ELE)**  
 Sponsorship: **DOE, NSF & MRSEC**

In selectively-doped semiconductor structures, the electrons are spatially separated from the dopant atoms to reduce scattering by the ionized impurities. Thanks to the reduced disorder and scattering, such clean structures provide nearly ideal systems for studies of electron-electron interaction phenomena, especially at low temperatures and high magnetic fields where the thermal and kinetic energies of the electrons are quenched. The dominant electron interaction leads to various fascinating and exotic ground states that are often unexpected. Studies of such states are at the forefront of condensed matter research. They could lead to a better fundamental understanding of interaction phenomena, and they might help advance new concepts such as topological quantum computing. We propose an experimental investigation of electron interaction physics in high-quality, quantum-confined semiconductor structures. The program will include studies of the electronic transport properties at low temperatures and high

magnetic fields where electron correlation phenomena dominate. The emphasis of the work will be on several systems, including high-quality two-dimensional electron systems (2DESs) confined to selectively-doped AlAs quantum wells (QWs), and electron and hole systems confined to wide or to double QWs of GaAs. The 2DESs in AlAs have parameters that are very different from those of the standard 2DESs in GaAs: they have a much larger and anisotropic effective mass, a much larger effective g-factor, and they occupy multiple conduction band valleys. The electron or hole systems in wide or double GaAs QWs, on the other hand, possess an additional subband or layer degree of freedom. Both AlAs and bilayer systems provide crucial and important test-beds for new many-body physics. Several exotic phases of these systems will be studied during the course of this project, including the fractional quantum Hall effect (FQHE), composite fermions, Wigner crystal, and stripe phases.

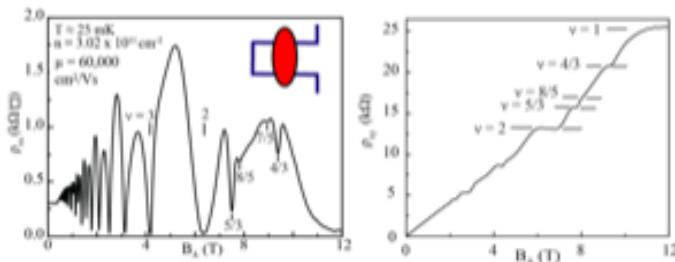


**Figure 1:** Longitudinal and Hall resistance transport measurement of a high quality AlAs 2DES sample with the out-of-plane conduction band valley occupied.

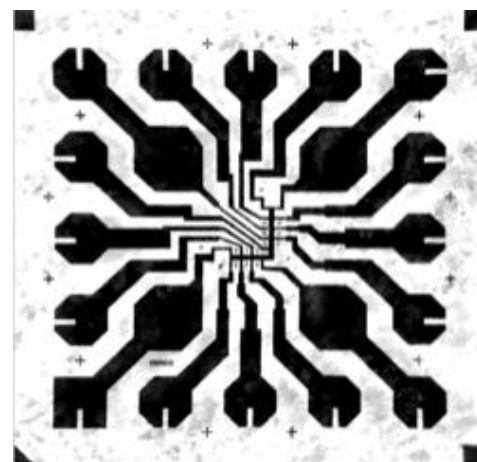


**Figure 2:** Image of a Hall bar geometry photomask fabricated here at the PRISM cleanroom used for making samples for transport measurement.

**CITATIONS**

- Phys. Rev. B **98**, 081109 (R)

Researcher: **Kevin Villegas Rosales**  
 Advisor: **Mansour Shayegan (ELE)**  
 Sponsorship: **NSF**

In a two-dimensional electron system (2DES) when a strong perpendicular field is applied, an anisotropic phase appears between filling factors 3 and 2, at tilted magnetic fields. We aim to study the anisotropic phase with a composite fermions sea. The structure of study is a double quantum well, grown by Molecular Beam Epitaxy.

In one of the quantum wells a stripe phase lives and in the other composite fermions. Specifically, our goal is to detect geometric resonances in the composite fermions layer due to an imposed periodicity of the anisotropic phase layer.

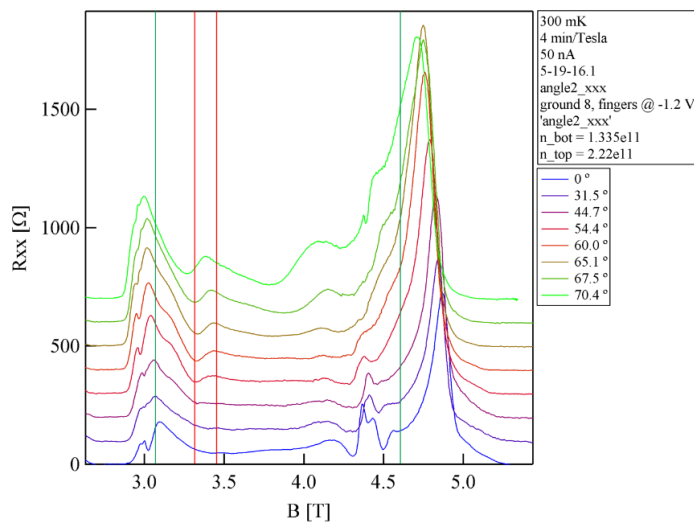
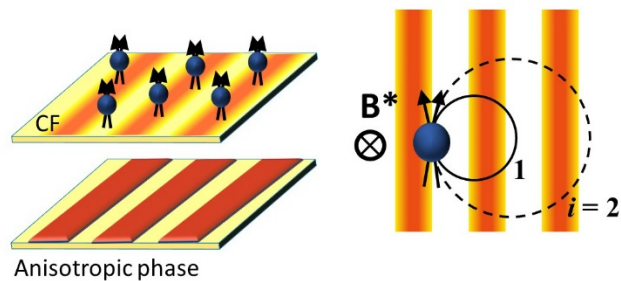


**Figure 1:** Angle-dependent magnetoresistance between integer filling factors 2 and 1 of the composite fermion layer. On the stripe phase layer an anisotropic phase should appear at high tilt angles. We could observe the increase in resistance in the flanks of filling factor 3/2. This could be indicative of an impose modulation from the stripe phase layer to the composite fermion layer.

**Figure 2:** Cartoon of the composite fermion layer next to the stripe phase layer. Because the stripe phase layer has a preferential axis of orientation it would act as a potential modulation to the composite fermion layer. We expect to detect geometric resonances in the composite fermions layer.



**CITATIONS**

- No publications yet

Researcher: **Levent Aygun**  
 Advisor: **James C. Sturm (ELE)**  
 Sponsorship: **Sturm Unrestricted**

Flexible hybrid electronics (FHE) is a technology that enables expansive sensor arrays over a large area (e.g.  $10\text{ m}^2$ ) on flexible substrates. They can interact/cover systems such as people and large physical infrastructure (e.g. bridges, vehicles). For the direct sensor interfacing, initial signal processing, and energy harvesting, an emerging route towards implementing electronics on large flexible surfaces is based on ZnO semiconductor thin films, with the ZnO layer deposited by plasma-enhanced atomic layer deposition (PEALD) on glass and plastic. An attractive approach is to build these separate functions (based on different materials) on different flexible sheets, and

lamine them together into a final system by using near-field inductive non-contact links to send signals and power between the different sheets. This method avoids metal-metal contacts between the sheets but requires high frequency diodes for demodulating signals from the AC carrier since the power transfer performance of the inductive interface improves with increasing frequency. We demonstrated a half wave rectifier (HWR) based on Au/ZnO Schottky diodes. with measured cutoff frequency ( $f_c=1/(2\pi R_s C_D)$ ,  $R_s$  and  $C_D$  are the series resistance and depletion capacitance) of 700 MHz (highest reported  $f_c$  for a ZnO based diode).

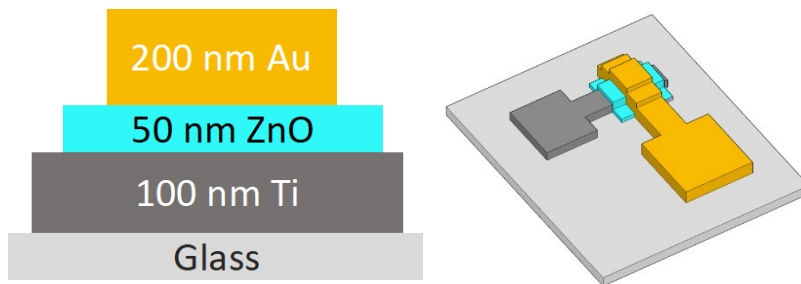


**Figure 1:** Cross section and device structure for the ZnO diode

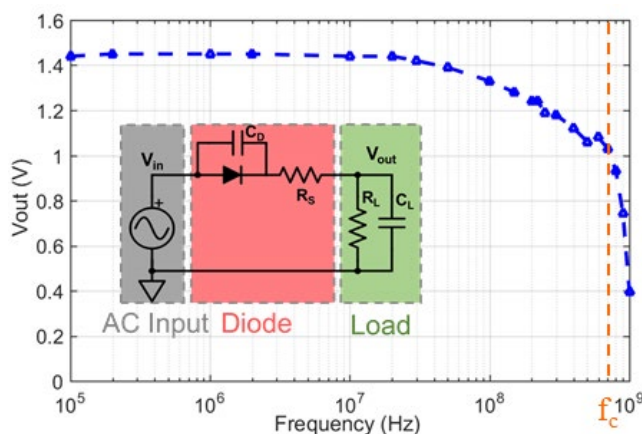


**Figure 2:** DC output voltage of the half wave rectifier as a function of input frequency ( $V_{in(p-p)}= 4\text{ V}$ ), with  $f_c=700\text{ MHz}$ . The inset shows the circuit diagram of the HWR,  $R_L= 1\text{ M}\Omega$  and  $C_L= 100\text{ pF}$ .

## CITATIONS

- L. E. Aygun, S. Wagner, N. Verma and J. C. Sturm, High-frequency ZnO schottky diodes for non-contact inductive power transfer in large-area electronics, in 75th Annual Device Research Conference (DRC), South Bend, IN, pp. 1-2, June 2017.

Researcher: **Alexander Berg**  
 Advisor: **James C. Sturm (ELE)**  
 Sponsorship: **DOE & Princeton**

The Sturm Solar group studies novel materials and device structures for solar cells, with a particular focus on metal oxides in silicon heterojunction cells [Fig. 1]. These cells could generate more power, at lower cost, than current state-of-the-art commercial cells. Use of the MNFL is critical in much of this work.

One current project is the study of ultrathin, thermally-grown silicon oxides [Fig. 2]. These layers can be inserted between silicon and selective contacts in heterojunction cells. Depending on the temperature and growth time, different lifetimes and series resistances can be obtained, increasing cell efficiency. For this, the MNFL's Rapid Thermal Annealer system, which can change temperatures by hundreds of degrees in a few seconds while also maintaining precise flow rates of three different gasses, is ideal. After this, device contacts (allowing electrical measurements) can be deposited in

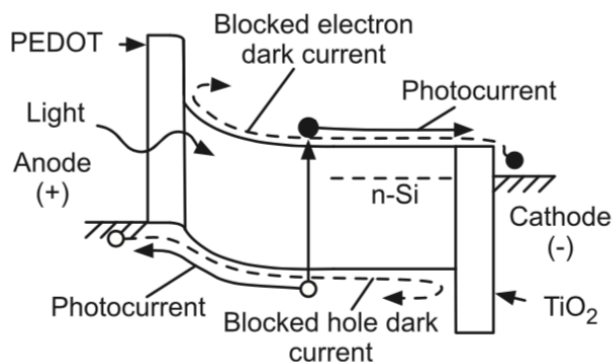


**Figure 1:** Silicon heterojunction solar cell under illumination

one of the MNFL's Angstrom metal deposition systems.

We are also currently studying nickel oxide (NiO) films as possible hole-selective contacts in silicon cells. By "blocking" electrons that try to move through them, the NiO layers lead to the creation of voltages and, ultimately, generated solar power. As we modulate the NiO's chemical composition, it's important to be able to characterize the resulting material. To make this possible, we use the MNFL's furnace systems to grow thick SiO<sub>2</sub> layers. We then use the MNFL's photolithography capabilities (encompassing a number of different tools spread across multiple cleanroom areas) to define device structures that enable materials-science measurements. Sometimes, we modify the films' properties directly in the cleanroom, using either the "metals RTA" or the UV-Ozone exposure system.

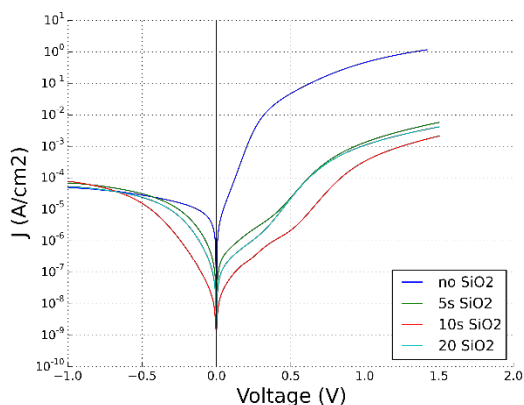


**Figure 2:** Effect of short oxygen anneals at 750C on IV characteristics of NiO/SiO<sub>2</sub>/n-Si diodes

## CITATIONS

- Nagamatsu et al JPV 2014, Berg et al IEEE-TED 2017, Sahasrabudhe et al ACS 2015, Jhaveri et al JPV 2018, etc

Researcher: **Weiguang Huo**  
 Advisor: **James C. Sturm (ELE)**  
 Sponsorship: **NSF**

Two-dimensional electron gases (2DEGs) in Si/SiGe heterostructures have been considered as a potential platform to fabricate single electron quantum dots for spin manipulations because silicon has an inherently longer

coherence time. The efforts to improve mobility of 2DEGs are the main focus of this project. We will fabricate Hall bar devices to measure the density of electrons and mobility.

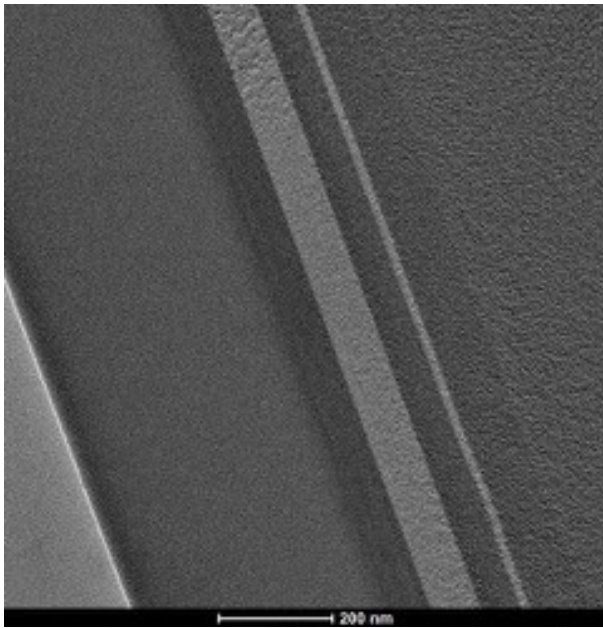


**Figure 1:** TEM image of Si/SiGe heterostructure grown by Chemical Vapor Deposition (CVD). The darker layer is SiGe and the lighter layer is Si.

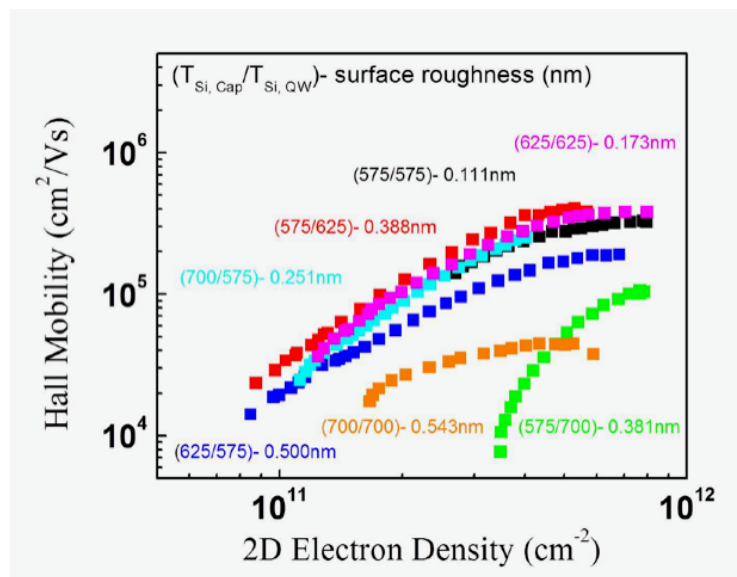


**Figure 2:** This figure shows mobility versus density labeled by individual growth temperature and its RMS surface roughness.

## CITATIONS

- Li J Y, Huang C T, Rokhinson L P, et al. Extremely high electron mobility in isotopically-enriched <sup>28</sup>Si two-dimensional electron gases grown by chemical vapor deposition[J]. Applied Physics Letters, 2013, 103(16): 162105.
- Huang C T, Li J Y, Chou K S, et al. Screening of remote charge scattering sites from the oxide/silicon interface of strained Si two-dimensional electron gases by an intermediate tunable shielding electron layer[J]. Applied Physics Letters, 2014, 104(24): 243510.

Researcher: **Weibin Liang**  
 Advisor: **James C. Sturm (ELE)**  
 Sponsorship: **NIH/GPB STTR**

Our bio group develops microfluidic sorters, bioreactors, and concentration gradient generators to study DNA, stem cells and cancer. High throughput cell separation by microfluidic methods, especially deterministic lateral displacement (DLD) array method, has a broad range of application, such as lymphocyte purification for immunotherapy, circulating

tumor cells (CTCs) separation for early diagnosis of cancer, cell sample washing, and aphaeresis. Currently, we focus on improving the separation efficiency, understanding the chip clogging mechanism and cell-fluid interaction which determine the performance of our microfluidic device.

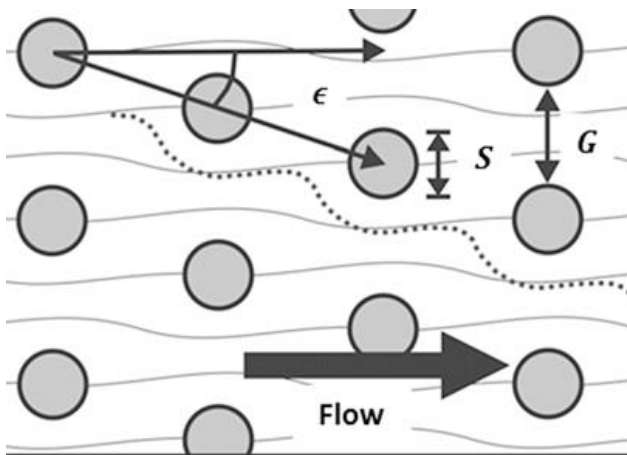


**Figure 1:** Deterministic Lateral Displacement (DLD) Array for Cell Separation

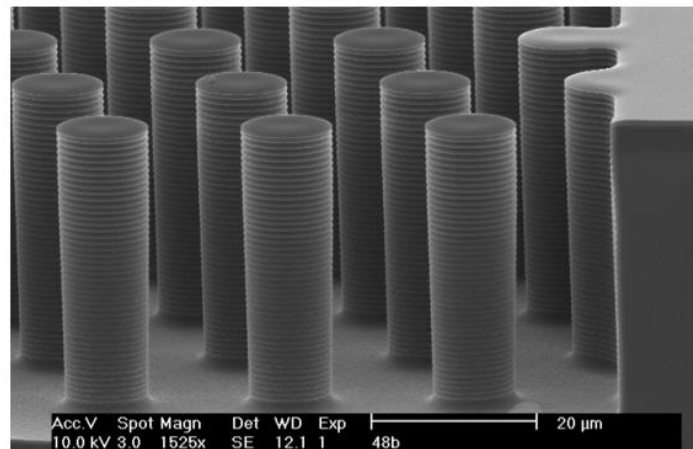


**Figure 2:** SEM Image of Silicon DLD Array (fabricated by DRIE)

## CITATIONS

- Microfluidic chemical processing with on-chip washing by deterministic lateral displacement arrays with separator walls. Chen Y, D'Silva J, Austin RH, Sturm JC. *Biomicrofluidics*. 2015 Sep 9;9(5):054105.
- On-chip cell labelling and washing by capture and release using microfluidic trap arrays. Chen Y, Austin RH, Sturm JC. *Biomicrofluidics*. 2017 Sep 27;11(5):054107

Researcher: **KC Lin**  
 Advisor: **James C. Sturm (ELE)**  
 Sponsorship: **Sturm**

We have designed a PDMS microfluidic cell culture platform, the Evolution Accelerator (EA), that generates an in vitro landscape of stress heterogeneity, which allows for accelerated adaption and evolution dynamics of multiple cell phenotypes in the cancer population. The utility of this technology is highlighted by analysis of heterogenous prostate cancer cell motility changes as a function of position in the stress landscape (Fig.1) as well as the downstream experiment capacities such as immunofluorescence assay on specific biomarkers (Fig.2). This newly developed system has the potential for broad application in fundamental cell biology study, preclinical drug development and assays of likely drug efficacy.

**Figure 2:** The mesenchymal biomarker ZEB1 expression level of PC3-Epi after being cultured in docetaxel gradient, from 0 to 5 nM for 20 days, which is associated with the invasiveness and metastatic potential of cancer cells. (A) The fluorescent image of the entire EA. The drug diffused into the chip from the bottom three edges. (B) The heatmap of ZEB1 expression level across the device. Each dot represents the average ZEB1 level of cells in the corresponding EA. (C) The normalized histogram of ZEB1 level of PGCCs and diploid PC3-Epi cells showing the significant elevation of ZEB1 expression in polyploidy giant cancer cells (PGCCs). (D) The color-mapped ZEB1 intensity in one EA element where PGCCs coexisted with diploid PC3-Epi cells. PGCCs stain more positively than diploid cells.

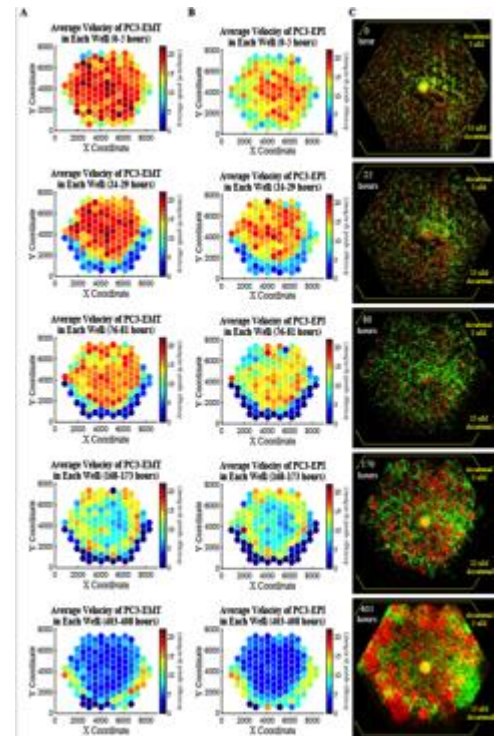
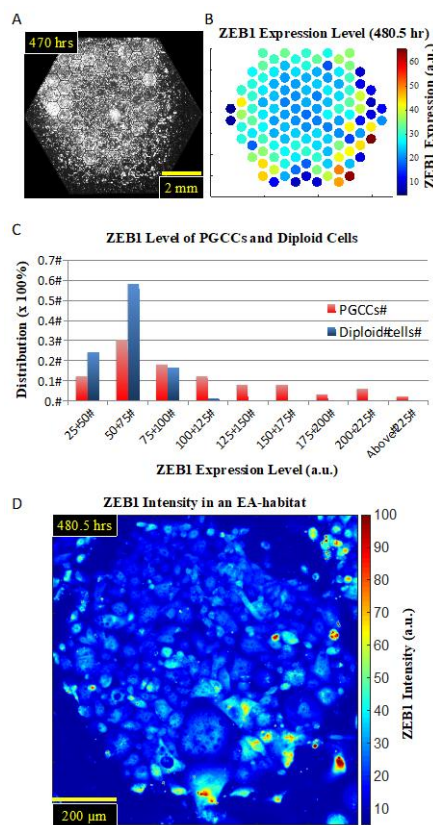


**Figure 1(Above):** The distribution of velocities and populations of PC3-EPI (red cells) and PC3-EMT (green cells) in the complex ecology with docetaxel gradient. The experiment was done under the existence of docetaxel gradient across the chip, from 10 nM at the bottom three edges to 0 nM at the top three edges. The distribution of the averaged speed of (A) PC3-EMT and (B) PC3-EPI in each micro-habitat is illustrated as the 2D color-scaled graph. (C) The red and green fluorescent images were taken respectively with 10X objective, stitched and displayed together to show a global view of the distribution of the two cell lines at different time points.

## CITATIONS

- Ke-Chih Lin, Gonzalo Torga, Amy Wu, Joshua D Rabinowitz, Wesley J Murray, James C Sturm, Kenneth J Pienta and Robert Austin, Epithelial and mesenchymal prostate cancer cell population dynamics on a complex drug landscape, *Convergent Science Physical Oncology*, 3(4): 045001 (2017)



Researcher: **Jonathan Mehlman**  
 Advisor: **James C. Sturm (ELE)**  
 Sponsorship: **PPST**

Large-area hybrid electronic systems are a powerful platform for enabling interactions between the microelectronic and meter-scale domains by combining the strengths of large area electronics for sensing and conventional integrated circuits for computation. In such systems, thin-film transistors (TFTs) are needed for instrumentation and communication circuitry integrated with thin-film sensors patterned over large surfaces on the scale of people or large equipment. When integrating transistors with sensors patterned on glass or especially flexible plastic sheets, low process temperatures are required for compatibility with the substrate. Low-temperature processing makes fabrication

of high performance devices difficult, so that realizing large sensor systems presents a considerable design challenge. Plasma-enhanced deposition techniques are typically used to improve material and device quality at low process temperatures. My research over the past year has focused on bringing significant improvements to the performance of metal oxide (ZnO) TFTs by scaling of transistor dimensions. This has enabled the highest frequency circuits utilizing metal-oxide TFTs reported in literature. My future research will focus on overcoming various non-idealities have been identified as limiting an even further increase in performance.

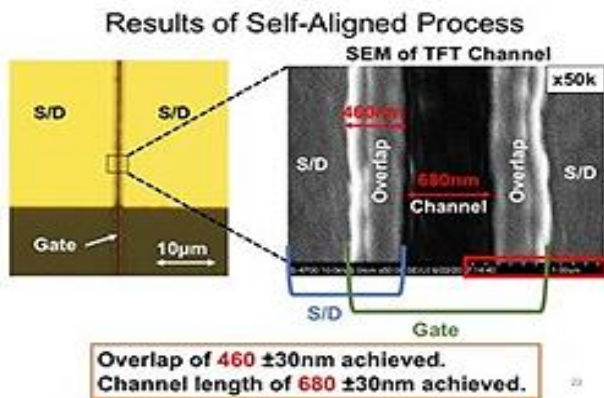


**Figure 1:** Optical micrograph (left) and SEM (right) of short-channel self-aligned transistors.

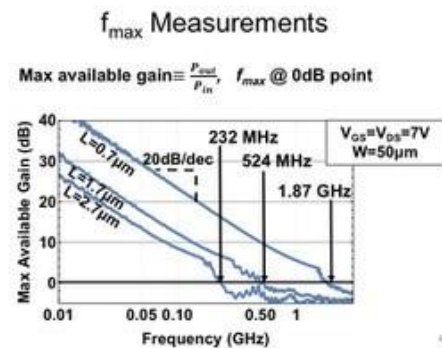


**Figure 2:** Max available power gain vs. frequency for three different channel lengths (L).  $f_{MAX}$  corresponds to 0dB, and increases with decreasing L. Measurements were taken using a VNA (Agilent E5061) with DC bias  $V_{DS}=V_{GS}=7V$ .

## CITATIONS

- C. Wu, Y. Mehlman, A. Pierre, T. Moy, A. Arias, and N. Verma, A Large-area Image Sensing and Compression System Based on Variation Tolerant Random Projections, presented at the SONIC Annual Meeting, Champaign, IL, 2015.
- Y. Mehlman, Y. Afsar, T. Moy, S. Wagner, J. C. Sturm, and N. Verma, High-Speed Scanning Circuit Based on Metal-Oxide Thin-Film-Transistors for Reduction of Large-Area to CMOS IC Connections, presented at the International Thin Film Transistor Conference, Austin, TX, 2017.
- Y. Mehlman, Y. Afsar, T. Moy, S. Wagner, J. C. Sturm, and N. Verma, Self-Aligned ZnO Thin-Film Transistors with 860 MHz ft and 2 GHz  $f_{max}$  for Large-Area Applications, presented at the Device Research Conference, Notre Dame, IN, 2017.
- M. Ozatay, L. Aygun, H. Jia, P. Kumar, Y. Mehlman, C. Wu, S. Wagner, J. C. Sturm, and N. Verma, "Artificial Intelligence Meets Large-scale Sensing: using Large-Area-Electronics (LAE) to enable intelligent spaces," presented at IEEE Custom Integrated Circuits Conference, San Diego, CA, 2018. (invited)

Researcher: **Matt Wang**  
Advisor: **James C. Sturm (ELE)**  
Sponsorship: **Princeton University**

I will work with Levent Aygun on fabricating flexible microelectrodes to obtain electrical measurements from SCG neurons. We will start with a commercial 50  $\mu\text{m}$  thick polyimide substrate and deposit/pattern metal traces (Ti, Au, Cr) via Sputterer or thermal evaporator. Phase 1: In order to encapsulate these metal traces, we will try: (a) spin coating and furnace baking polyimide (a few  $\mu\text{m}$  thick), and etching holes via oxygen plasma (PlasmaTherm 720)

using a Cr mask (b) depositing parylene-C (using the new coater - few  $\mu\text{m}$  thick), etching holes via oxygen plasma (PlasmaTherm 720) using Cr mask, and (c) if a and b don't work, try another biocompatible insulator layer (using PECVD or dielectric sputterer). Phase 2: Develop an oxygen plasma etch recipe to open through holes through 50  $\mu\text{m}$  thick polyimide layer and encapsulation layer without heating up the sample during the long etch process.

## CITATIONS

---

- None

Researcher: **Can Wu**  
 Advisor: **James C. Sturm (ELE)**  
 Sponsorship: **SONIC**

Our work focusses on novel system architectures for interfacing large numbers of sensors, such as applications in IoT (Internet of Things). The work is based on flexible compatible transistors that can be directly fabricated over large area at low cost, avoiding the packaging and bonding limitations of using many discrete integrated circuits. At the heart of our work is (1) record high frequency performance of thin film transistors, with maximum power gain frequency

$f_{max}$  over 1 GHz, enabling oscillators in the GHz range in TFT technology for the first time. (2) A novel circuit design allowing TFT operating above  $f_t$ . (3) A system architecture that synchronizes oscillators.

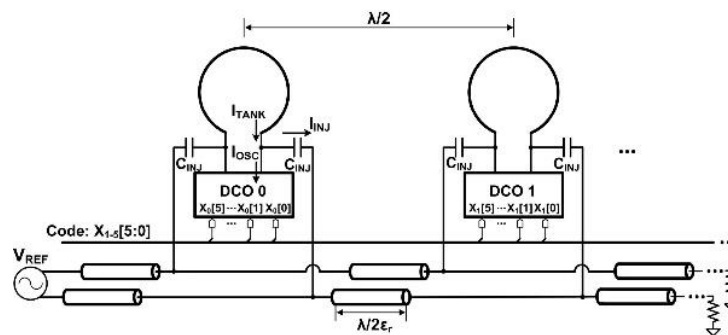


Figure 1:

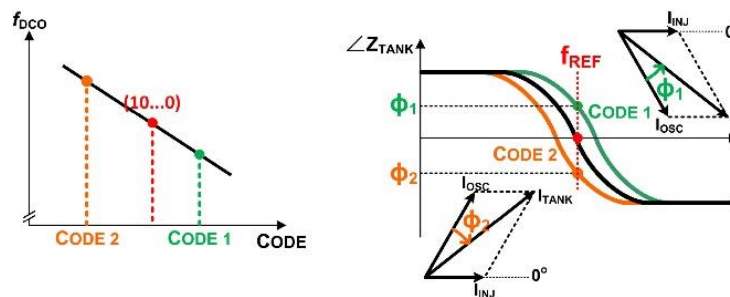


Figure 2:

## CITATIONS

- Haven't been published yet.

Researcher: **Alan Dibos, Songtao Chen**  
 Advisor: **Jeffery Thompson (ELE)**  
 Sponsorship: **AFOSR YIP**

Single atoms and atom-like defects in solids are ideal quantum light sources and memories for quantum networks. However, most atomic transitions are in the ultraviolet-visible portion of the electromagnetic spectrum, where propagation losses in optical fibers are prohibitively large. Here, we observe for the first time the emission of single photons from a single  $\text{Er}^{3+}$  ion in a solid-state host, whose optical transition is at a wavelength of 1.5 microns is in the telecom band, allowing for low-loss propagation in optical fiber. This is enabled by integrating

$\text{Er}^{3+}$  ions with silicon nanophotonic structures, which results in an enhancement of the photon emission rate by a factor of more than 650. Dozens of distinct ions can be addressed in a single device, and the splitting of the lines in a magnetic field confirms that the optical transitions are coupled to the electronic spin of the  $\text{Er}^{3+}$  ions. These results are a significant step towards long-distance quantum networks and deterministic quantum logic for photons based on a **scalable silicon nanophotonics architecture**.

**Figure 1:** Schematic diagram of experiment. Silicon photonic crystal nanobeam cavities couple light to isolated  $\text{Er}^{3+}$  ion defects in a  $\text{Y}_2\text{SiO}_5$  substrate.

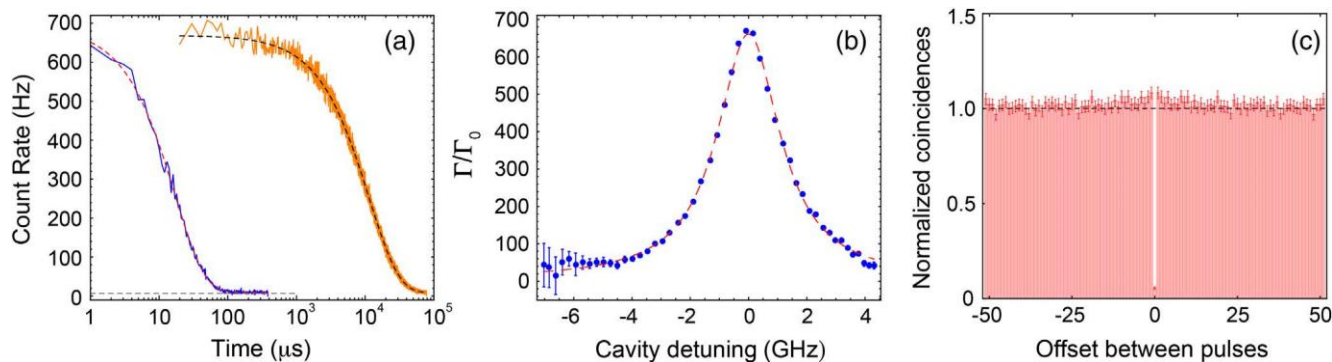
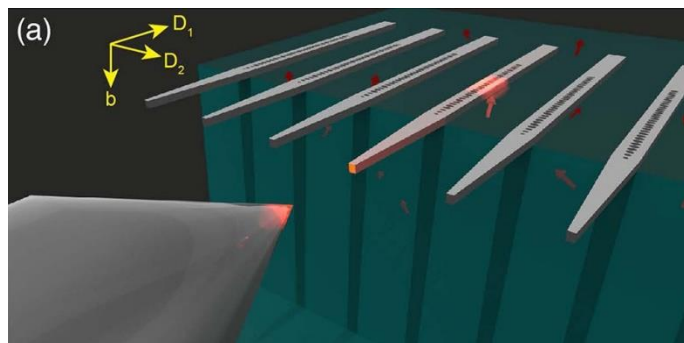


**Figure 2:** (a) The fluorescence lifetime of cavity-coupled ions is  $17 \mu\text{s}$  (blue), over 600 times shorter than bulk ions (11.4 ms, orange). (b) Tuning the optical cavity away from the ion resonance shows that the enhancement is purely radiative. (c)  $g^{(2)}(0) = 0.05$  confirms that the fluorescence originates from a single  $\text{Er}^{3+}$  ion.

**CITATIONS**

- A.M. Dibos, M. Raha, C.M. Phenicie, and J.D. Thompson. Phys. Rev. Lett. 120, 243601 (2018).

Researcher: **Chris Phenicie**

Advisor: **Jeffrey D. Thompson (ELE)**

Sponsorship: **Eric and Wendy Schmidt Transformative Technology Fund**

This project is aimed at identifying new materials to use in quantum information processing. The materials that are current leading candidates for these applications have serious limitations to the wavelength of light used to address the system as well as the coherence properties (and, thus applicability to quantum information). One promising candidate to address both of these issues is the electronic spin associated with erbium defects in solids. These spins have excellent coherence properties and are addressable in the “telecommunication wavelength” of light used in modern

communication networks. In the initial stages of this project, I am implanting erbium into various materials such as silicon and diamond. I am screening the properties of these materials with electron spin resonance (ESR). To use this technique, I have fabricated superconducting microwave resonators that can manipulate and measure the properties of these spins. Using this technique, I should be able to screen the properties of many materials and determine their promise in future quantum information applications.

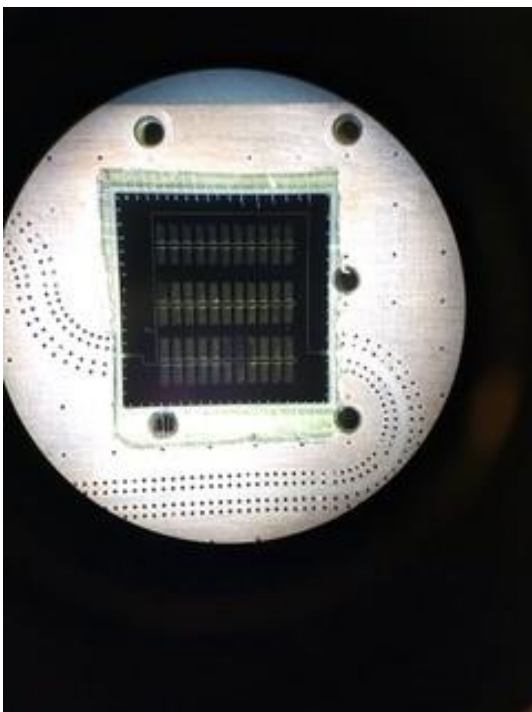


**Figure 1:** Example device used to characterize the materials. This central chip contains a series of superconducting microwave resonators that act like antennas to drive spin transitions

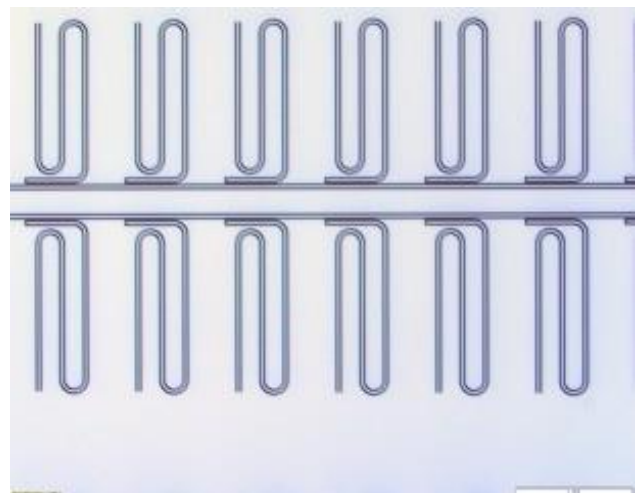


**Figure 2:** Close-up image of the series of superconducting microwave resonators. Each paperclip shaped blue curve is an individual resonator capable of driving and measuring spin properties in the host materials

## CITATIONS

- None

Researcher: **SeungYeon Kang**  
 Advisor: **Craig B. Arnold (MAE)**  
 Sponsorship: **Industrial, NSF**

Increasing the printing resolution of drop-on-demand printing and deposition techniques is important for many industrial applications. We are investigating ways to minimize the jet size and reduce the laser threshold energy of a variant of the laser-induced forward transfer (LIFT) process called blister-actuated LIFT. We

fabricate micrometer-sized holes onto the solid polyimide thin-film substrate which hosts the donor liquid ink film to be printed. Due to the micrometer size of the holes, surface tension effects are enhanced, a meniscus is formed at the air-ink interface, and the resulting focused jets are thinner and faster than regular jets.

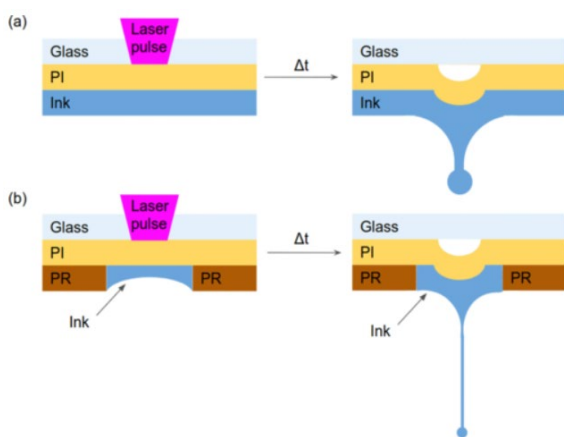


**Figure 1:** Schematic of blister-actuated laser-induced forward transfer (BA-LIFT) with and without flow-focusing. (a) The conventional BA-LIFT technique. The laser pulse is absorbed by the polyimide (PI) layer which leads to the rapid formation of a blister. This leads to the deformation of the ink film and jet formation. (b) BA-LIFT with flow-focusing. The ink inside the hole of the photoresist (PR) layer forms a meniscus at the liquid-air interface. The curved interface leads to the flow-focusing with the pressure impulse from the blister.

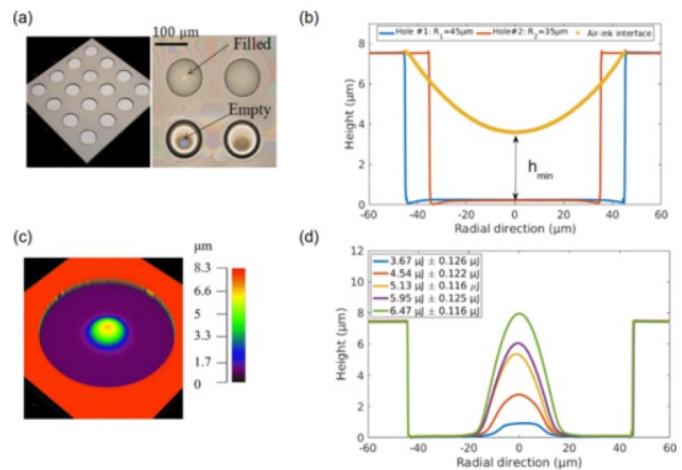


**Figure 2:** Profiles of machined holes, blisters generated by the laser pulse, and meniscus on the air-ink interface. (a) A 3D image of the hole pattern fabricated on the polyimide substrate along with the confocal image showing the filled and empty holes together. (b) Profiles of the two types of holes used in the study ( $R_1=45\mu\text{m}$  and  $R_2=35\mu\text{m}$ ). The ink layer follows a parabolic-like profile with a measured  $h_{\min}=3.8\mu\text{m} \pm 0.9\mu\text{m}$  value that defines the minimum distance between the hole bottom surface and the air-ink interface. (c) A 3D image and variation in height as a contour plot of a blister generated inside a 45- $\mu\text{m}$ -radius hole. (d) Blister profiles as the result of the five different laser pulse energy levels used in this study. The profiles of the blisters and the holes are measured using confocal microscopy.

## CITATIONS

- PHYSICAL REVIEW FLUIDS 3, 082201(R) (2018)

Researcher: **Juliane Preimesberger**  
 Advisor: **Craig B. Arnold (MAE)**  
 Sponsorship: **Internal Funding**

As technology becomes smaller and smaller, the need for micro-energy sources becomes increasingly imperative. One promising technology to address this need is piezoelectrochemical harvesting, a recently identified mechanism to directly convert mechanical energy to electrochemical potential. In piezoelectrochemical (PEC) materials, the chemical potential of ions is affected by an applied stress, and under such circumstances these materials can be used in a thermodynamic cycle to harvest energy, at a relatively slow rate commensurate with the kinetic

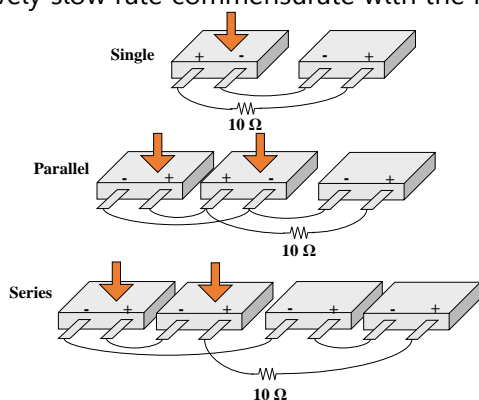


**Figure 1:** To test how the PEC effect works in multiple batteries, three wiring configurations of commercial LCO pouch cells were tested: single, parallel, and series. To minimize instrumental error, active cells were connected in parallel to reference cells through a resistor. Then the active cells (denoted by arrows) were mechanically cycle as the voltage across the resistor was measured.

transport in electrochemical systems. Previous work has demonstrated that commercial lithium cobalt oxide (LCO) batteries exhibit the PEC effect, as both the lithium cobalt oxide cathode and lithium-intercalated graphite anode are PEC materials. Current work investigates how the piezoelectrochemical effect works in multiple batteries wired together. However, commercial batteries are not ideal systems to study due to their complexity. Single-crystal and solid-state systems would provide insight into how the mechanism works.

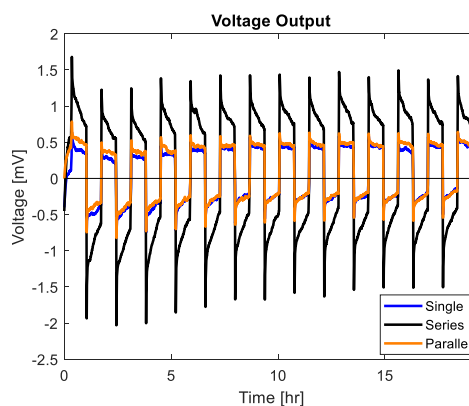


**Figure 2:** The voltage across the resistor of the three configurations in Figure 1 is plotted in Figure 2. As expected, in series the voltage increases. This indicates that a straightforward way to increase the energy harvested from piezoelectrochemical systems is to compress multiple systems connected in series.

## CITATIONS

- J. Cannarella and C. B. Arnold, "Toward Low-Frequency Mechanical Energy Harvesting Using Energy-Dense Piezoelectrochemical Materials," *Advanced Materials*, 27, 7440 (2015).
- N. Muralidharan, M. Li, R. E. Carter, N. Galioto, and C. L. Pint, "Ultralow Frequency Electrochemical-Mechanical Strain Energy Harvester Using 2D Black Phosphorus Nanosheets," *ACS Energy Lett.*, 2, 1797 (2017).
- S. Kim, S. J. Choi, K. Zhao, H. Yang, G. Gobbi, S. Zhang, and J. Li, "Electrochemically driven mechanical energy harvesting," *Nature Communications*, 7, 10146 (2016).
- E. Jacques, G. Lindbergh, D. Zenkert, S. Leijonmarck, and M. H. Kjell, "Piezo-Electrochemical Energy Harvesting with Lithium-Intercalating Carbon Fibers," *ACS Appl. Mater. Interfaces*, 7, 13898 (2015).
- V. A. Sethuraman, V. Srinivasan, A. F. Bower, and P. R. Guduru. "In Situ Measurements of Stress-Potential Coupling in Lithiated Silicon." *J. Electrochemical Society*, 157, 11 (2010).
- C. Massey, G. McKnight, W. Barvosa-Carter, and P. Liu. "Reversible work by electrochemical intercalation of graphitic materials." *SPIE*, 5759 (2005).
- Z. J. Schiffer, J. Cannarella, and C. B. Arnold. "Strain Derivatives for Practical Charge Rate Characterization of Lithium Ion Electrodes." *J. Electrochemical Society*, 163, 3 (2016).
- J. Cannarella, C. Z. Leng, and C. B. Arnold. "On the Coupling Between Stress and Voltage in Lithium Ion Pouch Cells." *SPIE*, 9115(2014).
- G. Bucci et al. "The Effect of Stress on Battery-Electrode Capacity." *J. Electrochemical Society*, 164, 4 (2017).

Researcher: **Matt Heinrich**  
Advisor: **Daniel J. Cohen (MAE)**  
Sponsorship: **N/A**

We are exploring the ability to control migration of tissues through micropatterned channels. First we will explore asymmetric boundary features in 2D (using protein patterning), and then construct

3D microchannels. Later we will treat the sides of the 3D microchannels with protein functionalizations that are relevant to the tissue setting, such as Cadherin, Fibronectin, etc.

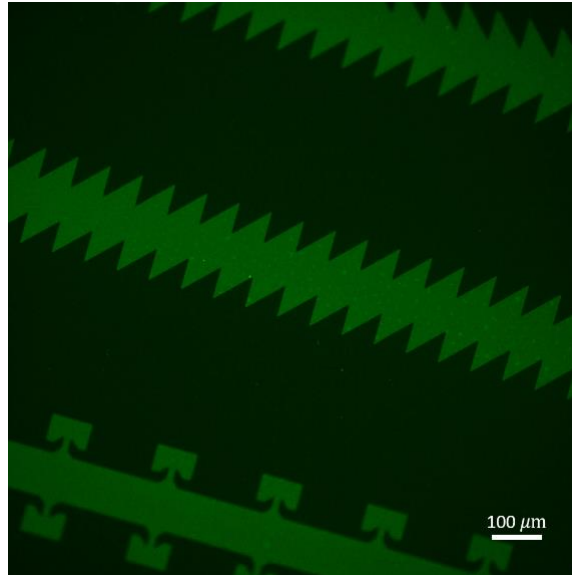


**Figure 1:** The above image shows a cell culture dish micropatterned with fluorescent extracellular matrix. Cultured cells will only form tissues where there is matrix present.

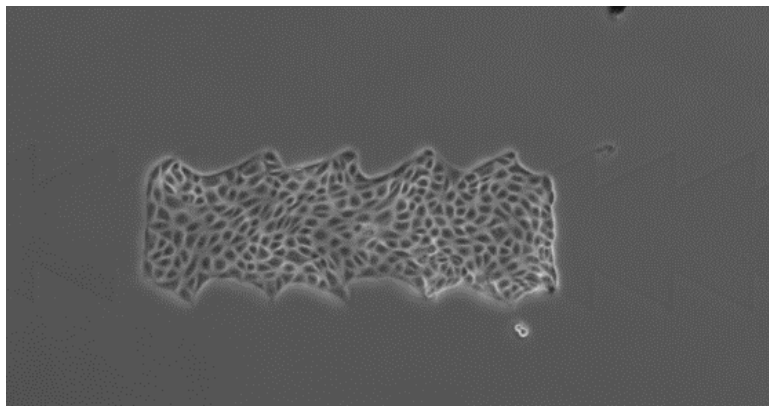


**Figure 2:** Here we show the initial configuration of a tissue cultured on this patterned substrate. It will expand laterally to fill the patterns.

## CITATIONS

- N/A



Researcher: **Yi-Chun (Kelly) Huang**  
 Advisor: **Marcus N. Hultmark (MAE)**  
 Sponsorship: **NSF**

A robust and scalable nano-scale hot-and-cold-wire system was constructed and deployed at the Surface Layer Turbulence and Environmental Science Test (SLTEST) facility on the playa of western Utah as part of the Idealized Planar Array experiment for Quantifying Surface heterogeneity or IPAQS2018 experiment. This experiment aims to improve the reliability of numerical weather predictions by providing an accurate representation of the lower-boundary conditions that shape the near-surface micro-climate. Host to a myriad of important meteorological processes such as fog, dew, subsidence, and intense momentum jets, the near-surface velocity and temperature fields are crucial information that need to be obtained. Unfortunately, conventional instrumentation used in studies of the atmospheric surface layer (ASL) are often limited in spatial or temporal resolution. Moreover, there is often a trade-off between cost and resolution. Thus, utilizing Nano-Scale Thermal Anemometer Probes (NSTAPs) will allow for well-resolved data with unprecedented spatiotemporal resolution.

Developed and manufactured in-house at Princeton University using standard MEMS (Micro Electro-Mechanical Systems) techniques, Nano-Scale Thermal Anemometry Probes (NSTAPs) were used in this experiment to capture single-



**Figure 1:** One station of the set-up deployed at Utah's SLTEST facility. An NSTAP, a TNSTAP, a pitot tube, and a thermocouple are mounted.

component velocity data in the atmospheric surface layer. The small size of the NSTAP results in a spatial resolution three orders of magnitude greater than conventional sonic anemometers and ten times greater than conventional hot-wires. Its small size and silicon support structure also contribute to its high survival rate in the severe field environment. Although constant temperature anemometry (CTA) hot-wire systems offer greater ease of use, they are not economically feasible for applications demanding multiple sensors. The cheaper, alternative constant current anemometry (CCA) mode of operation comes at the cost of reduced bandwidth and higher sensitivity to heat transfer relations. The setup used in the experiment addresses both these drawbacks to render CCA a viable option in the atmospheric surface layer. The small size of the NSTAP enables CCA measurements with a bandwidth of 10 kHz, and to account for the drastic temperature changes that occur, the temperature variant of the NSTAP, the TNSTAP, is mounted adjacent to each NSTAP. Simultaneous sampling of well-resolved temperature and velocity data then allows for an instantaneous application of the temperature compensation scheme proposed by Hultmark and Smits (2010), which can be used in both CTA and CCA mode.

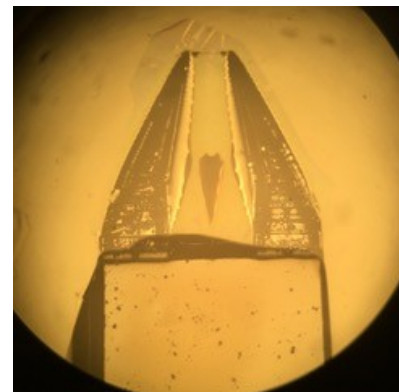


**Figure 2:** Close-up of the TNSTAP. The wire (suspended at the tip of the silicon structures) has dimensions of 200 microns x 6 microns x 120nm.

## CITATIONS

- Hultmark, M. and Smits, A. J., "Temperature corrections for constant temperature and constant current hot-wire anemometers", *Meas. Sci. Technol.* Vol. 21, 105404, 2010.

Researcher: **Katherine Kokmanian**  
 Advisor: **Marcus N. Hultmark (MAE)**  
 Sponsorship: **AFOSR**

Our group focuses on the development of sensors which can be placed in a wide variety of flows and acquire reliable information such as velocity (in one or two directions), mass flux, temperature and humidity. We are currently developing nano-scale hot-wires to extract spatially and temporally resolved turbulence statistics in compressible flows. Hot-wires consist of a heated metallic filament through which the change in resistance (or change in current, depending on the circuit's mode of operation) registers as a change in heat transfer. The sensor currently being manufactured is a variant of the already established nano-scale thermal anemometry probe (NSTAP) developed at Princeton in 2010. Design changes were performed in order for the NSTAP to be more robust and aerodynamic in order to withstand supersonic flows ( $M > 1$ ); the two-dimensional pattern was modified for the wire to sense unobstructed flow (see Figure 1) and the thickness of the metallic sensing element was

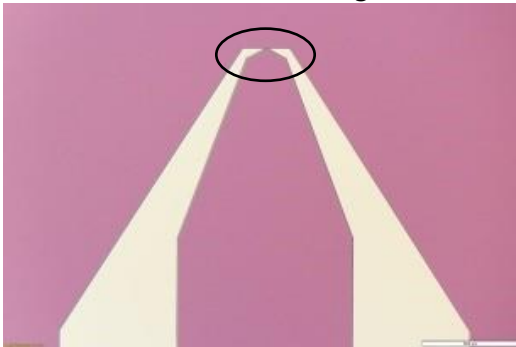


**Figure 1:** Two-dimensional design of the sensor currently being manufactured in the micro/nano-fabrication laboratory. A thin layer of titanium followed by a thicker layer of platinum is sputtered onto a silicon wafer.

increased in order to mitigate undesirable vibrational effects. The possibility of using electron-beam evaporation to deposit different metals was investigated and multiple lithography dose tests were performed in order to satisfy all new design requirements (see Figure 2). The current design consists of a  $\sim 300$  nm thick,  $2 \mu\text{m}$  wide and  $30 \mu\text{m}$  long freestanding platinum wire, supported on each end by a silicon structure. Deep reactive ion etching (DRIE) followed by RIE lag provide a tapered profile of the silicon support. After removing the thin layer of silicon dioxide which serves as a protective layer for the sensing element, the sensor is placed in a trisonic flow facility ( $0.3 < M < 2$ ) where reliable high frequency data is acquired. The objectives of this research project are to obtain more accurate data regarding supersonic wall-bounded flows and to fill the knowledge gap concerning the behavior of the NSTAP in compressible flows.

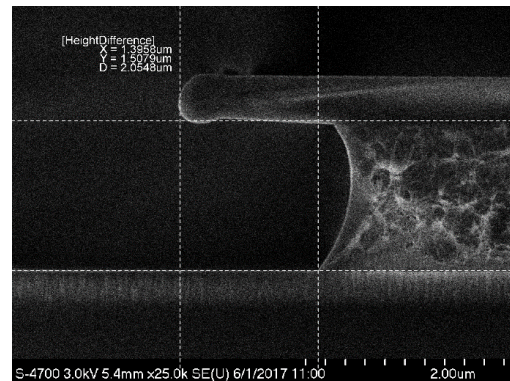


**Figure 2:** Scanning electron microscope image of a bilayer of photoresist. In order to mitigate the appearance of large wings on the edges of the metallic layer, a new spin coating recipe was developed.

## CITATIONS

- Nanoscale sensing devices for turbulence measurements (Fan Y. et al, 2015)
- Fabrication and Characterization of a Novel Nanoscale Thermal Anemometry Probe (Vallikivi M. and Smits A. J., 2014)
- Turbulence measurements using a nanoscale thermal anemometry probe (Bailey S. C. C. et al., 2010)

Researcher: **Anthony Harness**  
 Advisor: **N. Jeremy Kasdin (MAE)**  
 Sponsorship: **NASA, Jet Propulsion Laboratory (CalTech)**

Starshades are a promising technology to enable the direct detection and spectroscopic characterization of Earth-like exoplanets. Two key aspects to advancing starshade technology are the demonstration of starlight suppression at science-enabling levels and validation of optical models at this high level of suppression. The Princeton Starshade Testbed was designed to perform the sub-scale tests of starshades needed to experimentally validate the optical models at a flight-like Fresnel number. The

starshade masks, manufactured at the Microdevices Laboratory at JPL, are lithographically etched in a Silicon wafer and coated with a thin metallic layer. PRISM facilities are used to characterize the as-built masks to high precision to enable validation between experimental results and optical models. The facilities also provide the opportunity to explore additional manufacturing techniques that will enable the masks to be manufactured to the required tolerances.

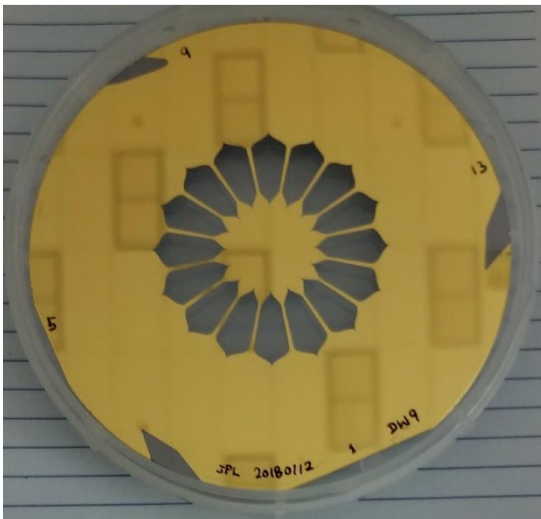


**Figure 1:** Starshade mask manufactured at the Microdevices Laboratory at JPL. The pattern etched through the Silicon wafer controls the diffraction of light to create a dark shadow; suppressing laser light by 9 orders of magnitude.



**Figure 2:** Princeton Starshade Testbed located on campus. This 80 meter long, 1 meter diameter tube provides a clean and dark environment for conducting optical tests on the starshade masks. Data from this experiment are used to validate optical models predicting the starshade's starlight suppression capabilities.

## CITATIONS

- M. Galvin, Y. Kim, N. J. Kasdin, et al., Design and construction of a 76m long-travel laser enclosure for a space occulter testbed, Proc. SPIE 9912, 18 (2016).
- Y. Kim, A. Harness, N. J. Kasdin, et al., Optical demonstration of a starshade at flight Fresnel numbers in the laboratory, Proc. SPIE 10400, 43 (2017).
- K. Balasubramanian, et al., Recent progress in the fabrication of starshade masks for laboratory demonstration of concepts, Proc. SPIE 10698, 224 (2018).
- A. Harness, S. Shaklan, P. Dumont, Y. Kim, and N. J. Kasdin, Modeling and performance predictions for the Princeton starshade testbed, Proc. SPIE 10400, 20 (2017).

Researcher: **Mrudhula Baskaran**  
 Advisor: **Howard A. Stone and Clarence W. Rowley (MAE)**  
 Sponsorship: **MAE Department**

The aim of this senior thesis is to implement control theory and develop a control model for solving a fluid mechanics problem. Professor Rowley’s research group is currently studying flow separation from the top of an airfoil with a high angle of attack. This flow separation is being studied in wind tunnels as the formation of a separation layer along the base of the wind tunnel. In this system, a fan is used to pull fluid away from the main flow, which causes flow separation in the channel, and reintroduce the fluid back into the main flow later downstream, which causes reattachment. We are determining whether this principle can be studied in microfluidic channels, prepared using poly-

dimethyl siloxane (PDMS). Instead of using pumps to withdraw and infuse fluid as is done in the wind tunnel with fans, the geometry of the microfluidic channel will be used to create a separation zone, by the placement of a bump or curve in the channel wall so that the flow naturally undergoes separation. Water will be used as the fluid for these experiments, and the system will have a Reynolds number on the order of  $10^2$ . We are also considering whether this system can also be studied as a controls problem, to see whether parameters such as an incoming flow rate can be modified to change the properties of the separation bubble.

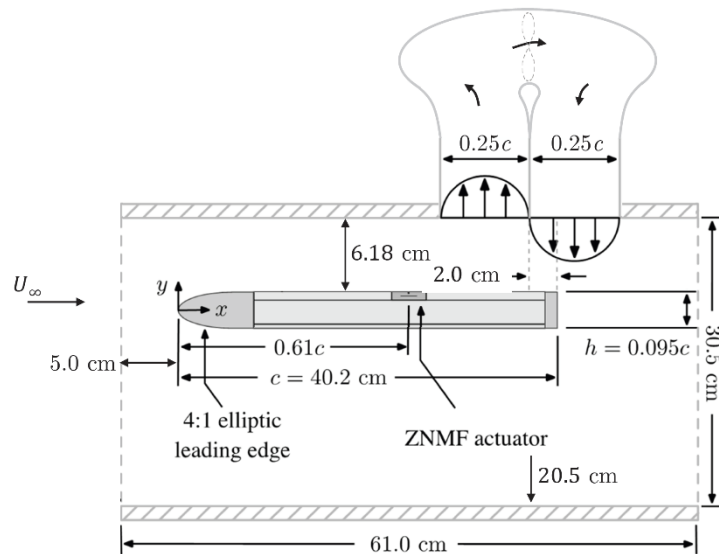


**Figure 1:** A side view of the experimental setup used by Deem et. al. (2017) is shown. In the wind tunnel, flow separation and reattachment are created using the fan and blower shown along the top.

## CITATIONS

- Deem, Eric A., et al. "Identifying Dynamic Modes of Separated Flow Subject to ZNMF-Based Control from Surface Pressure Measurements." *47th AIAA Fluid Dynamics Conference*, Feb. 2017, doi:10.2514/6.2017-3309.

Researcher: **Ya Gai**

Advisor: **Howard A. Stone (MAE) & Sabine Petry (MOL)**

Sponsorship: **Princeton Catalysis Initiative**

1) To build a minimal mitotic spindle within drops or vesicles and engineer it to segregate chromosomes (bottom up approach).

2) To assemble a physiological mitotic spindle within a compartment and study how multiple copies of chromosomes can be aligned and separated.

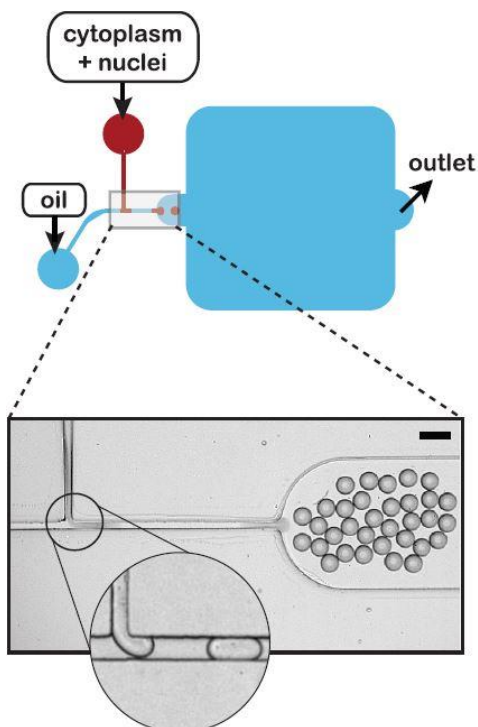


**Figure 1:** A microfluidic setup to encapsulate cell extract in droplets 1.

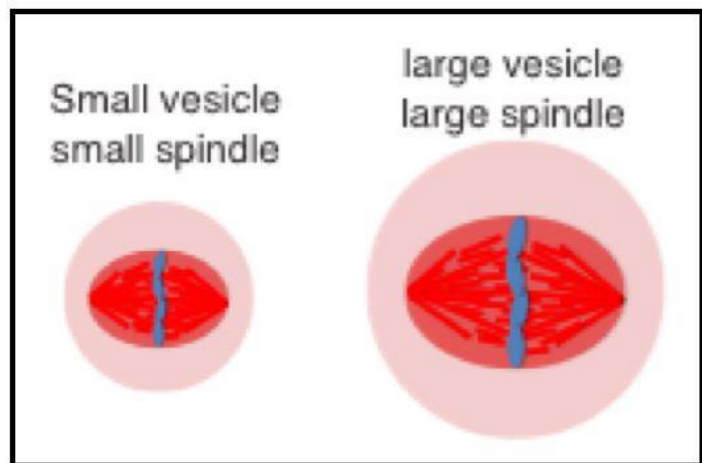


**Figure 2:** Effect of vesicle size on spindle size.

## CITATIONS

- Hazel, James, et al. "Changes in cytoplasmic volume are sufficient to drive spindle scaling." *Science* 342.6160 (2013): 853-856.

Researchers: **Janine Nunes & Sophie Slutzky**  
 Advisor: **Howard A. Stone (MAE)**  
 Sponsorship: **NSF**

Suspensions of flexible fibers usually behave as shear thinning fluids; that is, their effective viscosity, or resistance to flow, decreases as they are exposed to higher shear stresses. Here we demonstrate that for suspensions created with very-high-aspect-ratio and highly flexible fibers produced using a microfluidic method, shear thickening behavior of the fiber suspension is obtained. Such a property can be exploited to

produce a biocompatible hydrogel by injecting the suspension from a standard needle and syringe without any chemical reactions (unlike a chemically cross-linked hydrogel) or chemical interactions (unlike a traditional physical hydrogel). Once extruded, the hydrogel is a yield-stress material with potentially useful mechanical properties for bioengineering and biomedical applications.

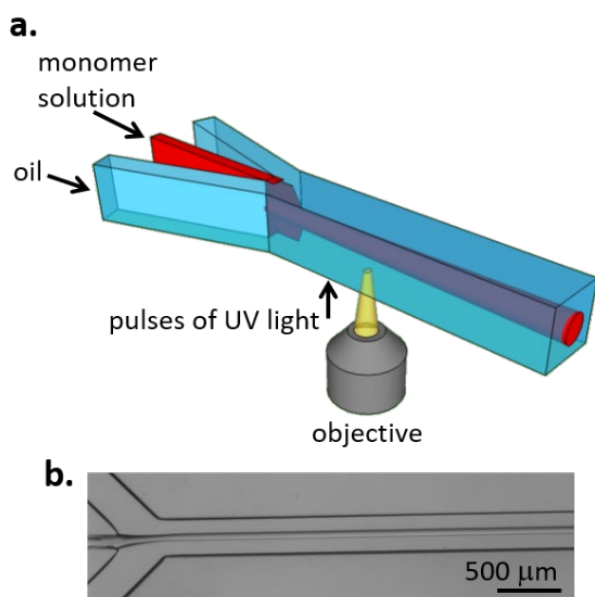


**Figure 1: Microfluidic production of flexible microfibers.** (a) Schematic showing the photoreactive fluid jet flowing in a microchannel exposed to UV light. (b) Microscope image of the jet flowing in the device.

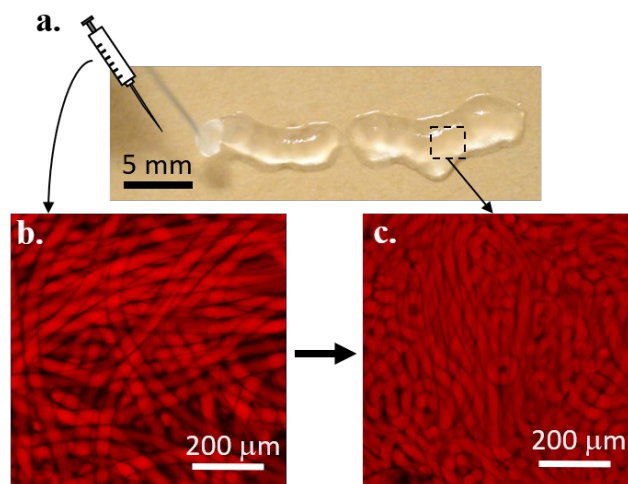


**Figure 2: Flow-induced gelation of a microfiber suspension.** (a) Photograph showing the extrusion of a suspension of microfibers by a syringe needle to form a hydrogel. (b) and (c) are confocal projections of the suspension and the hydrogel, respectively.

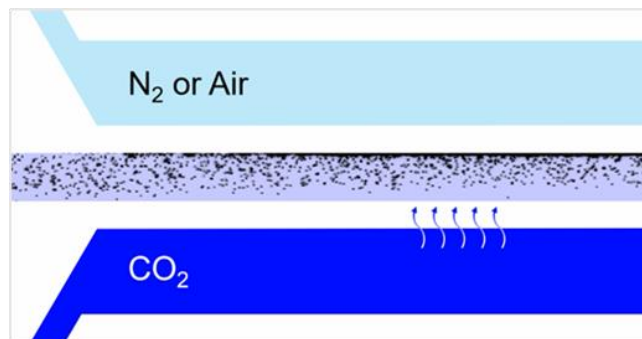
## CITATIONS

- Perazzo, A.; Nunes, J. K.; Guido, S.; Stone, H. A. Flow-induced gelation of microfiber suspensions. *Proc. Natl. Acad. Sci. U.S.A.* 2017, 114, E8557-E8564.

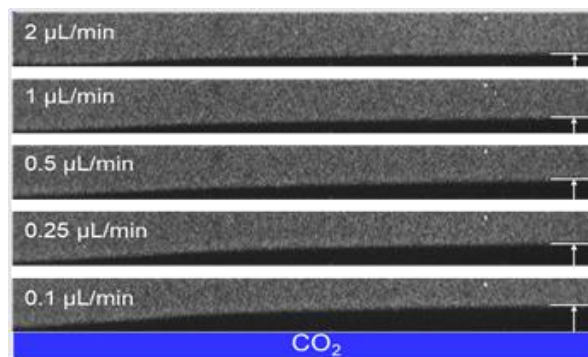
Researcher: **Suin Shim**  
 Advisor: **Howard A. Stone (MAE)**  
 Sponsorship: **NSF**

We investigate diffusiophoretic separation of positively- and negatively charged particles in a dead-end pore and a rectangular channel flow, driven by CO<sub>2</sub> dissolution from one boundary. Since the negatively charged particles create an exclusion zone near the boundary where CO<sub>2</sub> is introduced, we model the channel flow problem by applying a shear flow approximation in a 2D configuration. From the form of the equations we define a similarity variable to transform the reaction-diffusion equations and particle

distribution equations to ODEs. The definition of the similarity variable suggests a characteristic length scale for the particle exclusion zone. We consider height averaged and different orientation of the flow behaviors in rectangular channels to rationalize and connect our experimental observations with the model. Our observations and the theoretical model provide design parameters such as flow rate, channel dimensions and CO<sub>2</sub> pressure for the in-flow water cleaning systems.



**Caption 1:** Schematic of exclusion zone formation in the channel flow.



**Caption 2:** Change in the exclusion zone thickness at different flow rates.

## CITATIONS

- O. Shardt, B. Rallabandi, S. Shim, S. Shin, P. B. Warren, and H. A. Stone, Driving diffusiophoresis by the dissolution gas under review

Researcher: **Salman Sohrabi**  
Advisor: **Coleen T. Murphy (MOL)**  
Sponsorship: **NIH**

Making SU-8 Mold and fabricating a microfluidics chip to perform experiments with *C. elegans*.

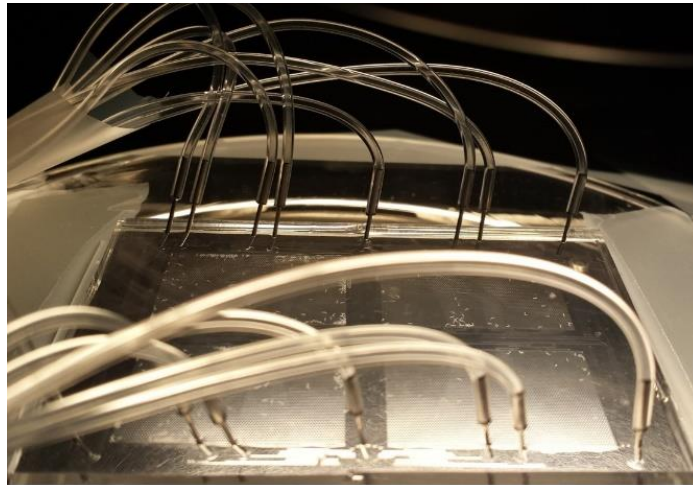


**Figure 1:** SU-8 Mold is used to fabricate PDMS microfluidics chip.

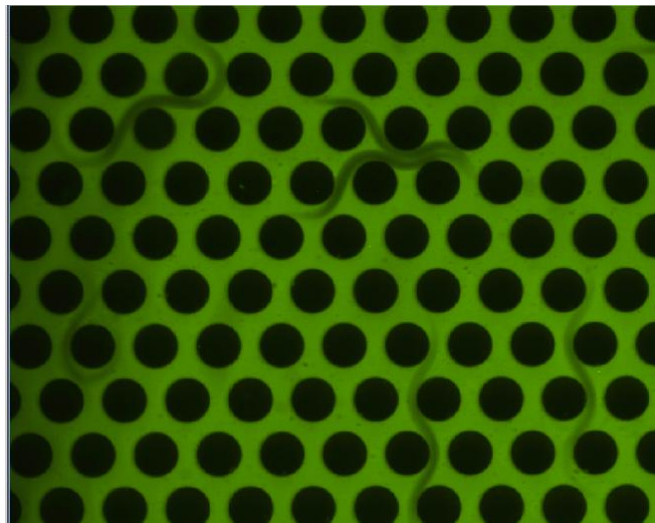


**Figure 2:** *C. elegans* moving between pillars inside microfluidic chip.

## CITATIONS

- Princeton University



Researcher: **Yimo Han**  
 Advisor: **Nieng Yan (MOL)**  
 Sponsorship: **Princeton University, Yan Lab**

I will explore the applications of graphene and other 2D materials in cryo-EM. Although single particle cryo-electron microscopy (cryo-EM) reaches 3-angstrom resolution by averaging many protein particles in solution, it fails to uncover *in vivo* high-resolution protein structures and interactions in cells. The main challenge to see proteins *in situ* is the electron dose: biological sample can tolerate only 50 electrons per angstrom square in total. In theory,

graphene as a 2D conductor with strong mechanical strength, can contribute to reducing sample damages by the electron beam (both ionization and knock-on). This approach may increase the electron dose limits of biological samples, thus allowing for high dose cryo-EM techniques such as cryo-electron tomography (Cryo-ET) and cryo-scanning TEM (cryo-STEM) to study protein complex in situ.

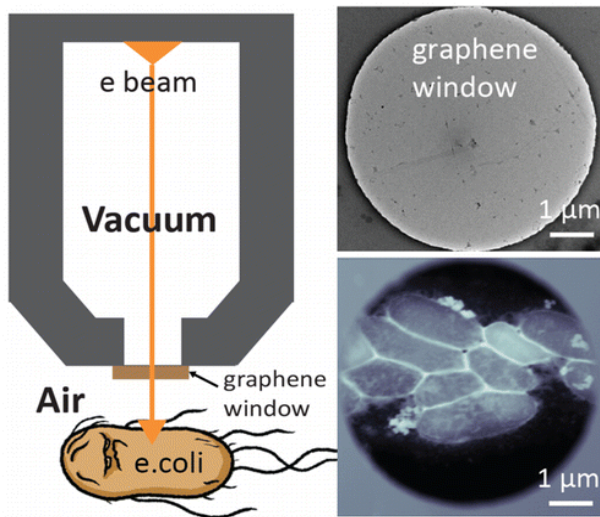


**Figure 1:** Atomically thin graphene windows enable high contrast vacuum-less *in situ* SEM (airSEM) for imaging biological specimens in their native environments.

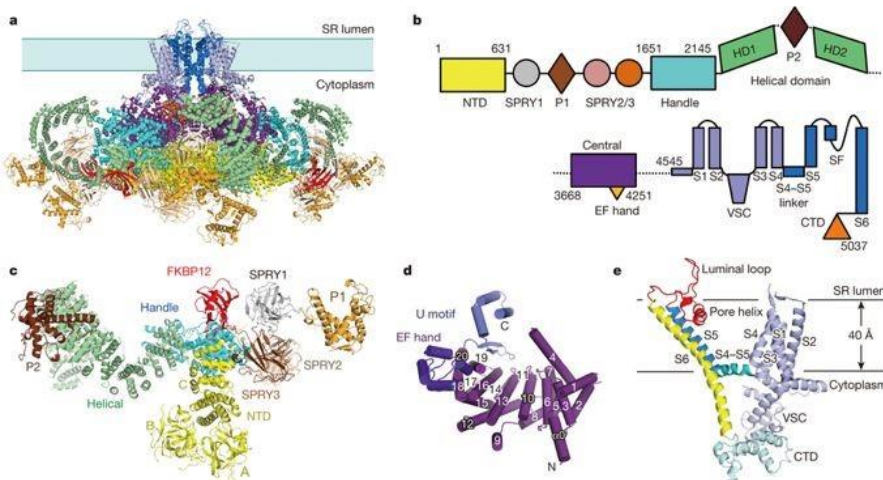


**Figure 2:** Overall structure and domain organization of the rabbit RyR1 solved by single particle Cryo-EM at a 3.8 angstrom resolution. We are interested in studying their interactions with Cav1.1 in cells using cryo-ET.

**CITATIONS**

- Nano Letters 16, 7427-7432
- Nature 517, 50-55

Researcher: **Xinran Li**

Advisor: **Cristiano Galbiati (PHY)**

Sponsorship: **Waiting for confirmation from Adviser**

This research is dedicated to the development of high-resolution amorphous selenium (a-Se) based imaging detector for the search of neutrinoless double  $\beta$  decay, which could reveal the nature of neutrinos. While being a double  $\beta$  decay source,  $^{82}\text{Se}$  could be evaporated on a complementary metal-oxide-semiconductor (CMOS) pixel array in amorphous format to produce two-dimensional images of ionizing tracks of utmost energy and spatial resolution, effectively akin to an electronic bubble chamber in the solid-state regime. Still to be experimentally demonstrated, a detector consisting of a large array of these devices could

have great background rejection and possibly reaching  $1 \times 10^6$  (kg y) exposure with zero background, making it feasible to probe the neutrinoless double  $\beta$  decay parameter space in the most unfavorable condition of a strongly quenched nucleon axial coupling constant.

The first stage of experiment aims to measure intrinsic energy resolution of a-Se in the energy region of interest. We use photolithography to fabricate comb like coplanar electrode to achieve hole carrier unipolar sensing in order to disentangle the effect of electron trapping in a-Se.

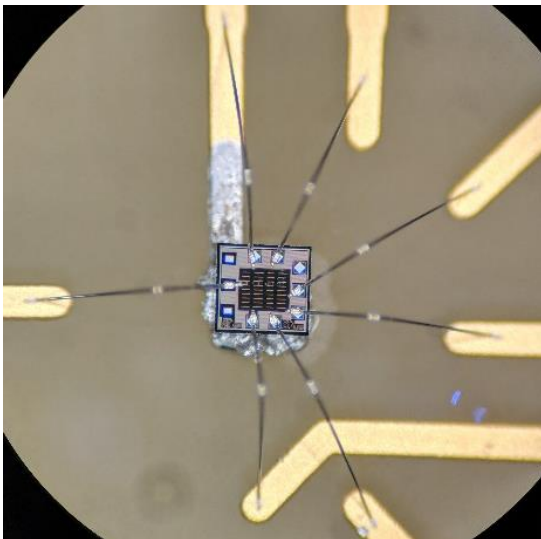


**Figure 1:** Wire bonding from charge amplifier (CUBE, produced by XGlab) to carrier board.

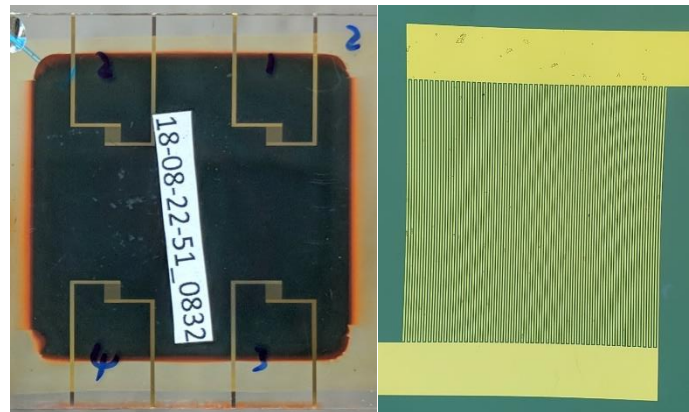


**Figure 2:** Left: Back side look of glass substrate with fabricated coplanar electrode (gold traces). The black film is a-Se deposited by collaboration company. Right: A microscope picture of coplanar electrode.

## CITATIONS

- [PDF] from arxiv.org  
A high-resolution CMOS imaging detector for the search of neutrinoless double decay in  $^{82}\text{Se}$   
Authors: AE Chavarria, C Galbiati, X Li, JA Rowlands  
Publication date: 2017/3/20  
Journal: Journal of Instrumentation Volume 12 Issue 03 Pages P03022  
Publisher: IOP Publishing

Researcher: **Xinwei Yu**

Advisor: **Andrew M. Leifer (PHY & PNI)**

Sponsorship: **Simon's Foundation**

It is widely known that male *C.elegans* can sense the scent of hermaphrodites, including pheromones such as *ascr#10* and *ascr#3* (Srinivasan et al., 2008). In response, males alter their behavior to increase the probability of mating. Such pheromone sensing is evolutionarily important because it is required for the male to pass on its genes. However, little is known about the brain-wide neural dynamics that mediate this behavioral response. Here, we study the animals behavioral and neural response to the odor of the opposite sex using an artificial dirt-style microfluidic chip (Lockery et al., 2008) where worms can crawl freely. We

deliver time varying quantities of supernatant carrying pheromones and other odors from hermaphrodites and observe the males' behavioral response and neural dynamics of neurons in the animal's head using pan-neuronally expressed GCaMP6s. Consistent with previous studyings, we observe that males increase their reversal rate in response to the scent of hermaphrodites (Srinivasan et al., 2008). Moreover, the animal exhibits different patterns of calcium activity in response to odor compared to buffer. Furthermore, we present preliminary results investigating whether neural coding of the animal's turning and velocity differ in these two odor contexts.

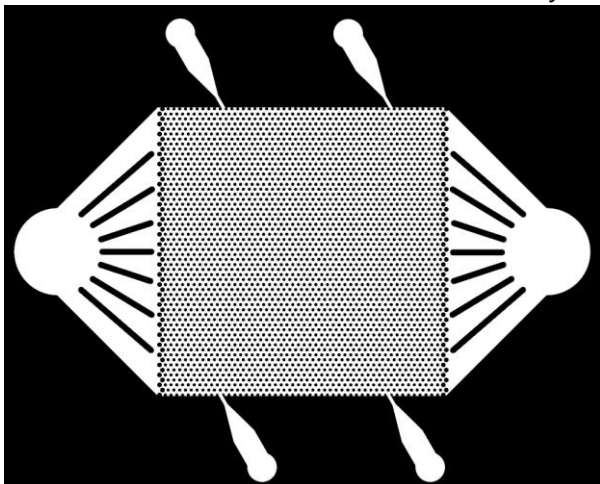


**Figure 1:** Artificial dirt chip

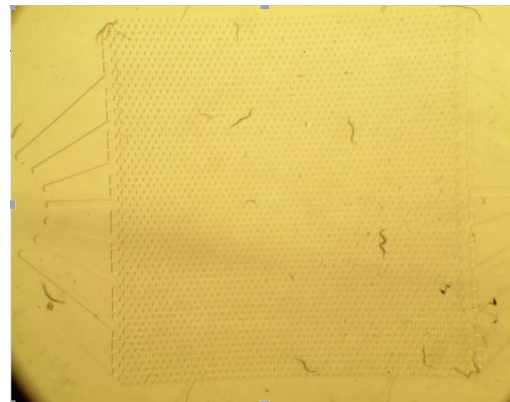


**Figure 2:** *C.elegans* freely moving in chip.

## CITATIONS

- Jeffrey P. Nguyen, Frederick B. Shipleya, Ashley N. Linder, George S. Plummer, Mochi Liu, Sagar U. Setru, Joshua W. Shaevitz, and Andrew M. Leifer, (2015). Whole-brain calcium imaging with cellular resolution in freely behaving *Caenorhabditis elegans*. *Proceedings of the National Academy of Sciences of the United States of America*, 10.1073/pnas.1507110112.
- Jeffrey P. Nguyen, Ashley N. Linder, George S. Plummer, Joshua W. Shaevitz, Andrew M. Leifer. Automatically tracking neurons in a moving and deforming brain. *PLOS Computational Biology* 13(5):e1005517(2017).
- Jagan Srinivasan, Fatma Kaplan, Ramadan Ajredini, Cherian Zachariah, Hans T. Alborn, Peter E. A. Teal, Rabia U. Malik, Arthur S. Edison, Paul W. Sternberg & Frank C. Schroeder. A blend of small molecules regulates both mating and development in *Caenorhabditis elegans*. *Nature*, Vol 454| 28 August 2008| doi:10.1038/nature07168
- S. R. Lockery, K. J. Lawton<sup>1</sup>, J. C. Doll, S. Faumont<sup>1</sup>, S. M. Coulthard, T. R. Thiele, N. Chronis, K. E. McCormick, M. B. Goodman, and B. L. Pruitt. Artificial dirt: Microfluidic substrates for nematode neurobiology. *J Neurophysiol*. Author manuscript; available in PMC

Researcher: **Stephan Kim**  
Advisor: **Nai Phuan Ong (PHY)**  
Sponsorship: **MURI**

We measure superconductivity in topological materials to discover new underlying physics.

## CITATIONS

---

- No publication yet

Researcher: **Nick Quirk**

Advisor: **Nai Phuan Ong (PHY)**

Sponsorship: **DOE**

I make nano/microscale electronic devices to study the exotic transport phenomena exhibited by topological materials of different kinds.

## CITATIONS

---

- None as of yet

Researcher: **Wudi Wang**  
 Advisor: **Nai Phuan Ong (PHY)**  
 Sponsorship: **MURI Foundation**

We are focusing on the study of superconductivity in various topological materials, like Weyl semimetal WTe<sub>2</sub> and MoTe<sub>2</sub>.

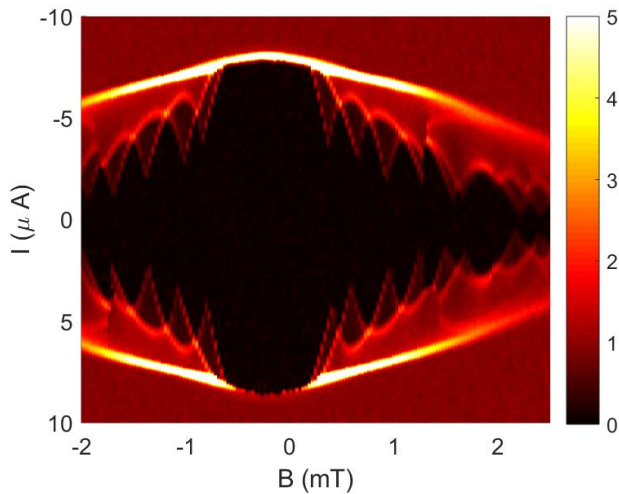


**Figure 1:** Differential resistance curves under various magnetic field measured on MoTe<sub>2</sub> sample with Au contacts at 20mK. Two oscillations show in Fig indicate periodical change of critical current.

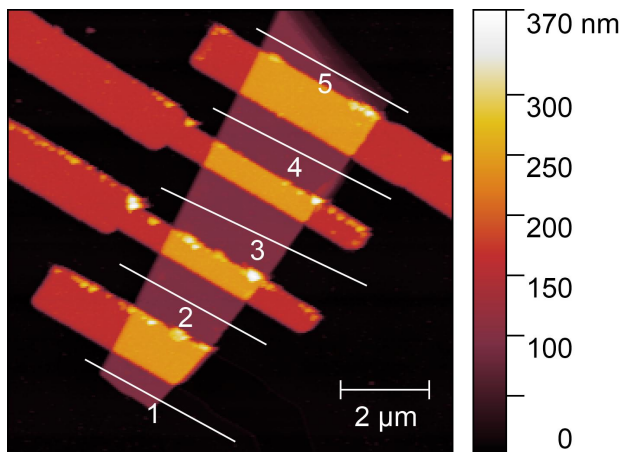


**Figure 2:** AFM image of a MoTe<sub>2</sub> device with Au contacts. Device fabricated with Raith Electron Beam Writer in PRISM cleanroom. AFM image was taken using NanoMan AFM in IAC.

## CITATIONS

- Wang, Wudi, et al. "Measurement of proximity induced superconductivity in MoTe<sub>2</sub>." APS Meeting Abstracts. 2017.

Researcher: **Zheyi Zhu**  
Advisor: **Nai Phuan Ong (PHY)**  
Sponsorship: **DOE**

This project focuses on the transport properties of topological material. This includes making devices with exfoliated crystal of quantum spin liquid candidates, preparing

substrates and making contacts for transport experiments involving 3D topological insulators and Weyl/Dirac semimetals, and more.

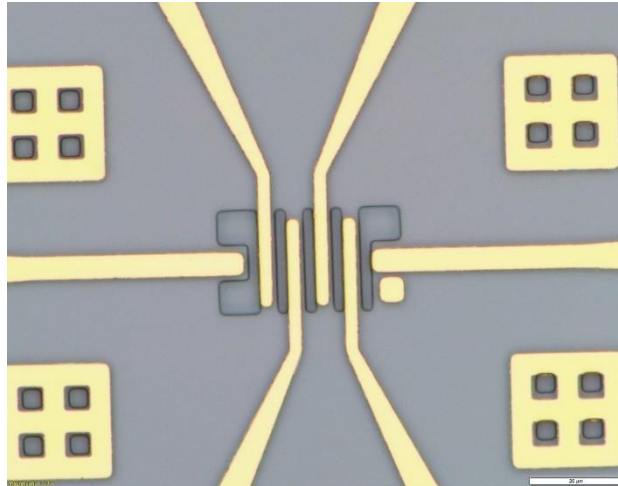


Figure 1

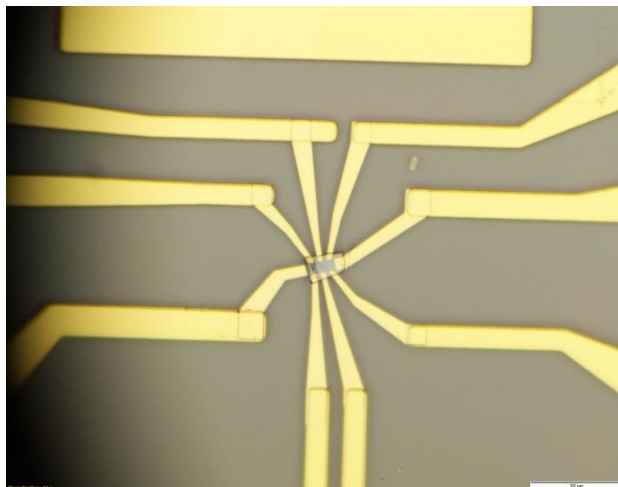


Figure 2

## CITATIONS

- N/A

Researcher: **Yaqiong Li**  
 Advisor: **Suzanne T. Staggs (PHY)**  
 Sponsorship: **Simons Foundation**

The Simons Observatory will be located in the high Atacama Desert in Northern Chile inside the Chajnantor Science Preserve. At 5,200 meters (17,000 ft) the site hosts some of the highest telescopes in the world. The Atacama Cosmology Telescope (ACT) and the Simons Array are currently making observations of the Cosmic Microwave Background (CMB). Their

goals are to study how the universe began, what it is made of, and how it evolved to its current state. The Simons Observatory will add to these several new telescopes and new cameras with state of the art detector arrays. The result will set the stage for the next generation of CMB experiments.

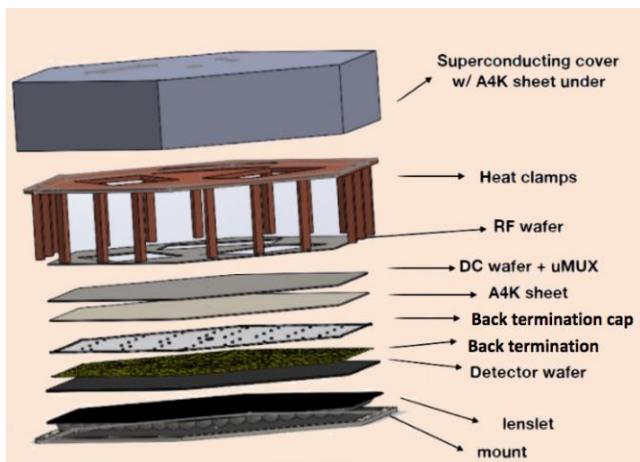


**Figure 1:** Simons Observatory detector array.

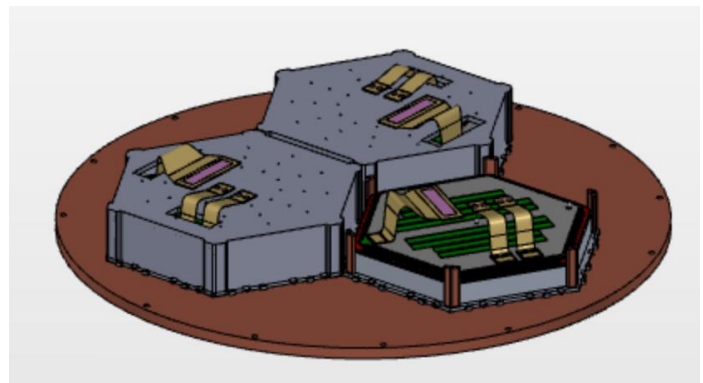


**Figure 2:** Simons Observatory focal plane.

## CITATIONS

- [arXiv:1808.07445v1 \[astro-ph.CO\]](https://arxiv.org/abs/1808.07445v1)



Researcher: **Yuhan Wang**  
Advisor: **Suzanne T. Staggs (PHY)**  
Sponsorship: **Simons Foundation**

The Simons Observatory will be located in the high Atacama Desert in Northern Chile inside the Chajnantor Science Preserve. At 5,200 meters (17,000 ft) the site hosts some of the highest telescopes in the world. The Atacama Cosmology Telescope (ACT) and the Simons Array are currently making observations of the Cosmic Microwave Background (CMB). Their

goals are to study how the universe began, what it is made of, and how it evolved to its current state. The Simons Observatory will add to these several new telescopes and new cameras with state of the art detector arrays. The result will set the stage for the next generation of CMB experiments.

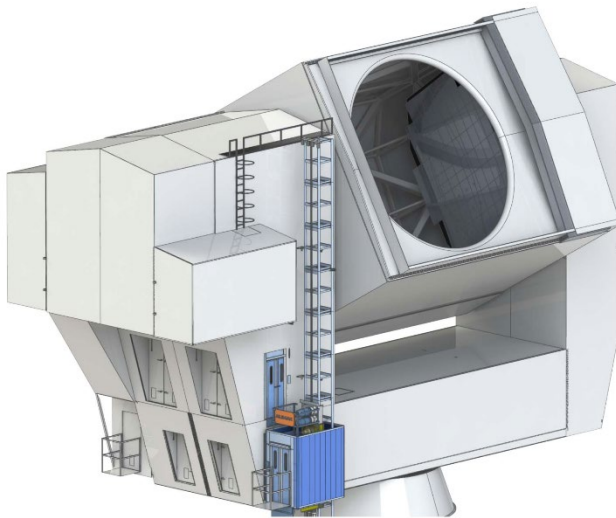


**Figure 1:**

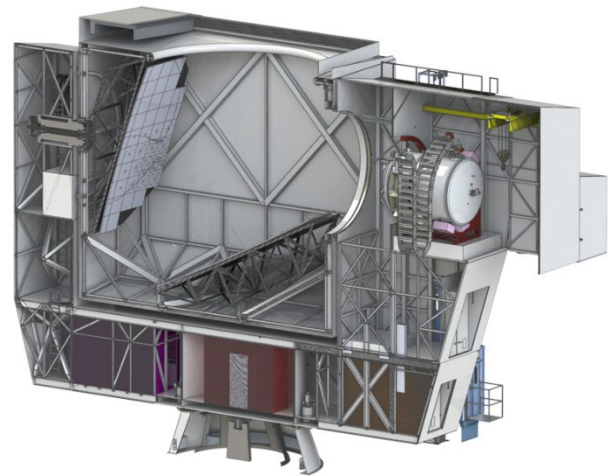


**Figure 2:**

## CITATIONS

- [arXiv:1808.07445v1](https://arxiv.org/abs/1808.07445v1) [astro-ph.CO]

Researcher: **Fang Zhao**

Advisor: **Christopher G. Tully (PHY)**

Sponsorship: **Simons Foundation (#377485), John Templeton Foundation (#58851), Department of Energy (DE-SC0007968)**

1. Graphene nanoribbon transistors with top and bottom gates are fabricated for the first time direct directional detection of MeV dark matter. The GNFET sensor has a tunable meV band gap, a full three orders of magnitude smaller than cryogenic germanium detectors. This sensitivity is used to switch on and off the conductivity of the GNFET channel by 10 orders of magnitude in charge carriers in response to the gate voltage shift from a single scattered electron. The width of GNs are from sub-10nm to 100nm. Single and

ribbon array FETs will be fabricated for electronic properties low measurements at temperature from 4K to room temperature. CVD and exfoliated graphene is applied.

2. Greyscale lens structure will be fabricated by Heidelberger greyscale lithography to coat on our photodetectors for the light collection of precision timing detectors for the LHC at CERN.

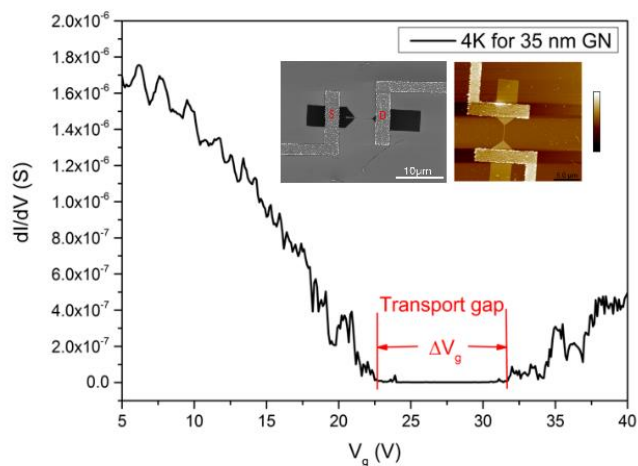


**Figure 1:**  $dI/dV$  of a GNFET with  $W=35\text{nm}$  and  $L=2.5\mu\text{m}$ , plotted as a function of  $V_g$ . Right inset shows an SEM image and left inset shows an AFM image.

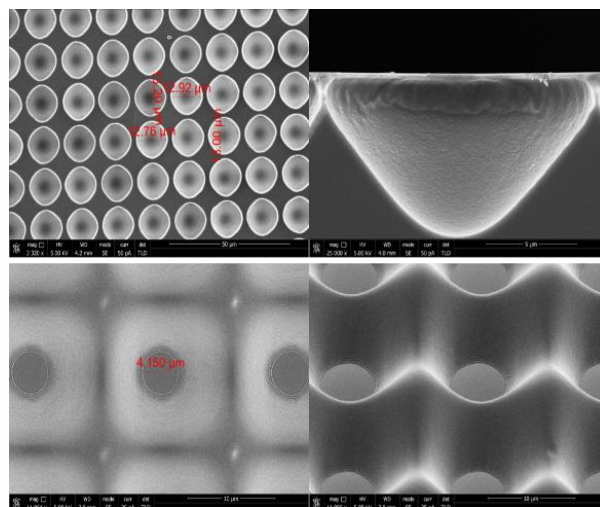


**Figure 2:** SEM images of lens and cone structure by greyscale lithography.

**CITATIONS**

- Have not published yet

Researcher: **Yanyu Jia**  
 Advisor: **Sanfeng Wu (PHY)**  
 Sponsorship: **Princeton Physics new faculty startup**

This project aims to fabricate quantum devices based on 2D materials, such as graphene, boron nitride and Tungsten ditelluride (WTe<sub>2</sub>), for quantum transport measurements. We will study the topological phases and novel

superconducting states in these materials. To accomplish that, we will create nanoscale devices using equipment in MNFL, such as E-beam lithography, dry etch, metal evaporator and wire bonder.

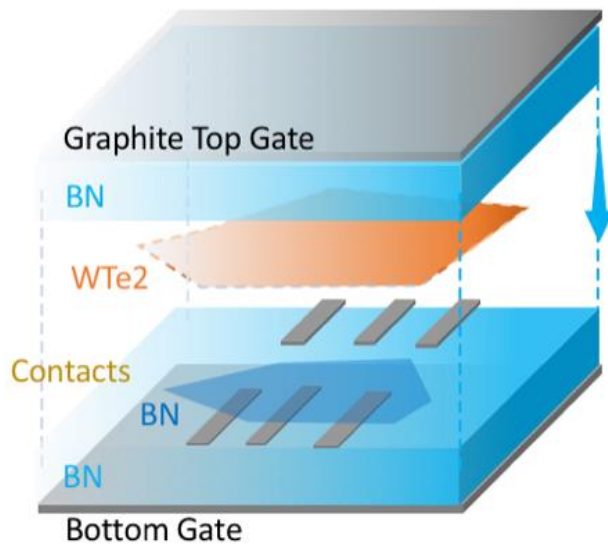


**Figure 1:** WTe<sub>2</sub> Quantum Tunneling Spectroscopy Device Diagram

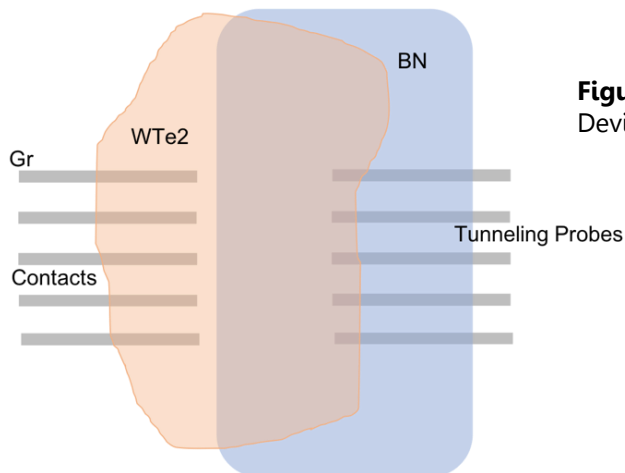


**Figure 2:** WTe<sub>2</sub> Quantum Tunneling Spectroscopy Device Diagram 2

**CITATIONS**

- None

Researcher: **Mike Onyszczak**

Advisor: **Sanfeng Wu (PHY)**

Sponsorship: **Princeton Physics New Faculty Start-up**

This project aims to fabricate quantum devices based on 2D materials, such as graphene, boron nitride and tungsten ditelluride (WTe<sub>2</sub>), for quantum transport measurements. We will study the topological phases and novel

superconducting states in these materials. To accomplish that, we will create nanoscale devices using equipment in MNFL, such as E-beam lithography, dry etch, metal evaporator and wire bonder.

## CITATIONS

---

- None

## OTHER RESEARCH PERFORMED IN THE PRISM CLEANROOM

### NANOPRINTING AND MICROFLUIDIC

Researcher: **Bing Xu**

Advisor: **Stephen Y. Chou (ELE)**

Sponsorship: **Industrial**

### ULTRASENSITIVE NANOSTRUCTURED BIOSENSOR

Researcher: **Faheng Zang**

Advisor: **Stephen Y. Chou (ELE)**

Sponsorship: **DTRA**

### ELECTRONS ON HELIUM

Researcher: **Ethan Kleinbaum**

Advisor: **Stephen A. Lyon (ELE)**

Sponsorship: **Stephen Lyon**

### FAST OPTICAL SWITCH

Researcher: **Siamak Abbaslou**

Advisor: **Paul R. Prucnal (ELE)**

Sponsorship: **General Dynamics**

### MAGNETIC PARTICLE SENSING BASED ON CMOS OSCILLATOR ARRAY

Researcher: **Hao Tang**

Advisor: **Kaushik Sengupta (ELE)**

Sponsorship: **NSF**

### MULTIPLE ION DIFFUSIOPHORESIS

Researcher: **Jessica Wilson**

Advisor: **Howard A. Stone (MAE)**

Sponsorship: **NSF**

### HIGH-YIELD FABRICATION ON THIN FILM TRANSISTORS

Researcher: **Zhiwu Zheng**

Advisor: **James C. Sturm (ELE)**

Sponsorship: **James C. Sturm**

## EXAMPLES OF CITATIONS RESULTING FROM RESEARCH UTILIZING THE PRISM CLEANROOM

**Average index for this partial citation listing is: 16**

**This partial citation listing includes 43 citations**

E.W.-H. Sun, I. C. Bourg, "Molecular Dynamics Simulation Prediction of Quartz Wetting by Water and Supercritical CO<sub>2</sub> and the Potential Impact of Organic Residues", *Goldschmidt Abstracts*. [In preparation]

Y. Zhang, W. Fan, A. Y. Song, D. L. Sivco, and C. F. Gmachl, "Optoelectronic Plasmonic Metamaterials with a Quantum Cascade Structure", In *Conference on Lasers and Electro-Optics, The Optical Society Technical Digest (online)*.

Y. Zhang, W. Fan, A. Y. Song, D. L. Sivco, and C. F. Gmachl, "Optical Response of Plasmonic Metamaterials with Quantum Cascade Structure for Loss Compensation", *SPIE Photonics West*.

A. J. Kollar, M. Fitzpatrick, and A. A. Houck, "Hyperbolic Lattices in Circuit Quantum Electrodynamics", *Quantum Physics archive*.

M. Fitzpatrick, N. M. Sundaresan, A. C. Y. Li, J. Koch, and A. A. Houck, "Observations of a Dissipative Phase Transitions in One-Dimensional Circuit QED Lattice", *Physical Review X, Vol. 7, Iss. 1*.

T. M. Hazard, A. Gyenis, A. Di Paolo, A. T. Asfaw, S. A. Lyon, A. Blais, and A. A. Houck, "Nanowire Superinductance Fluxonium Qubit", *Quantum Physics and Mesoscale and Nanoscale Physics archive*.

N. M. Sundaresan, R. Lundgren, G. Zhu, A. V. Gorshkov, and A. A. Houck, "Interacting Qubit-Photon Bound States with Superconducting Circuits", *Quantum Physics archive*.

A.T. Asfaw, E. I. Kleinbaum, T. M. Hazard, A. Gyenis, A. A. Houck and S. A. Lyon, "Superconducting Kinetic Inductance Field-Frequency Sensors for Sensitive Magnetometry in Moderate Background Magnetic Fields", *Applied Physics Letters*. Vol. 113, Iss. 17.

A. T. Asfaw, A. J. Sigillito, A. M. Tyryshkin, T. Schenkel and S. A. Lyon, "Multi-frequency Spinmanipulation Using Rapidly Tunable Superconducting Coplanar Waveguide Microresonators", *Applied Physics Letters*, Vol. 111.

A. T. Asfaw, E. I. Kleinbaum and S. A. Lyon, "Transport Measurements of Surface Electrons in 200 nm Deep Helium-Filled Microchannels Above Amorphous Metallic Electrodes", *Mesoscale and Nanoscale Physics archive*.

J.-S. Kim, A. M. Tyryshkin, and S. A. Lyon, "Annealing Shallow Si/SiO<sub>2</sub> Interface Traps in Electron-Beam Irradiated High-Mobility Metal-Oxide-Silicon Transistors", *Applied Physics Letters, Vol. 110, Iss. 12*.

S. Chen, K. Roh, J. Lee, W. K. Chong, Y. Lu, N. Mathews, T. C. Sum, and A. Nurmikko, "A Photonic Crystal Laser from Solution Based Organo-Lead Iodide Perovskite Thin Films", *ACS Nano Publications*.

L. Zhao, Y.-W. Yeh, N. L. Tran, F. Wu, Z. Xiao, R. A. Kerner, Y. L. Lin, G. D. Scholes, N. Y. Yao, and B. P. Rand, "In Situ Preparation of Metal Halide Perovskite Nanocrystal Thin Films for Improved Light-Emitting Devices", *ACS Nano Publications*.

## EXAMPLES OF CITATIONS RESULTING FROM RESEARCH UTILIZING THE PRISM CLEANROOM

- C. R. Chappidi, X. Wu, and K. Sengupta, "Simultaneously Broadband and Back-Off Efficient mm-Wave PAs: A Multi-Port Network Synthesis Approach", *IEEE Journal of Solid-State Circuits*, Volume 53, No. 9.
- C. Chappidi, X. Wu, and K. Sengupta, "A Digital mm-Wave PA Architecture with Simultaneous Frequency and Back-Off Reconfigurability", *IEEE Radio Frequency Integrated Circuits Symposium*.
- C. Chappidi and K. Sengupta, "A W-Band SiGe Power Amplifier with PSAT of 23 dBm and PAE of 16.8% at 95GHz", *IEEE International Microwave Symposium*.
- C. R. Chappidi and K. Sengupta, "Globally Optimal Matching Networks with Lossy Passives and Efficiency Bounds", *IEEE Transactions on Circuits and Systems*.
- C. R. Chappidi and K. Sengupta, "20.2 A Frequency-Reconfigurable mm-Wave Power Amplifier with Active-Impedance Synthesis in An Asymmetrical Non-Isolated Combiner", *IEEE International Solid-State Circuits Conference*.
- Md. S. Hossain, M. K. Ma, M. A. Mueed, L. N. Pfeiffer, K. W. West, K. W. Baldwin, and M. Shayegan, "Direct Observation of Composite Fermions and their Fully Spin-Polarized Fermi Sea Near  $\nu=5/2$ ", *Physical Review Letters*.
- M. A. Mueed, Md. S. Hossain, I. Jo, L.N. Pfeiffer, K. W. West, K. W. Baldwin, and M. Shayegan, "Realization of a Valley Superlattice", *Physical Review Letters*.
- Md. S. Hossain, M. A. Mueed, M. K. Ma, Y. J. Chung, L. N. Pfeiffer, K. W. West, K. W. Baldwin, and M. Shayegan, "Anomalous Coupling Between Magnetic and Nematic Orders in Quantum Hall Systems", *Physical Review Letters*.
- L. E. Aygun, S. Wagner, N. Verma, and J.C. Sturm, "High-frequency ZnO Schottky Diodes for Non-Contact Inductive Power Transfer in Large-Area Electronics", *IEEE 75th Annual Device Research Conference*.
- A. H. Berg, K. A. Nagamatsu, J. C. Sturm, "Extraction of Front-and Rear-Interface Recombination in Silicon Double-Heterojunction Solar Cells by Reverse Bias Transients", *IEEE Transactions on Electron Devices*, Vol. 64, No. 11.
- G. Sahasrabudhe, S. M. Rupich, J. Jhaveri, A. H. Berg, K. A. Nagamatsu, G. Man, Yves. J. Chabal, A. Kahn, S. Wagner, J. C. Sturm, and J. Schwartz, "Low-Temperature Synthesis of a TiO<sub>2</sub>/Si Heterojunction", *Journal of the American Chemical Society*.
- K. A. Nagamatsu, S. Avasthi, G. Sahasrabudhe, G. Man, J. Jhaveri, A. H. Berg, J. Schwartz, A. Kahn, S. Wagner, and J. C. Sturm, "Titanium Dioxide/Silicon Hole-Blocking Selective Contact to Enable Double-Heterojunction Crystalline Silicon-Based Solar Cell", *Applied Physics Letters*.
- J. Jhaveri, A. H. Berg, and J. C. Sturm, "Isolation of Hole Versus Electron Current at p-Si/TiO<sub>2</sub> Selective Contact Using a Heterojunction Bipolar Transistor Structure", *IEEE Journal of Photovoltaics*, Vol. 8, Iss. 3.

## EXAMPLES OF CITATIONS RESULTING FROM RESEARCH UTILIZING THE PRISM CLEANROOM

- K.-C. L, G. Torga, A. Wu, J. D. Rabinowitz, W. J. Murray, J. C. Sturm, K. J. Pienta, and R. Austin, "Epithelial and Mesenchymal Prostate Cancer Cell Population Dynamics on a Complex Drug Landscape", *Convergent Science Physical Oncology*.
- C. Wu, Y. Mehlman, A. Pierre, T. Moy, A. Arias, and N. Verma, "A Large-Area Image Sensing and Compression System Based on Variation Tolerant Random Projections", *SONIC Annual Meeting*.
- Y. Mehlman, Y. Asfar, T. Moy, S. Wagner, J. C. Sturm, and N. Verma, "High-Speed Scanning Circuit Based on Metal-Oxide Thin-Film-Transistors for Reduction of Large-Area to CMOS IC Connections, *International Thin Film Transistor Conference*.
- Y. Mehlman, Y. Asfar, T. Moy, S. Wagner, J. C. Sturm, and N. Verma, "Self-Aligned ZnO Thin-Film Transistors with 860 MHz fT and 2 GHz fmax for Large-Area Applications, *75th Device Research Conference*.
- M. Oztay, L. Aygun, H. Jia, P. Kimar, Y. Mehlman, C. Wu, S. Wagner, J. C. Sturm, and N. Verma, "Artificial Intelligence Meets Large-Scale Sensing: Using Large-Area Electronics (LAE) to Enable Intelligent Spaces", *IEEE Custom Integrated Circuits Conference*.
- A. M. Dibos, M. Raha, C. M. Phenicie, and J. D. Thompson, "Atomic Source of Single Photons in the Telecom Band", *Physical Review Letters*. Vol. 120. Iss. 24.
- E. Turkoz, SY. Lang, L. Deike, and C. B. Arnold, "Subthreshold Laser Jetting Via Flow-Focusing in Laser-Induced Forward Transfer", *Physical Review Fluids*, Vol. 3, Iss. 8.
- Y. Kim, A. Harness, D. Sirbu, M. Hu, M. B. Galvin, N. J. Kasdin, R. Vanderbei, and S. B. Shaklan, "Optical Demonstration of a Starshade at Flight Fresnel Numbers", *Proceedings of the SPIE*, Vol. 10400.
- A. Harness, S. Shaklan, P. Dumont, Y. Kim, and N. J. Kasdin, "Modeling and Performance Predictions for the Princeton Starshade Testbed", *Proceedings of the SPIE*, Vol. 10400.
- A. Perazzo, J.K. Nunes, S. Guido, and H. A. Stone, "Flow-Induced Gelation of Microfiber Suspensions", *Proceedings of the National Academy of Sciences of the United States of America*.
- O. Shardt, B. Rallabandi, S. Shim, S. Shin, P. B. Warren, and H. A. Stone, "Driving Diffusiophoresis by the Dissolution Gas". [under review]
- Y. Han, K. X. Nguyen, Y. Ogawa, J. Park, and D. A. Muller, "Atomically Thin Graphene Windows That Enable High Contrast Electron Microscopy without a Specimen Vacuum Chamber", *Nano Letters*.
- A. E. Chavarria, C. Galbiati, X. Li, and J. A. Rowlands, "A High Resolution CMOS Imaging Detector for the Search of Neutrinoless Double Decay in  $82\text{Se}$ ", *Journal of Instrumentation* Vol. 12, Iss. 03.
- M. Scholz, A. N. Linder, F. Randi, A. K. Sharma, X. Yu, J. W. Shaevitz, and A. M. Leifer, "Predicting Natural Behavior from Whole-Brain Neural Dynamics", *BioRxiv: The Present Server for Biology*.



## EXAMPLES OF CITATIONS RESULTING FROM RESEARCH UTILIZING THE PRISM CLEANROOM

W. Wang, M. Liu, Q. Gibson, R. J. Cava, and N. P. Ong, "Measurement of Proximity Induced Superconductivity in MoTe<sub>2</sub>", *APS Meeting Abstracts*.

Y. Li and The Simons Observatory Collaboration, "The Simons Observatory: Science Goals and Forecasts", *Astrophysics: Cosmology and Nongalactic Astrophysics archive*.

Y. Wang and The Simons Observatory Collaboration, "The Simons Observatory: Science Goals and Forecasts", *Astrophysics: Cosmology and Nongalactic Astrophysics archive*.